

UNIVERSITÄTSKLINIKUM HAMBURG-EPPENDORF

Zentrum für Molekulare Neurobiologie Hamburg

Prof. Dr. Matthias Kneussel

**Functional deficits of mice mutated in the cell
adhesion molecule L1**

Dissertation

zur Erlangung des Dr. rer. biol. hum.

an der Medizinischen Fakultät der Universität Hamburg

vorgelegt von:

Ludovica Congiu

aus Cagliari, Italien

Hamburg 2023

Angenommen von der Medizinischen Fakultät der Universität Hamburg am: 24.05.2023_

Veröffentlicht mit Genehmigung der Medizinischen Fakultät der Universität Hamburg.

Prüfungsausschuss, der/die Vorsitzende: Prof. Dr. Dr. Melitta Schachner _

Prüfungsausschuss, zweite/r Gutachter/in: PD Dr. Sabine Hoffmeister-Ullerich

TABLE OF CONTENT

1. INTRODUCTION	5
1.1 The cell adhesion molecule L1	5
1.2 Proteolytic processing of L1	7
1.3 The L1-70 fragment	8
1.4 L1 syndrome and L1 mutant models	9
1.5 L1-agonist compounds	11
1.6 Mitochondria	12
1.6.1 Structure and functions	12
1.6.2 Mitochondrial electron transport chain and reactive oxygen species generation	14
1.6.3 AMPK and mitochondria	17
1.7 AIMS OF THE THESIS	21
2. MATERIALS AND METHODS.....	22
2.1 Animals	22
2.1.1 L1-deficient mice.....	22
2.1.2 L1-201 mice	22
2.1.3 L1/858-863 mice	23
2.1.4 L1/687 mice.....	24
2.2 Suppliers of chemical, kits, reagents and laboratory equipment	25
2.3 Solutions and buffers	26
2.4 Antibodies	29
2.5 Cell culture methods and assays.....	30
2.5.1 Preparation of coverslips	30
2.5.2 Culture of mouse primary cerebellar granule cells.....	30
2.5.3 Isolation of mitochondrial fractions for import and enzymatic assays.....	31
2.5.4 Determination of the protein concentration.....	31
2.5.5 Western blot	32
2.5.6 Schwann cell process formation.....	32
2.6 Mitochondrial motility	32
2.6.1 Mitochondrial membrane potential	33
2.6.2 Mitochondrial complex I activity	34

2.6.3 ATP level.....	34
2.6.4 Measurement of reactive oxygen species in cells.....	35
2.6.5 Measurement of reactive oxygen species in tissue with 2-Thiobarbituric acid (TBARS) assay	35
2.7 Golgi staining	36
2.8 Behavior and histology.....	37
2.8.1 Histology	37
2.8.2 Behavior analysis	38
2.8.2.1 Open field and elevated plus maze	38
2.8.2.2 Marble burying test.....	39
2.8.2.3 Social interaction.....	39
2.8.2.4 Home cage activity.....	39
2.8.2.5 Rotarod and pole test.....	40
2.8.2.6 Beam walking.....	40
2.8.2.7 Grip strength test	40
2.9 Statistics	41
3. RESULTS.....	42
3.1 Impaired mitochondrial motility in neurons from L1 mutant mice.....	42
3.2 The mitochondrial membrane potential is differently impaired in neurons of L1/858-863 and L1-201 mice.....	46
3.3 Complex 1 activity and ATP production are differently affected in neurons of L1-201 and L1/858-863 mice.....	48
3.4 Cerebellar neurons from L1-201 and L1/858-863 mice show enhanced levels of reactive oxygen species.....	51
3.5 Oxidative stress is higher in young but not in adult brains of L1-mutant mice.....	53
3.6 Phospho-AMPK/AMPK levels are normal in 10-day-old L1-201 mice	54
3.7 Schwann cell process formation is impaired in L1-201 neurons.....	56
3.8 Behavior	58
3.8.1 Body weight and grip strength	58
3.8.2 Open field.....	60
3.8.3 Elevated plus maze	62
3.8.4 Social interaction.....	63
3.8.5 Circadian activity.....	64
3.8.6 Rotarod and pole test.....	65
3.8.7 Marble burying	67
3.9 Morphological analysis	68

3.9.1 L1/858-863 mice have normal ventricle size and corpus callosum thickness	68
3.9.2 Spine density and spine type determination in L1-201 male mice	70
3.9.3 Normal arborization of dendrites from pyramidal neurons in the prefrontal cortex of L1-201 male mice	73
4. DISCUSSION.....	75
4.1 The L1-70 fragment regulates mitochondrial membrane potential and complex I activity	75
4.2 L1-70 fragment is not responsible for the increased oxidative stress in both L1-201 and L1/858-863 neurons.....	78
4.3 L1-70 fragment absence reduces mitochondrial motility but is not responsible for the increased retrograde transport of mitochondria	81
4.4 Morphological and histological features of L1-201 mutant mice	82
4.5 Morphological characterization of adult L1/858-863 mice	83
4.6 Behavioral characterization of adult L1/858-863 mice	84
4.6.1 L1/858-863 female mice show alterations in their anxiety state	85
4.6.2 L1/858-863 male mice show altered activity in the marble burying test	86
4.6.3 Normal social interest of L1/858-863 mice.....	87
4.6.4 Lack of L1-70 fragment does not influence motor performance and general motor coordination	87
5. SUMMARY	89
6. ZUSAMMENFASSUNG.....	91
7. REFERENCES	99
8. ACKNOWLEDGEMENTS	111
9. CURRICULUM VITAE	112
10. Eidesstattliche Versicherung	114

1. INTRODUCTION

1.1 The cell adhesion molecule L1

Cell adhesion molecules (CAMs) are cell surface glycoproteins involved in neural development, axons growth, synapse formation, apoptosis, gene expression, migration and adhesion of neuronal cells (Togashi et al., 2009), as well as memory and learning processes (Sanes and Yamagata, 1999, Yamagata et al., 2003, Washbourne et al., 2004). They are grouped into four superfamilies: cadherins, the immunoglobulin (Ig)-like superfamily, selectins and integrins (Fields and Itoh, 1996). L1 belongs to the Ig-like superfamily and is a member of the L1 subfamily which also includes the close homolog of L1 (CHL1), neuron-glia CAM-related cell adhesion molecule and neurofascin (Herron et al., 2009, Wei and Ryu, 2012). L1 mediates cell-cell adhesion to activate various signaling pathways by homophilic interaction or heterophilic binding to other neural cell adhesion molecules and to extracellular matrix proteins (Maness and Schachner, 2007, Colombo and Meldolesi, 2015).

L1 is a 200-220 kDa membrane glycoprotein and consists of an extracellular part with six Ig-like domains and five fibronectin type III homologous repeats, followed by a transmembrane region and a cytoplasmic tail (Fig. 1) (Moos et al., 1988).

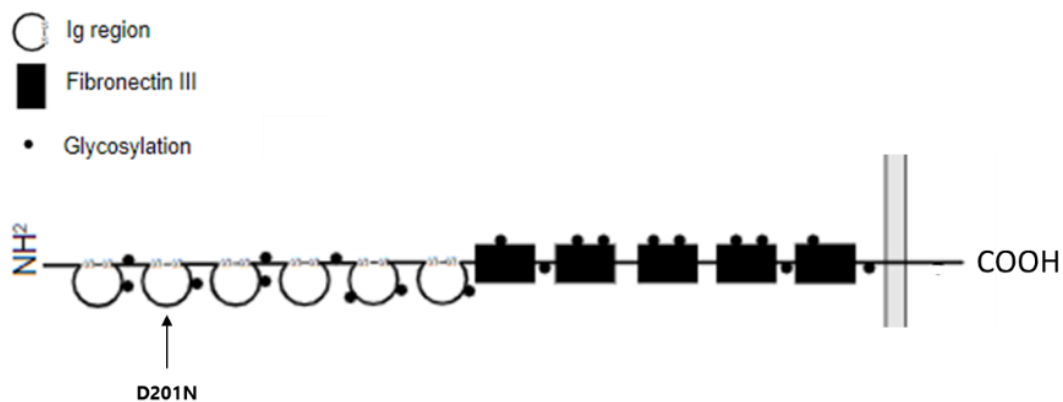


Figure 1. Protein domain structure of the cell adhesion molecule L1. L1 is a 200-220 kDa glycoprotein with six Ig-like domains at the amino terminal end followed by five fibronectin type III homologous repeats, a single transmembrane region and an intracellular tail at the C-terminal end (modified from Fields and Itoh, 1996).

The cytoplasmic domain of L1 contains the conserved sequence FIGQ/AY that reversibly binds ankyrin, a spectrin adaptor that couples L1 to the actin cytoskeleton. L1 also binds to the actin cytoskeleton via ezrin-radixin-moesin (ERM) proteins. Furthermore, alternative splicing generates a neuronal isoform of L1 containing the sequence RSLE in the cytoplasmic domain that enables L1's recruitment to the adaptor protein 2-clatrin for endocytosis. At the plasma membrane, L1 is capable of cis binding to neuropilin-1 (NP-1), a component of the semaphorin 3A (Sema3A) receptor complex, through the sequence FASNKL in the first immunoglobulin-like domain of L1 (Maness and Schachner, 2007).

The L1 gene is located on the X chromosome, and it is preferentially expressed in the developing peripheral nervous system by neurons as well as by non-myelinating Schwann cells and in the central nervous system by non-myelinated neurons. L1 protein is present in axons of non-myelinated neurons and in growth cones of differentiating neurons (Hortsch, 1996, Dahme et al., 1997, Kamiguchi and Lemmon, 1998, Kenwrick et al., 2000, Wang et al., 2012). Furthermore, L1 is also expressed by leukocytes and epithelial cells of the intestine and urogenital tract (Probstmeier et al., 1990, Kowitz et al., 1992, Kujat et al., 1995). L1 has various functions in the nervous system: it plays important roles in neuronal cell migration and survival, neurite outgrowth, axonal fasciculation (Lindner et al., 1983, Kruse et al., 1984, Fischer et al., 1986, Martini and Schachner, 1986, Moos et al., 1988, Seilheimer et al., 1989, Appel et al., 1993), myelination and synaptic plasticity (Wood et al., 1990, Lüthl et al., 1994) as well as regeneration after injury (Guseva et al., 2009). Expression of the L1 gene is regulated by the RE-1-Silencing Transcription factor (REST), which is also involved in neuronal cell differentiation (Mikulak et al., 2012). It has been shown that L1 protein expression is differently regulated depending on the cell type: the β -caterin/T-cell factor transcription system is responsible for L1 expression in some tumors (Gavert et al., 2005), while another transcription factor called SLUG is involved in L1 expression in pancreatic adenocarcinoma (Pfeiffer et al. 2010, Geismann et al. 2011). L1 exists in two alternatively spliced isoforms: the full-length one is composed by 28 exons, and it is present in neurons. The other isoform is expressed in other non-neural cell types, and it lacks two mini exons (2 and 27) that code for sequences which mediate the binding of L1 with extracellular and cytoplasmatic proteins (Mikulak et al., 2012). The alternative splicing of L1 is controlled by REST

through two different mechanisms: the first one involves the direct repression of the L1 gene, the second one involves the repression of the Nova2 gene, which plays a key role in the expression of full-length L1 and thus contributes to L1-dependent migration, outgrowth/fasciculation/regeneration of axons and synaptic plasticity (Mikulak et al., 2012). Furthermore, L1 carries twenty-one potential glycosylation sites, which affect its homophilic interactions (Wei and Ryu., 2012).

1.2 Proteolytic processing of L1

Full-length L1 can be proteolytically processed by several proteases which cleave L1 in the extracellular transmembrane domain (Kalus et al., 2003, Lutz et al., 2014a, Lutz et al., 2014b). Cleavage of L1 within the third fibronectin type III domain at the dibasic sequence 858RKHSKR863 by trypsin (Sadoul et al., 1988), proprotein convertase 5a (Kalus et al., 2003) or plasmin (Nayeem et al., 1999, Silletti et al., 2000, Mechtersheimer et al., 2001) results in a 140 kDa extracellular fragment and an 80 kDa transmembrane fragment. Furthermore, full-length L1 can be cleaved by a serine protease in its extracellular domain at arginine 687 (R687V) in the first fibronectin type III domain within a highly conserved sialic-acid binding site in the first FNIII domain (Kleene et al., 2020). This serine protease is an active myelin basic protein (MBP) form of approximately 60 kDa which is released into the extracellular space after stimulation of L1-dependent signaling and represents a fusion between the 21.5-kDa MBP form and the C-terminal part of dynamin I or a dynamin I-related protein (Lutz et al., 2014). This cleavage of L1 leads to the generation of a transmembrane C-terminal fragment of approximately 70 kDa, called L1-70, and of a soluble N-terminal extracellular fragment of approximately 135 kDa, called L1-135 (Fig. 2) (Lutz et al., 2014a, Lutz et al., 2012). Two members of the disintegrin and metalloprotease family, ADAM10 and ADAM17, are also involved in the cleavage of L1, stimulating cellular migration and neurite outgrowth (Maretzky et al., 2005).

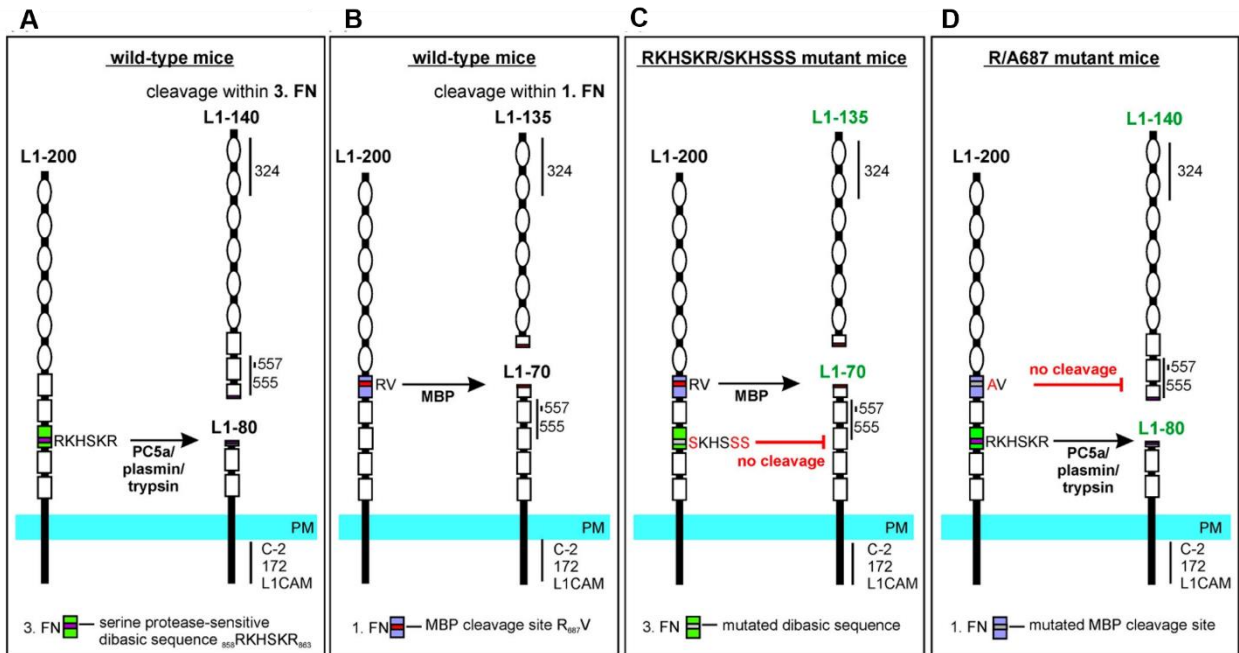


Figure 2. Generation of L1-70 and L1-80 in L1/687 and L1/858-863 mice. Full-length L1 can undergo proteolytical cleavage in its third FNIII domain within the dibasic sequence $^{858}\text{RKHSKR}_{863}$ by PC5a, plasmin or trypsin, leading to the generation of 140 kDa and 80 kDa fragments that contain the epitopes for the L1 antibodies 557, 555, ones for C-2, 172-R and L1CAM, respectively (A). Cleavage in the first FN domain by MBP in the R687V site leads to the generation of 135 kDa and a 70 kDa fragments, containing the epitopes for L1-antibodies 324, 555, 557, C-2, 172-R and L1CAM, respectively (B). Mutations of L1 in the dibasic sequence $^{858}\text{RKHSKR}_{863}$ prevent the generation of L1-80 (C), while mutation of MBP cleavage site in the first FN domain prevents the generation of L1-70 (D) (figure from Kleene et al., 2020).

1.3 The L1-70 fragment

Once generated, L1-70 is transported into the nucleus and suggested to function in nuclear signaling and transcription (Lutz et al., 2014a). L1-70 can be proteolytically processed by cathepsin E, leading to the generation of a sumoylated 30 kDa fragment (Lutz et al., 2014b). L1-70 is transferred to endosomes, released from the endosomes into the cytoplasm and then imported into the nucleus (Lutz et al., 2012). It has been demonstrated that L1-70 is involved not only in the regulation of neuronal migration and neurite outgrowth but also in the regulation of mitochondrial functions (Kraus et al., 2018). Recent studies on L1-deficient and wild-type mice

show that MBP-generated L1-70 is imported into mitochondria where it interacts with the complex I subunit NADH:ubiquinone oxidoreductase core subunit V2 (NDUFV2) and plays important roles in regulation of complex I activity and generation of the mitochondrial membrane potential. Moreover, L1-70 was suggested to be involved in controlling mitochondrial fusion, fission, motility and trafficking (Kraus et al., 2018a). The import of L1-70 is abolished by treatment with anti-TOM70 antibody, meaning that L1-70 can be recognized by TOM70 and imported from the cytoplasm to the mitochondrial intermembrane space via the TOM complex. It has been proposed that the TOM complex also mediates the transport of L1-70 from the intermembrane space to the mitochondrial matrix through the direct or indirect binding with TOM70 (Kraus et al., 2018). The interaction between the L1-70 and NDUFV2 was suggested to be important for the oxidation of NADH by the N module of complex I and given this role of L1-70 it can be assumed that impaired NADH oxidation in the absence of L1-70 may reduce the complex I-mediated transfer of protons from the matrix into the intermembrane space and may thus lead to an impairment of the proton gradient and of the mitochondrial membrane potential. L1-70 also interacts with RhoT1, which is involved in mitochondrial trafficking and control of anterograde transport of mitochondria. It also interacts with the dynamin-related protein 1 (Drp1), which is important for mitochondrial fission. Thus, it is likely that the interaction of L1-70 with RhoT1 and Drp1 at the outer surface of mitochondria leads to an enhancement of motility and to a reduction of fission, and that lack of L1-70 reduces motility and enhances fission and fragmentation, thereby decreasing the fusion of mitochondria (Kraus et al., 2018).

1.4 L1 syndrome and L1 mutant models

Mutations in the L1 gene on the X chromosome have been related to a rare genetic disease called L1 syndrome, which affect 1:30,000 newborn males. It comprises a spectrum of X-linked disorders, such as hydrocephalus with stenosis of the Sylvius aqueduct, mental retardation, aphasia, spastic paraplegia, adducted thumbs, complicated hereditary spastic paraplegia, and agenesis of the corpus callosum (Basel-Vanagaite et al., 2006). Missense mutations of L1 represent the largest group of mutations that can cause the L1-syndrome and they can affect either the extracellular domain, resulting in a more severe clinical phenotype, or the cytoplasmatic part (Schäfer and Altevogt, 2010). Mutations that affect the extracellular domain of

L1 induce structural and functional changes of important amino acid residues that are key players for molecular interactions and intracellular trafficking (Loers et al., 2021, Hortsch et al., 2014, Kenwrick et al., 2000). Dysfunctions of L1 are also associated with other neural disorders, such as fetal alcohol syndrome, and schizophrenia as well as Alzheimer's disease (AD), Parkinson, Huntington, and Hirschsprung diseases (Hortsch et al., 2014, Kenwrick et al., 2000, Schäfer and Altevogt, 2010).

In order to further understand the molecular mechanisms that underlie these vast spectra of X-linked disorders, several L1 mutant murine models have been used so far.

L1-deficient mice (L1-ko): these mice present several morphological features that characterize also the L1-syndrome in humans. L1-ko mice are smaller compared to their wild-type littermates, they present a mild to severe hydrocephalus and an enlarged skull due to stenosis of the aqueduct of Sylvius (Rolf et al., 2001). Genetic ablation of L1 leads to a severe impairment of mitochondrial activity (Kraus et al., 2018a). Mitochondria from L1-ko cerebellar primary cells show a lower membrane potential compared to mitochondria from the wild-type cells, as well as reduced complex I activity and impaired fusion and fission mechanisms (Kraus et al., 2018a). Absence of L1 also leads to impaired mitochondria motility: mitochondria from L1-ko mice move slower compared to the wild-type mitochondria, and they move more retrogradely than anterogradely (Kraus et al., 2018a). L1-deficient mice also exhibit impaired motor performance and motor learning in the rotarod test (Kraus et al., 2018a).

L1/687 and L1/858-863 mice: Gene-edited L1/687 and L1/858-863 mice were shown to express full-length L1, but no or only low levels of L1-70. Neurons from these mutant mice exhibited reduced neurite outgrowth and neuronal survival and migration when the cells are stimulated with antibody 557 or L1 agonists but were not affected without stimulation (Congiu et al., 2022). Interestingly, in contrast to L1-ko males, the transgenic males from these lines are fertile and thus females from the L1/687 and L1/858-863 lines can be transgenic.

L1-201: This novel L1-syndrome mouse line has a mutation of aspartic acid at position 201 in the extracellular part of L1 (p.D201N, called L1-201) that displays a cell surface-exposed L1 accessible to L1 mimetics. The percentage of transgenic newborn is usually very low, suggesting that this mutation leads to premature death already in the embryonic state. When mice survive,

transgenic L1-201 male mice show a reduced body weight (20-30% less) compared to their wild-type littermates in the first weeks of life. Like L1-ko males, the L1-201 male mice are infertile. Histological characterization of L1-201 male mice show reduced ventricle size and reduction of corpus callosum thickness, as well as several neurological deficits that are similar to the ones of the L1-syndrome in humans. Neuronal migration, neurite outgrowth and neuronal survival, as well as Schwann cells process formation are impaired in L1-201 cells as observed also in L1-ko cells (Loers et al., 2021).

1.5 L1-agonist compounds

Interestingly, all these cellular mechanisms are rescued by L1 mimetics. Eight small molecule L1 agonists (duloxetine, tacrine, crotamiton, ethinyl estradiol, phenelzine sulfate, honokiol, trimebutine maleate and piceid) were identified and used to trigger L1-mediated functions in mice both in vitro and vivo. It has been found that these compounds are able to enhance neuronal migration and survival, neurite outgrowth of cerebellar and cortical neurons and spinal motor neurons, plus process formation and migration of Schwann cells (Kataria et al., 2016). Among them, duloxetine and tacrine were taken more into account due to their stronger effect in triggering L1-functions, not only in mice but also in zebrafish where tacrine promotes functional recovery after spinal cord injury (Sahu et al., 2018).

Duloxetine is a serotonin and norepinephrine reuptake inhibitor, largely used in the treatment of major depressive disorder, anxiety, neuropathic pain, and stress urinary incontinence (Ball et al., 2013, Li et al., 2013). This compound also modulates N-methyl-D-aspartate (NMDA) receptors (Calabrese et al., 2012), that work together with L1 through the NMDA receptor-adhesion protein signaling complexes and modulate synaptic plasticity (Frederiske et al., 2016).

Tacrine is a choline esterase inhibitor that increases acetylcholine levels in cholinergic synapses, preventing amyloid beta (A β) aggregation. It also acts as antagonist of NMDA receptor, block sodium and potassium channels, it also modulates monoamine uptake and release of serotonin, noradrenaline and dopamine. It is one of the first drugs of choice for the treatment of Alzheimer`s disease and dementia (Bautista-Aguilera et al., 2021).

The functional topography of the L1 molecule can explain the ability of L1 mimetics to restore impaired functions caused by L1 mutation. In this L1-201 mutant model, the protein is expressed at the cell surface and the mutation is located less close to the signal transducing active site (Loers et al., 2021). This allows L1 mimetics to have access to the protein and then functionally normalize impaired functions.

Finally, behavioral analysis of this model revealed an increased locomotor activity and neuronal deficits evaluated by neurological deficit score test (Loers et al., 2021). It has been shown that L1 is involved in the regulation of mitochondrial activity and suggested that this function is performed by L1-70 (Kraus et al., 2018a). What is still not known is how L1-70 or the different mutations of L1 influence mitochondrial dynamic and functions and the final proof that L1-70 modulates mitochondrial functions.

1.6 Mitochondria

1.6.1 Structure and functions

Mitochondria are highly dynamic organelles that play a pivotal role in the regulation of energy metabolism, signaling pathways, cell differentiation, cell proliferation and cell death (Kabekkodu et al., 2015). They undergo coordinated cycles of fission and fusion, in order to maintain their shape, distribution and size (Tilokani et al., 2018). Mitochondria are made up of a double membrane, the outer membrane (OMM) which forms a semi-permeable barrier to the cytosol and the inner membrane (IMM) with its typical invaginations, so called cristae, which separates the intermembrane space from the matrix. The proton gradient between the intermembrane space (pH 7.2-7.4) and the matrix (pH 7.9-8.0) drives the adenosine triphosphate (ATP) production by the ATP synthase in the membranes of the cristae (Taanman, 1999, Friedman and Nunnari, 2014). Mitochondrial membranes are mainly composed of phosphatidylcholine and phosphoethanolamine but also contain minor amounts of other phospholipids like phosphatidic acid and cardiolipin, which play a major role in membrane remodelling.

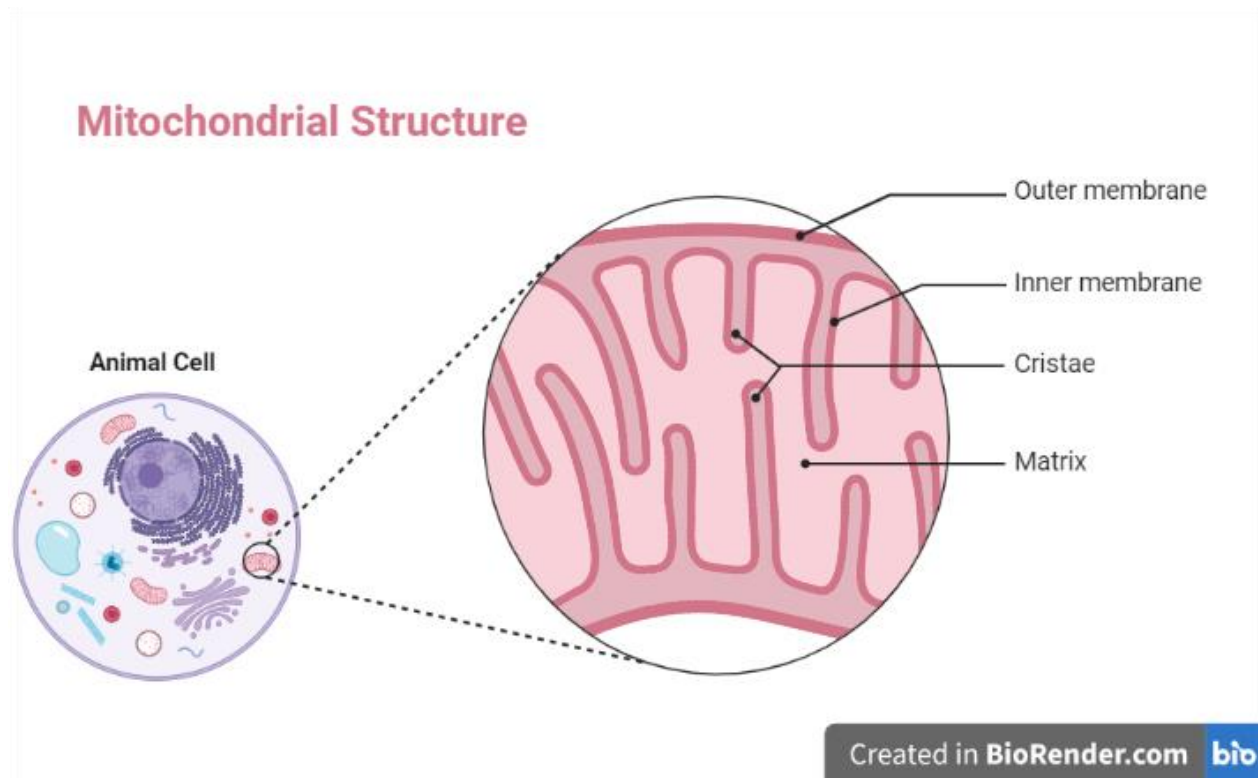


Figure 3. Mitochondrial structure. Mitochondria consist of a double membrane: an outer membrane in contact with the cytosol and an inner membrane with its characteristic invaginations so called cristae, containing the matrix with the mtDNA and where the ATP synthase machinery is located. The space between the membrane is the intermembrane space.

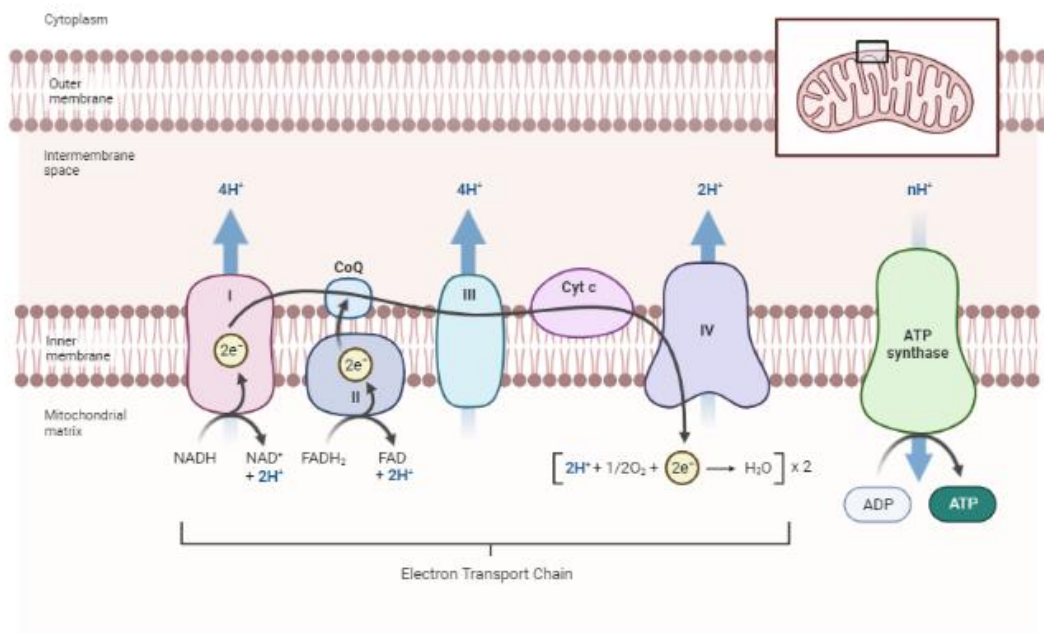
The inner membrane cristae are well known to be the location of the respiratory complexes and the F_1F_0 -ATP synthase, transporters and channels for metabolites and ions in both mitochondrial membranes, and numerous metabolic pathways are mainly localized in the matrix and inner membrane (Van der Blik et al., 2017). The mitochondrial matrix contains also a complete genetic system, including the mitochondrial genome, which encodes for inner membrane's proteins, numerous factors for maintaining, regulating, and expressing the mitochondrial genome, and the mitochondrial ribosomes (Ott et al., 2016). Mitochondrial proteins are mainly synthesized in the cytosol and from there they reach their final destination through the translocase of the outer mitochondrial membrane (TOM) complex (Schmidt et al., 2010). Four main pathways direct proteins to their intramitochondrial destination: the presequence pathway to the matrix and inner membrane, the carrier protein pathway to the inner membrane, the redox-regulated import

pathway into the intermembrane space, and the β -barrel pathway into the outer membrane (Chacinska et al., 2009). The presequence pathway leads proteins to the matrix by the presequence translocase of the inner membrane (TIM23) complex and the presequence translocase-associated motor. Then, the presequences are removed by mitochondrial processing peptidase. The TIM23 complex also performs the task of releasing some proteins into the lipid phase of the inner membrane. The mitochondrial intermembrane space assembly (MIA) machinery drives the import and oxidative folding of many intermembrane space proteins. From the intermembrane space the Tim9–Tim10 chaperone complex transfers hydrophobic precursor proteins, such as β -barrel proteins of the outer membrane, to the sorting and assembly machinery complex, while inner membrane carrier proteins are transferred through the carrier pathway to the TIM22 complex. The precursors of α -helical outer membrane proteins do not use the TOM channel but are inserted into the membrane by different pathways, some involving mitochondrial import 1. A few proteins are synthesized on matrix ribosomes and are exported into the inner membrane by the oxidase assembly machinery (Schmidt et al., 2010).

1.6.2 Mitochondrial electron transport chain and reactive oxygen species generation

Major metabolic pathways involve the energy metabolism, such as the tricarboxylic acid cycle (TCA) also known as citric acid cycle or Krebs cycle, and the metabolism of amino acids, lipids, and nucleotides. The respiratory chain, which plays a key role in the regulation of energy metabolism, consists of two electron transport pathways: complex I/III/IV, with NADH as the substrate and complex II/III/IV, with succinic acid as the substrate (Zhao et al., 2019). Electrons derived from oxidation of metabolites are fed into the respiratory chain that generates an electrochemical gradient by transferring protons from the matrix to the intern membrane space side. The proton gradient is then used to drive ATP synthesis by the F_1F_0 -ATP synthase (complex V), as well as the import of precursor proteins and the transfer of some metabolites across the inner membrane (Pfanner et al., 2019). Some electrons are directly transferred to O_2 to generate reactive oxygen species (ROS). These are signaling molecules that regulate cell proliferation, hypoxia adaptation and cell fate determination as well as cell damage and cell death when their production exceeds (Zhao et al., 2019). The electron transport chain (ETC) is composed of transmembrane protein complexes (I-IV) and the freely mobile electron transfer carriers

ubiquinone and cytochrome c. These elements together with complex V are the main producers of ATP during oxidative phosphorylation (OXPHOS) (Fig. 4).



Created in BioRender.com 

Figure 4. Mitochondrial electron transport chain. The electron transport chain complex consists of four major protein complexes (I-IV) and the ATP synthase (V). Complex I, III and IV generate the electrochemical proton gradient across the intermembrane space that leads to the synthesis of ATP by complex V. Complex I oxidizes NADH to NAD⁺ by transfer of two electrons to ubiquinone, leading to the synthesis of ubiquinol and release of protons into the intermembrane space. Complex II oxidizes succinate to fumarate and reduces ubiquinone to ubiquinol. Complex III catalyzes the oxidation of ubiquinol and reduction of cytochrome c. Complex IV uses electrons from the cytochrome c to generate 2 molecules of water from the molecular oxygen and to create a proton gradient across the inner membrane used then by the complex V (or ATP synthase) to generate ATP from ADP.

The first multisubunit enzyme complex of the ECT is the **Complex I**. It is also called NADH-ubiquinone oxidoreductase and its main role is to transfer electrons from matrix NADH to

ubiquinone. Complex I has a matrix arm with seven core subunits (NDUFS1, NDUFS2, NDUFS3, NDUFS7, NDUFS8, NDUFV1 and NDUFV2) that contain several co-factors such as flavin mononucleotide (FMN) and a membrane arm containing seven hydrophobic subunits (ND1-6 and ND4L), all of which are encoded by the mitochondrial genome (Zhao et al., 2019). Complex I oxidizes NADH to NAD⁺ by transfer of two electrons from NADH to ubiquinone. In this reaction, ubiquinol is generated and protons (H⁺) are transported across the inner mitochondrial membrane to the intermembrane space (Kadenbach et al., 2012).

Complex II, or succinate dehydrogenase, is a component of the Krebs cycle as well as the ETC, and it acts like a link between metabolism and OXPHOS. It consists of four subunits that catalyze the oxidation of succinate to fumarate and reduce FAD to FADH₂ by donating electrons via FeS clusters to CoQ that is then reduced to QH₂. In this second step, no translocation of protons occurs (Iverson et al., 2013).

Complex III, or cytochrome bc₁ complex or CoQ-cytochrome c reductase, is the mediator of the electrons transfer to cytochrome c from QH₂. QH₂ is then oxidized to ubisemiquinone (QH⁻) after transferring an electron to the (2Fe-2S) cluster and two protons are concurrently released into the mitochondrial intermembrane space. The electrons are transferred to cytochrome c via cytochromes b and c1 of complex III (Rich and Maréchal, 2010).

Complex IV, also known as cytochrome c oxidase, transfers electrons from cytochrome c to the terminal electron acceptor O₂ to generate H₂O. Four electrons from cytochrome c are also transferred to bind dioxygen, and eight protons in total are removed from the matrix, four of which are used to create the two water molecules and the other four are transferred across the membrane to the inner membrane (Zhao et al., 2019).

Finally, **complex V**, or F₁F₀-ATP synthase, consist of two functional domains: F₀, which transfers the stored energy created by the proton gradient, and F₁ which receives the protons and mediates the conformational change in complex V, leading to the phosphorylation of ADP to ATP (Jonckheere et al., 2012).

Under physiological conditions, 0.2-2% of the electrons in the ETC do not follow the normal transfer order but instead directly leak out of the ETC and interact with oxygen to produce superoxide anion or hydrogen peroxide (Turrens JF., 2003, Cadenas et al., 2000). Most

intracellular ROS are derived from superoxide anion ($O_2^{\cdot-}$), which is generated by the one electron reduction of O_2 . Superoxide is converted to hydrogen peroxide (H_2O_2) by superoxide dismutases (SODs) (Sena and Chandel., 2012).

Mitochondrial ROS are biologically important in a variety of physiological systems, including adaptation to hypoxia, regulation of autophagy, immunity, differentiation, and regulation of longevity. The major determinant of ROS production is the redox state of the ETC and the proton motive force (pmf), composed of an electrical gradient (ψ , mitochondrial membrane potential) and chemical gradient (pH) across the inner mitochondrial membrane. The proton motive force is generated as protons are extruded out of the matrix into the intermembrane space by complexes I, III and IV as electrons are transferred through the ETC. An increase in ROS production is observed when pmf increases (Echtay et al., 2002). Interestingly, ROS have been shown to be required for both AMP-activated protein kinase (AMPK) activation and endocytosis of the α subunit of the Na/K ATPase under hypoxia (Gusarova et al., 2011). AMPK is classically activated by an increase in the intracellular AMP/ATP ratio (Emerling et al., 2009), but under hypoxic condition, AMPK is activated by ROS regulation of Ca^{2+} /calmodulin-dependent kinase (CaMKK) (Mungai et al., 2011). ROS have also been demonstrated to regulate synaptic plasticity-related signaling molecules, receptors, and channels, including N-methyl-d-aspartate receptor, Ca^{2+} channel, Ca^{2+} kinase II (CaMKII), extracellular signal-regulated kinase and cyclic adenosine monophosphate (cAMP) response element binding protein (CREB) (Zhao et al., 2019). ROS are implicated in a variety of diseases including diabetes, cancer, inflammatory disorders, and neurodegeneration through lipid peroxidation, DNA damage, protein oxidation, irreversible impairment of mitochondria, insufficient ATP generation and cell death (Orrenius et al., 2007).

1.6.3 AMPK and mitochondria

AMPK is a well-known energy sensor of eukaryotic cells. It is activated under condition of low energy, when ATP levels decrease, and it phosphorylates specific enzymes to increase ATP generation and decrease ATP consumption (Herzig and Shaw., 2018). Several studies focused on the role of AMPK in promoting mitochondrial health and they have demonstrated its involvement in regulating mitochondrial homeostasis (Herzig and Shaw., 2018). When cells use up almost all the ATP for cellular processes, energy saving mechanisms are activated, including the conversion

of ATP into ADP, which can be further converted to AMP. Furthermore, emergency measures have to be taken to restore the cellular energy supply, such as increasing nutrient intake, activating alternative energy-producing pathways or turning over existing macromolecules into nutrients (Herzig and Shaw., 2018).

AMPK is activated by an allosteric mechanism that stimulates its kinase activity. Once activated, AMPK redirects metabolism towards increased catabolism and decreased anabolism through the phosphorylation of key proteins in multiple pathways, including mTOR complex 1 (mTORC1), lipid homeostasis, glycolysis, and mitochondrial homeostasis. In addition to directly regulating key enzymes involved in these pathways, AMPK also rewires cellular metabolism in a prolonged manner by targeting transcriptional regulators (Herzig and Shaw., 2018).

AMPK is a heterotrimeric complex with two catalytic α - subunits, two β -subunits and three γ -subunits (Fig. 5) (Ross et al., 2016). γ -subunit stimulates AMPK activity by binding adenine nucleotides and allowing AMPK to respond to changes in the ATP-AMP ratio (Xiao et al., 2007). AMP exercises its function through three mechanisms: by stimulating phosphorylation of Thr172, by inhibiting the dephosphorylation of Thr172 and by inducing allosteric activation of AMPK already phosphorylated on Thr172 (Gowans et al., 2013, Suter et al., 2006).

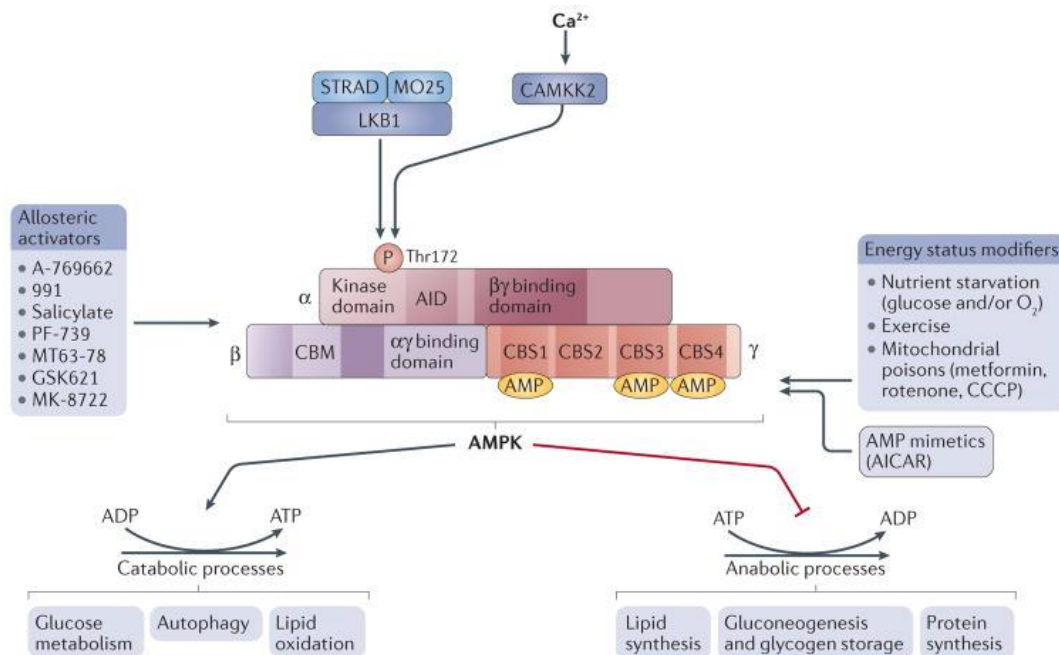


Figure 5. AMPK structure and activation. Domain structure of the AMP-activated protein kinase (AMPK) trimer, showing the α -, β - and γ -subunits with their respective domains. The upstream kinases calcium/calmodulin-dependent protein kinase kinase 2 (CAMKK2) and liver kinase B1 (LKB1) are shown above the AMPK complex. LKB1 is a heterotrimer composed of LKB1, STe20-related adaptor and armadillo repeat scaffolding-like protein (MO). CAMKK2 is activated by intracellular calcium. Several factors lead to AMPK activation, such as mitochondrial poisons and oxygen or glucose starvation, as well as exercise. The effect of AMPK activation is to rewire metabolism to decrease anabolic processes (that is, ATP consumption) and increase catabolism (that is, ATP production) (figure modified from Herzig and Shaw, 2018).

More studies are now focused on AMPK and its role in regulating mitochondrial activity. It has been shown that the AMPK complexes are able to control mitochondrial biogenesis and shape as well as autophagy and mitophagy processes (Herzig and Shaw, 2018). AMPK directly phosphorylates mitochondrial fission factor (MFF) to regulate mitochondrial fission through DRP1 and activates the Unc-51-like kinase 1, the upstream kinase in autophagy and mitophagy (Otera et al., 2010). AMPK also activates peroxisome proliferator-activated receptor- γ (PPAR γ) co-activator 1 α (PGC1 α), which activates mitochondrial biogenesis genes through interaction with PPAR γ or estrogen-related receptors (ERRs) (Wuz et al., 1999, Eichner and Giguère., 2011).

1.6.4 Mitochondrial trafficking

In neurons, regions with a high energy demand, such as synapses and active growth cones, contain a higher percentage of mitochondria. In axons and dendrites, around the 10%-40% of mitochondria are in motion, while 60%-90% are stationary (Wang and Schwarz., 2003). The moving organelles can move bidirectionally: anterogradely (away from the cell body) and retrogradely (toward the cell body). It has been hypothesized that anterograde movements are associated with a healthy status of mitochondria, while retrograde movements are representative of older, damaged mitochondria, with an altered membrane potential (Schwarz, 2013).

Transport of mitochondria is controlled by a motor/ adaptor complex which consists of three proteins: kinesin-1 (or kinesin heavy chain or Hif5), that regulates anterograde movements, Miro (RhoT1 and RhoT2) an outer membrane protein, and Milton (TRAK1 and TRAK2) that links kinesin and Miro. The other component of this complex is dynein that interacts with Miro and Milton and regulates retrograde movements (Schwarz, 2013). Several mechanisms are involved in regulating trafficking of mitochondria. For example, cytosolic Ca^{2+} levels are responsible for activation/deactivation of the motor machine: when Ca^{2+} concentration decreases, Miro binds Milton and activates the motor complex, while higher Ca^{2+} levels lead to a rearrangement of the complex such that the motor domain of kinesin directly binds to Miro and is blocked from binding to microtubules (Wang and Schwarz 2009). The PTEN-induced kinase 1 (PINK1)/ Parkin pathway causes an irreversible dissociation of the motors from the mitochondrial surface by causing Miro to be degraded. Miro degradation by the proteasome is triggered by PINK1 phosphorylation of Miro and Parkin ubiquitinylation of Miro (Wang et al. 2011). Finally, syntaphilin, which is bounded to the OMM of mitochondria and contains a microtubule-binding domain, is the main responsible of the stationary pool of mitochondria in axons (Kang et al., 2008).

1.7 AIMS OF THE THESIS

Given the role of L1 and L1-70 in regulating mitochondrial dynamics and functions (Kraus et al., 2018a), and given also its involvement in influencing motor and cognitive performances in mice (Kraus et al., 2018a), the aims of my project were 1. to evaluate mitochondrial deficits, 2. to characterize morphological features and 3. to determine the behavioral phenotype in the L1-mutant mouse models L1-201, L1/858-863 and L1/687.

These aims were addressed by:

1. Evaluation of mitochondrial metabolism and oxidative status through measurement of complex I activity, ATP levels, mitochondrial membrane potential, mitochondrial motility, ROS production and phosphorylation status of AMPK in both cells and tissue. Also, evaluation of the potential effect of L1 agonist compounds duloxetine and tacrine in rescuing mitochondrial deficits.
2. Analysis of morphological differences of brain structures, morphology of neurons from the cortex and spine type and spine density, using different tissue-staining methods.
3. Study of the functional role of L1-70 in behavior, through characterization of motor, cognitive and social performances of the L1-70 lacking mouse line L1/858-863 by using behavioral tests.

2. MATERIALS AND METHODS

2.1 Animals

Animals were housed at standard laboratory conditions with food and water supply ad libitum and with an artificial 12 h light/dark cycle. All procedures used were approved by the responsible authorities of the State of Hamburg (Behörde für Wissenschaft und Gesundheit, Amt für Gesundheit und Verbraucherschutz, Lebensmittelsicherheit und Veterinärmedizin; animal permit numbers ORG_679 Morph, ORG_1022, N118/0095, N116/2021 and N 073/2020) and in agreement to the guidelines set by the European Union and Germany. The experiments were conducted and evaluated following the ARRIVE guidelines for animal research (Kilkenny et al., 2010).

2.1.1 L1-deficient mice

L1-deficient mice (L1^{-y}) were generated by inserting a tetracycline controlled transactivator inside of the second exon of the X chromosome-linked L1 gene (Rolf et al., 2001). Heterozygous females (L1^{+/-}) and wild-type males 129SVJ background were used for breeding and obtaining L1^{-y} male mice and L1^{+y} male age-matched littermates (Guseva et al., 2009).

2.1.2 L1-201 mice

For generation of L1-201 mutant mice, the wild-type L1 sequence of mouse X-chromosome (NC_000086.7; Gene ID: 16728) was used for designing and screening of the zinc finger nuclease pair ZNF1/ZNF2 (Sigma-Aldrich) binding at position 73,864,197-73,864,216 and 73,864,167-73,864,194 and close to the codon for aspartic acid 201 (D201) at position 73,864,249. The codon GAC was replaced by AAC which codes for asparagine (N). The G to A exchange at Position 73,864,249 disrupts the restriction site for DdeI and corresponds to a human missense mutation. The zinc finger nuclease plasmids were linearized, purified, and subjected to reverse transcription. The transcripts and a 1655 bp donor sequence comprising sequences from 73,864,604 to 73,863,418 and carrying the ex-changed codon in a pUC-vector (Genewiz, Leipzig, Germany) were injected under constant pressure into the pronuclei of one-cell-stage embryos derived from C57BL6/JxCBA mice and im-planted into foster mothers according to standard procedures. The correct insertion of the mutation into the genomic DNA was confirmed by sequencing. Mice used were backcrossed to 129 background for 5-8 generations.

For genotyping, mouse tail biopsies were processed using the Phire Animal Tissue Direct PCR Kit (Thermo Fisher Scientific) according to the manufacturer's instructions. Primers L1_202_FW (5'- TAGGATCTACTGGATGAACAGCA-3'; 73,864,424-73,864,446) and L1_202_Rev (5'- AAAAC TTCTGGGACTTACTGGG-3'; 73,864,141-73,864,162) were used for amplification of a 306 bp region according to the following program: 98°C for 5 minutes; 35 cycles: 98°C for 10 seconds, 60°C for 45 seconds and 72°C for 20 seconds; 72°C for 7 minutes; 4°C until further use. The amplification product was digested with DdeI (New England Biolabs, Frankfurt am Main, Germany) in CutSmart buffer (New England Biolabs) at 37°C for 3 hours. The 306 bp amplicon from wild-type mice was cleaved into 194 and 112 bp products and visualized on a 3% agarose gel stained with ethidium bromide.

2.1.3 L1/858-863 mice

For the generation of mice expressing L1 with the RKHSKR/SKHSSS mutation, the wild-type L1 sequence on mouse X chromosome (NC_000086.7; Gene ID: 16728) was used for the design and screening of suitable zinc finger nuclease pairs (Sigma-Aldrich, Customer & Sales Services), which were found to bind at positions 73,857,884–73,857,870 (zinc finger nuclease 1) and 73,857,863–73,857,845 (zinc finger nuclease 2) and close to the codons coding for 858RKHSKR863 at positions 73,857,812–73,857,795. The gene sequence AGAAAGCACAGCAAGAGG (coding for 858RKHSKR863) was replaced by AGCAAGCACAGCTCGAGC (coding for SKHSSS) generating thereby a restriction site for *Ava*I (Kleene et al., 2021). The zinc finger nuclease transcripts were transcribed according to the manufacturer's instructions (Sigma-Aldrich) after linearization using the MessageMaxT7 ARCA-capped Transcription Kit with subsequent tailing with the Poly (A) Polymerase Tailing Kit (both Epicentre, Biozym, Hessisch Oldendorf, Germany). Transcripts purified using the MEGAClear™ Transcription Clean-Up Kit (AM1908, ThermoFisher Scientific, Darmstadt, Germany) and an 1,800 bp donor sequence (73,858,666–73,856,995) carrying the exchanged codons in a pUC vector (Genewiz, Leipzig, Germany) were injected under constant pressure into the pronuclei of one-cell-stage embryos. Mice were then backcrossed onto C57Bl6 background.

For genotyping the primers 25 nM of L1-DD fw, and 25 nM of L1-DD and rev were used (sequence in section '2. 8'). The tubes were incubated in the SimpliAmp Thermal Cycler (Life Technologies) as shown in Table 2.8.

Table 1. PCR cycling scheme for genotyping of L1/858-863 mice.

Step	Temperature	Time	Cycles
Initial denaturation	98°C	3 min	1
Denaturation	98°C	10 s	1
Annealing	60°C	1 min	35
Extension	72°C	20 s	35
Final extension	72°C	1 min	1
Cooling	4°C	∞	1

Following PCR, restriction digestion of the PCR product was performed, preparing a restriction master mix for all samples+1. For one sample the mix contained: 3 µl of Cutsmart Buffer (NEB), 1.8 µl of nuclease free water, and 0.2 µl (2 units) of AclI (NEB) for L1/858-863.

15 µl of the restriction master mix were added to 10 µl of PCR product, mixed, and incubated at 37°C for 3 hours.

Finally, 20 µl of digestion product was loaded into an agarose gel, in the same way as in the genotyping of L1 mice (previous section).

2.1.4 L1/687 mice

For the generation of mice expressing L1 with the R/A867 mutation, a single-guide RNA (sgRNA) was chosen after submitting the targeting region, exon 15 of murine L1, to the CRISPOR design tool (<http://crispor.tefor.net>; Haeussler et al., 2016). The template for transcription with the targeting sequence (GTAAATGGCAGTGACCCGAA) was generated by PCR using Q5™ DNA Polymerase (New England Biolabs, Frankfurt am Main, Germany). Transcription was performed using the HiScribe™ T7 High Yield RNA Synthesis Kit (#E2040S, New England Biolabs) with subsequent purification of the transcript with the

MEGAClear™ Transcription Clean-Up Kit (#AM1908, ThermoFisher Scientific) according to the manufacturer's instructions. A repair oligonucleotide designed to knock-in the p.R682A substitution, a restriction site for screening (AciI) and a further silent mutation for a degenerated PAM sequence had the following sequence: 5'-AGGTGCCAGG AAATCAGACC TCTACTACCCTCAAGCTGTCCCCCTATGTCCACTACACaTTTgcGGTCACTGCCATTAA CAAATATGGTCCTGGAGAACCCAGCCCTGTCTCTGAGACTG-3' (mutations are indicated by small letters). This donor DNA (Sigma-Aldrich) (1 µg/µl), sgRNA (600 ng/µl), and Cas9 protein (Alt-R® S.p. Cas9 Nuclease V3, #1081058, Integrated DNA Technologies (IDT), Leuven, Belgium) (500 ng/µl) in Gibco™ Opti-MEM™ (ThermoFisher Scientific) were used for electroporation into one-cell-stage embryos using the NEPA 21 electroporator (Nepa Gene, Ichikawa-City, Japan; for settings, see Remy et al., 2017). For genotyping of the mutant mouse line expressing the L1 with the R/A687 mutation, primers L1-RA fw (5'-TGAGGACAAGGAAATGGCTCC-3') and L1-RA rev (5'-GCTGTAGCAAGGACAAGGAAC-3') were used with the following program: 98°C for 5 min; 35 cycles: 98°C for 10 s, 56°C for 45 s, and 72°C for 20 s; 72°C for 7 min; 4°C until further use. The amplification product was digested with AciI (New England Biolabs) in CutSmart buffer (New England Biolabs) at 37°C for 2 hr. The 400 bp amplicon of mutant mice was cleaved into 107 bp and 293 bp products.

The PCR and digestion products were visualized on 3% agarose gels stained with ethidium bromide.

2.2 Suppliers of chemical, kits, reagents and laboratory equipment

All chemicals, reagents and kits were purchased from the following companies: Abcam (Cambridge, UK), Abnova (Taipei, Taiwan), Addgene Inc. (Teddington, UK), Applied Biosystems (Foster City, CA, USA), BioLegend (Fell, Germany), BIOMOL (Hamburg, Germany), Bio-Rad Laboratories (Munich, Germany), Bio&SELL, Nürnberg, Germany), Biozol (Eching, Germany), Carl Roth (Karlsruhe, Germany), Corning (Wiesbaden, Germany), Creative BioMart (Shirely, NY, USA), Dako/Agilent Technologies (Santa Clara, CA, USA), Dianova (Hamburg, Germany), DWK Life Sciences (Millville, NJ USA), Enzo Life Sciences (Farmingdale, NY, USA), Eppendorf AG (Hamburg, Germany), GenWay Biotech (San Diego,

CA, USA), Hamilton Company (Reno, NE, USA), INVIVO BioTech Service (Hennigsdorf, Germany), Jackson ImmunoResearch (West Grove, PA, UK), LifeTechnologies (Darmstadt, Germany), Macherey-Nagel (Düren, Germany), Merck Chemicals (Darmstadt, Germany), Mundipharma (Limburg, Germany), New England Biolabs (Ipswich, MA, USA), Nunc (Roskilde, Denmark), PAA Laboratories (Cölbe, Germany), PAN Biotech (Aidenbach, Germany), Santa Cruz Biotechnologies (Dallas, TX, USA), Roche Diagnostics (Mannheim, Germany), SERVA Electrophoresis (Heidelberg, Germany), Schafer-N (Copenhagen, Denmark), Sigma-Aldrich (Taufkirchen, Germany), T. H. Geyer (Hamburg, Germany), Thermo Fisher Scientific (Waltham, MA, USA), VWR International GmbH (Darmstadt, Germany), Wheaton (Millville, USA).

2.3 Solutions and buffers

50xTAE	2 M Tris 1 M acetic acid 50 mM EDTA pH 8.0
Agarose gel solution with Roti-GelStain	3% agarose standard (Carl Roth) 1xTAE 0.05 µl/ml Roti-GelStain (Carl Roth)
DNA Ladders	1 kb Plus DNA Ladder (Thermo Fisher Scientific) 100 bp Plus DNA Ladder (Thermo Fisher Scientific)
Protease inhibitor solution (Complete, EDTA free tablets) (mitochondrial lysates)	1 tablet in 2 ml phosphate buffered saline (PBS) (25x stock)
Mitochondria Isolation Kit for Tissue	Thermo Fisher Scientific 89801
MitoTracker stock solution (staining of mitochondria)	MitoTracker® Red CMXRos 1 mM in dimethyl sulfoxide (DMSO)
Formaldehyde (PFA) solution (fixation)	4% paraformaldehyde (PFA) in dH ₂ O
Poly-L-lysine (PLL) (coating solution)	0.01% in dH ₂ O
HBSS (cell washing)	Hank's balanced salt solution without Ca ²⁺ and Mg ²⁺ containing 0.35 g/l NaHCO ₃ and

	phenol red
HBSS (cell washing, without phenol red)	Hank's balanced salt solution without Ca ²⁺ and Mg ²⁺ containing 0.35 g/l NaHCO ₃
Medium X-1 (cerebellar granule cells)	Neurobasal A containing: 1% penicillin/streptomycin 0.1% BSA 10 µg/ml insulin 4 nM L-thyroxine 100 µg/ml transferrin holo 30 nM sodium-selenite 0.5x B27 supplement
DNase I solution (cerebellar granule cells)	10 mg DNase I 50 mg glucose 20 ml Neurobasal A
Trypsin/DNase solution (cerebellar granule cells)	0.3 g trypsin 30 mg DNase I 300 µl 80 mM magnesium chloride (MgCl ₂) 30 ml HBSS
BacTiter-Glo® 2.0 Cell Viability Assay	Promega, Walldorf, Germany; catalog #G8230
ROS-sensitive fluorescent probe 2',7'-dichlorofluorescein diacetate (DCFH-DA)	Biomol, Hamburg, Germany
JC-1 iodide (1,1',3,3'-tetraethyl-5,5',6,6'-tetrachloroimidacarbocyanine iodide)	Santa Cruz Biotechnology, Heidelberg, Germany; catalog #sc-364116
MitoCheck® Mitochondrial Complex I Activity Assay Kit	Cayman Chemical, Ann Arbor, MA, USA; catalog #700930
Tris-buffered saline (TBS) 10x stock (Western Blotting)	10 mM Tris-HCl 150 mM NaCl pH 7.5
TBS-T (Western Blotting)	0.1% Tween-20 in 1x TBS

Blotting buffer (Western Blotting)	25 mM Tris 192 mM glycine 0.01% SDS 20% methanol
Blocking buffer (Western Blotting)	4% skim milk powder in 1x TBS-T
RIPA Buffer (pH 7.4)	50 mM Tris 180 mM NaCl 1 mM Na ₄ P ₂ O ₇ NP-40
Antibody dilution buffer (Western Blotting)	4% skim milk powder in 1x TBS-T
557 antibody	50 µg/ml for stimulation of cultured cells
Duloxetine	100 nM for stimulation of cultured cells
Tacrine	100 nM for stimulation of cultured cells
FD Rapid GolgiStain Kit	FD NeuroTechnologies, INC, catalog #PK401
Gelatin-coated microscope slides	Cat. #PO101
Eukitt® Quick-Hardening Mounting medium	Fluka, Buchs, Switzerland
Malondialdehyde (MDA)	Sigma-Aldrich, Lot# BCCD7045
2-Thiobarbituric acid (TBARS)	Sigma-Aldrich, Lot# BCBS4013V
Butylhydroxytoluol (BHT)	100 mM, Sigma-Aldrich, Lot# BCCF3416

2.4 Antibodies

Antigen	Host	Company	Catalog number	Dilution/ Concentration
L1CAM (C-20)	goat	Santa Cruz Biotechnology	sc-1508	WB: 1:1,000
L1CAM (C-2)	mouse	Santa Cruz Biotechnology	sc-514360	WB: 1:1,000
TOM40	goat	Santa Cruz Biotechnology	sc-11025	blocking assay: 30 µg/ml
β-actin	rabbit	Millipore Sigma	A2066	WB: 1:1,000
AMPKalpha	rabbit	Cell Signaling	Lot: 4 2532	WB: 1:1,000
phosphoAMPKalpha	rabbit	Cell Signaling	Lot: 8 2535S	WB: 1:1,000
anti-mouse, HRP	goat	Jackson ImmunoResearch	Lot: D00120- C4	WB: 1:10,000
anti-mouse, HRP	goat	Jackson ImmunoResearch	Lot: C91217-03	WB: 1:10,000

2.5 Cell culture methods and assays

2.5.1 Preparation of coverslips

For performing immunocytochemistry of cultured cerebellar primary granule cells, the glass coverslips needed to be coated with PLL, as follows: Glass coverslips were placed inside an Erlenmeyer flask, immersed in 3 M hydrochloric acid solution, at room temperature with gentle shaking. The coverslips were then washed twice with ddH₂O, immersed in acetone for 3 h at room temperature with gentle shaking, and washed 5 times with ddH₂O. The coverslips were then washed twice for 10 min with absolute ethanol. The Erlenmeyer flask containing the coverslips was then heated up to 160°C for 2 h. From this point the steps were performed under sterile conditions, the coverslips were cooled down at room temperature, and coated with sterile 0.01% PLL in ddH₂O overnight at 4°C with gentle shaking. The coverslips were washed twice with autoclaved ddH₂O and dried under the hood at room temperature. Finally, they were stored in a sterile 50 ml Falcon tube until use.

2.5.2 Culture of mouse primary cerebellar granule cells

In order to culture cerebellar granule cells, 6 to 8-day-old wild-type, L1-ko, L1-201, L1/867 or L1/858-863 mutant mice were used. The mice were sacrificed by decapitation, and using clean and sterilized dissection material (scissors, forceps and tweezers), the cerebella were extracted and placed inside of a petri dish containing ice-cold HBSS. Under the stereomicroscope, the cerebella were cleaned from blood vessels and meninges and placed into a new petri dish containing ice-cold HBSS. Each cerebellum was cut into 3 pieces and placed inside of a 15 ml Falcon tube and washed using 5 ml of ice-cold HBSS/ 3 cerebella. The HBSS was discarded, and 1 ml/ 3 cerebella of trypsin/DNase solution was added to the tube, which was incubated for 15 min at room temperature. The trypsin/DNase solution was discarded, the cerebella were washed 3 times using 5 ml/3 cerebella of ice-cold HBSS, and 1 ml/ 3 cerebella of DNase solution was added to the tube. The cerebella were then disrupted using 3 glass Pasteur pipettes with rounded tip, from wider to thinner diameter, till obtaining a single cell suspension. The cells were then centrifuged for 15 min at 1,000 x g at 4°C. The cell pellet was then suspended in medium X-1 without serum if cultured for 1-2 days, or with medium containing 5% fetal horse serum if cultured for a longer time.

To determine the cell number under the microscope using a glass Neubauer chamber 10 μl of the cell suspension were mixed 1:1 with 0.4% trypan blue solution. The cells were then diluted to a density of $1\text{-}2 \times 10^6$ cells/ml for all the experiments, seeded on PLL-coated 6-well-plates or glass coverslips, and cultured for at least 24 h at 37°C , in 5% CO_2 and in 90% relative humidity.

2.5.3 Isolation of mitochondrial fractions for import and enzymatic assays

Mitochondria were isolated from wild-type and L1-201 or L1/858-863 mutant mouse brains using male mice at the age of 7 days or two to six months by the Mitochondria Isolation Kit for Tissue (ThermoFisher Scientific) according to manufacturer's instructions. All steps were performed on ice or at 4°C . Brains were removed from mice (one brain for each mitochondrial isolation), washed with PBS (without Ca^{2+} and Mg^{2+}), cut into small pieces and homogenized in PBS (without Ca^{2+} and Mg^{2+}). The homogenates were centrifuged at $1,000 \times g$ for 3 min and the supernatant was discarded. The pellet was resuspended in the supplied BSA/Reagent A solution (1,000 μl per brain), mixed for 5 sec and incubated for 2 min on ice. Supplied Reagent B was added (10 μl per brain) and the samples were mixed and incubated for 5 min on ice with mixing every minute. Supplied Reagent C (800 μl per brain) was added and the tube was inverted several times. The samples were centrifuged at $700 \times g$ for 10 min, the pellet was discarded and the supernatant was transferred to a new pre-chilled tube. The supernatant was centrifuged at $8,000 \times g$ for 15 min and the mitochondrial pellet was washed in the supplied Wash Buffer at $12,000 \times g$ for 5 min. After isolation, the mitochondrial pellets were resuspended in PBS (without Ca^{2+} and Mg^{2+}), and used directly for the mitochondrial import assay or they were lysed in the mitochondrial lysis buffer and stored at -20°C .

2.5.4 Determination of the protein concentration

The BCA Protein Assay Reagent Kit (ThermoFisher Scientific) was used to determine the protein concentration of the samples. The assay was performed with 10 μl of the samples (dilution of 1:10 and 1:100 in dH_2O), 10 μl BSA standard solutions (50-1,000 $\mu\text{g/ml}$) and 200 μl of a mixture of Reagent A and Reagent B (50:1). The samples were incubated for 30 min at 37°C and the absorbance was measured at 562 nm with the $\mu\text{Quant}^{\text{TM}}$ microplate spectrophotometer (Biotek, Germany). The concentrations were calculated using the calibration curve of the BSA standard solutions.

2.5.5 Western blot

For identification of proteins, the proteins were transferred from the SDS-PAGE gel into a 0.22 µm or 0.45 µm nitrocellulose membrane (GE Healthcare) using the Mini-Protean II blotting system (Bio-Rad Laboratories GmbH, Germany). The blotting sandwich was prepared as described in the manufacturer's manual. The electrophoretic transfer was performed in blotting buffer at a constant voltage of 90 V for 90 min on ice. The membrane was placed protein-bound site up in glass vessels and incubated in blocking buffer for 1 h at room temperature. The membrane was incubated overnight with an appropriate primary antibody diluted in blocking buffer. The membrane was washed six times for 5 min in TBS-T, incubated for 1 h with an HRP-coupled secondary antibody (diluted 1:10,000 in blocking solution) at room temperature and washed again five times for 5 min in TBS-T. Proteins were detected using the ECL select or ECL prime reagents (GE Healthcare) and the LAS 4000 Mini camera (GE Healthcare, UK).

2.5.6 Schwann cell process formation

Monolayer cultures of dissociated Schwann cells were prepared from dorsal root ganglia and sciatic nerves of 7-day-old wild-type and L1-201 mice. Schwann cell process formation was measured from at least 100 cells per treatment and genotype. Cultures were treated with the L1 mimetic compound duloxetine at 100 nM and L1Fc (as positive control) at 20 µg/ml for 24 hours, fixed with 2.5% glutaraldehyde for 30 minutes and stained with 1% toluidine blue and 1% methylene blue in 1% sodium tetraborate. Duloxetine was chosen since it had been shown to stimulate Schwann cell migration and in vitro myelination of wild-type cells at this concentration (Kataria et al., 2016). The experiment was performed independently three times with two mice per genotype and experiment.

2.6 Mitochondrial motility

Mitochondria were labeled with MitoTracker® Red CMXRos (ThermoFisher Scientific; catalog #M7512). MitoTracker stock solution (1 mM) was diluted to the final concentration of 50 nM in the pre-warmed cerebellar neuron culture medium. Cerebellar granule neurons (density $1-2 \times 10^6$ cells/6-well containing a 20 mm glass coverslip) were cultured for two to three days in medium

as indicated above containing 5% fetal horse serum. Then the medium was replaced with serum-free medium, and cells were incubated with 50 nM MitoTracker for 30 min at 37°C. This solution was then replaced with fresh serum-free medium, and the cells were analyzed at 37°C under 5% CO₂ by time-lapse imaging using an upright Nikon Eclipse Ti microscope (Nikon Instruments, Amsterdam, The Netherlands) combined with spinning disk (Visitron, Puchheim, Germany) live-cell confocal technology (Visitron Systems) and a 100× objective (1.45 aperture). For live cell imaging, a 561 nm argon laser was used at 10% intensity, and images were taken at intervals of 2 s for a duration of 5 min. Videos were acquired using the VisiView software (Visitron Systems). To determine mitochondrial velocity, mobility, and the direction of mitochondrial transport (anterograde or retrograde), we used the kymograph (time space plot) plugin and the velocity tool from ImageJ (https://www.embl.de/eamnet/html/body_kymograph.html; ImageJ Kymograph Analysis handout, Rietdorf and Seitz, 2008, Heidelberg: Homepage of European Advanced Light Microscopy Network). The kymograph represents a time and space plot: the x-axis indicates the distance, and the y-axis shows the time. Vertical lines represent no movement, while diagonal lines show mobile mitochondria. With respect to the position of the cell soma, the direction (right or left) of diagonal lines indicates retrograde or anterograde transport, respectively (Marra et al., 2015). To calculate the motility of moving mitochondria, segmented lines were drawn along the diagonal lines of the kymograph and the velocity tool from ImageJ (Rietdorf and Seitz, 2008) was used for quantification of the motility. Experiments were carried out in duplicates and performed independently three times.

2.6.1 Mitochondrial membrane potential

The dual-emission potential-sensitive probe JC-1 iodide (1,1',3,3'-tetraethyl-5,5',6,6'-tetrachloroimidacarbocyanine iodide; Santa Cruz Biotechnology, Heidelberg, Germany; catalog #sc-364116) was used to measure the membrane potential of mitochondria (Menke et al., 2003). JC-1 enters mitochondria and shows a potential-dependent accumulation: at intact or normal mitochondrial membrane potentials, JC-1 forms red-fluorescent "J-aggregates", while in cells with a lower mitochondrial membrane potential it leaks out of mitochondria and is present as green fluorescent monomer in the cytosol. The ratio of red to green fluorescence of JC-1 is dependent only on the mitochondrial membrane potential and not influenced by mitochondrial size, shape, or density in the cell.

To determine the mitochondrial membrane potential cerebellar granule cells were plated at a density of $1-2 \times 10^6$ cells/ml onto 22 μm glass coverslips coated with PLL and cultured in serum-free medium for two days. Afterwards, cells were stained with 3 μM JC-1 in Hank's balanced salt solution (HBSS) for 30 min, incubated with HBSS alone for 15 min and then observed under a spinning disk microscope with a 60 \times objective (1.40 aperture). For detection of mitochondria with higher mitochondrial membrane potential compared to the mitochondrial membrane potential of the control group, a rhodamine filter set was used together with the fluorescein filter for detection of depolarized mitochondria with lower mitochondrial membrane potential compared to the control group. Experiments were carried out in duplicates and performed independently three times and the analysis was performed by Viviana Granato (Senior Gruppe Biosynthese Neuraler Strukturen, ZMNH, UKE, Hamburg).

The level of the fluorescence intensity in a given region of a green or red channel was analyzed by calculating the corrected total cell fluorescence (CTCF) with the ImageJ software. CTCF was determined with the formula (McCloy et al., 2014):

$$\text{CTCF} = \text{integrated density} - (\text{area of selected cell} \times \text{mean fluorescence of background readings})$$

2.6.2 Mitochondrial complex I activity

Brains were isolated from 6- to 8-day-old and 7- to 8-month-old mice, frozen in liquid nitrogen and stored at -80°C until use. For the isolation of mitochondria, the Mitochondria Isolation Kit for Tissue from ThermoFisher Scientific (catalog #89801) was used. For determination of complex I activity, mitochondria were applied to the Mitochondrial Complex I Activity Assay Kit (Cayman Chemical, Ann Arbor, MA, USA). Mitochondrial complex I (NADH oxidase/co-enzyme Q reductase) activity was determined by measuring the decrease in NADH oxidation, which is reflected by a decreased in absorbance at 340 nm in the presence of 2 mM potassium cyanide (KCN) to prevent the oxidation of Q. Experiments were carried out in duplicates and performed independently three times.

2.6.3 ATP level

ATP levels were determined using the BacTiter-Glo® 2.0 Cell Viability Assay (Promega, Walldorf, Germany; catalog #G8230) according to the manufacturer's protocol. In brief, cerebellar granule cells were cultured in serum-free medium as indicated above at a density of 2.5

$\times 10^5$ cells/well in 48-well plates for 2 days. Afterwards, cells were scraped off in 200 μ l serum-free medium, 100 μ l of the supernatant was transferred into white 96-well plates and 100 μ l BacTiter-Glo was added to the wells. Plates were incubated for 5 min at room temperature with gentle shaking and then luminescence was measured using a luminometer (Mithras LB943; Berthold Technologies, Bad Wildbad, Germany) The difference in the ATP production between wild-type and mutant group was calculated using wild-type as control group (100%). Experiments were carried out three times independently in triplicates.

2.6.4 Measurement of reactive oxygen species in cells

Intracellular ROS were monitored using the ROS-sensitive fluorescent probe 2',7'-dichlorofluorescein diacetate (DCFH-DA; Biomol, Hamburg, Germany), which penetrates into cells rapidly, is deacetylated by cellular esterases to a non-fluorescent compound and is oxidized by ROS into 2'-7' dichlorofluorescein, a green fluorescent dye. Cerebellar granule cells from 6- to 7-day-old mice were isolated and seeded on glass coverslips as mentioned above, maintained in culture for 3 days in serum-free medium, stained with 10 μ M DCFH-DA for 30 min at 37°C and 5% CO₂. Then the medium was replaced by Hank's balanced salt solution without phenol red and cells were imaged under a spinning disk microscope with a 40 \times objective (aperture 1.2) and with an excitation wavelength of 488 nm. Experiments were carried out in duplicates and performed independently three times and for each condition 10 images and 100 neurons for each genotype were taken for analysis.

2.6.5 Measurement of reactive oxygen species in tissue with 2-Thiobarbituric acid (TBARS) assay

To measure ROS in tissue, mice were killed by decapitation and brains were isolated on ice as quick as possible. Fresh brains from adult and 10-day-old L1-201 and wild-type mice were washed twice in cold PBS. A TBA stock solution was reconstituted in glacial acetic acid and filled up with ddH₂O to have a 25ml TBA solution. Precipitates, where present, were dissolved using a sonicator. A lysis solution of RIPA buffer and butylhydroxytoluol (BHT, 100nM dissolved in ethanol), which prevents sample peroxidation during processing, were prepared and BHT was diluted 1:100 in RIPA buffer. Tissue was homogenized in 303 μ l of lysis solution with a Dounce homogenizer sitting on ice. Next, brain homogenates were collected and centrifuged at

13,000 x g for 10 min to remove insoluble material. Supernatant was then taken and 200 μ l of sample and MDA standard (0.4 to 2 nmol/well) were added to 600 μ l of TBA reagent into a vial. Vials were incubated 95°C for 1 h and cooled down to room temperature on an ice bath for 10 min. 200 μ l of the reaction mix were added into a 96-well microplate for analysis and the output was read after processing at an absorption of 532 nm. Concentration of MDA in the test samples was calculated as: $\text{MDA concentration (nmol/mg)} = (A/mg) \times 4$

A is the amount of MDA in sample calculated from the standard curve (nmol), *mg* is the weight of the tissue used and *4* is the correction for using 200 μ l of the 800 μ l of reaction mix.

2.7 Golgi staining

Fresh brains from 10-month-old wild-type and L1-201 mutant mice were collected and washed two times with cold distilled water. Next, tissues were immersed in 6 ml of impregnation solution (A/B) and stored at room temperature in the dark for 24 h. The solution was replaced the day after, and brains were stored in the dark at RT for two weeks. Brains were then transfer into 7 ml of solution C and stored at RT in the dark for 24h, then old solution C was replaced by fresh solution C, and samples were kept one week at RT in the dark. After one week, brains were put at -20°C for 24 h. The cutting of 100 μ m thick sections was performed using a cryostat (Cryostar Nx70, Thermo Fisher Scientific) with -25°C and -27°C as temperature respectively for the chamber and the blade. Sections were washed two times with cold dH₂O and stained with staining solution (solution D + solution E and H₂O) for 10 minutes under gentle shaking. For dehydration, sections were washed 6 times with dH₂O and next treated for 4 min with 50%, 75%, 95% and 100% ethanol. Finally, sections were treated three times with xylene for 4 min and mounted with Eukitt® Quick-Hardening Mounting medium (Fluka, Buchs, Switzerland). Imaging of the samples was performed using an Apotome 3 microscope (Carl Zeiss). Spine density and arborization of pyramidal neurons from the prefrontal cortex and motor cortex were quantified using Imagej software. Spines were traced and quantified on 30 μ m segments of the first branch of apical or basal dendrites from apotome 3 z-stack images (5 mice/genotype). Mean spine number per 10 μ m of dendritic length (density) was calculated. Mean spine densities/10 μ m \pm SEM were compared by Mann-Whitney two-tailed t-tests (unequal variance, $p < 0.05$). Dendritic arborization of Golgi-labeled pyramidal neurons was performed by Sholl analysis of image stacks

captured at lower magnification (20x/0.5 NA). The Sholl center was defined as the midpoint of the cell body, and the automatic tracing mode was used to seed and trace dendritic arbors.

2.8 Behavior and histology

2.8.1 Histology

Animals were deeply anesthetized by intraperitoneal injections of ketamin and xylazin (80 mg Ketanest® (Pfizer Pharma PFE GmbH, Berlin, Germany) and 10 mg Xylazine® (WDT, Garbsen, Germany), per kg body weight) and then transcardially perfused with fixative (4% w/v paraformaldehyde and 0.1 % w/v CaCl₂ in phosphate buffered saline (PBS), pH 7.4). Brains were extracted and postfixed for at least 24 h at 4°C in the same fixative. Tissue was then immersed in a 15% w/v sucrose solution in PBS, pH 7.4, for 2 days at 4°C and then in 30% w/v sucrose solution in PBS, pH 7.4, for 2 days at 4°C. Then, brains were embedded in Tissue Tek (Sakura Finetek, Umkirch, Germany), frozen by a 2-min immersion into 2-methylbutane precooled to -80°C and stored at -80°C until sectioned. Brains were cut into 40 µm-thick coronal sections in a cryostat (Cryostar NX70; ThermoFisher Scientific, Waltham, MS, USA) and collected in section storage buffer (0.02% sodium azide in PBS) and stored at 4°C.

Free-floating cryosections were mounted on glass slides (Superfrost Plus, ThermoFisher Scientific), air dried and stained with cresyl violet and Luxol Fast Blue to visualize neurons and myelin. Luxol Fast Blue solution (0.1% w/v Lxol Fast Blue, 95% ethanol and 0.5% glacial acetic acid in distilled water) at 57°C overnight. Sections were then washed in 95% ethanol and distilled water before being stained in a 0.05% w/v lithium carbonate solution for 3 minutes. The differentiation was then continued with 70% ethanol and distilled water. Afterwards, sections were stained in a cresyl violet solution (0.1% w/v cresyl violet acetate in water) at 57°C for 5-10 minutes. Finally, sections were differentiated with several changes of 95% ethanol, dehydrated in absolute ethanol, cleared in xylene and mounted with Eukitt quick-hardening mounting medium (Fluka, Buchs, Switzerland). Image acquisition and digitalization were performed using a Apotome 3 microscope, (Zeiss). Ventricle size was measured at two different Bregma levels (0.74 and -0.34), and calculated relative to the entire area of the section. Corpus callosum thickness (vertical dimension) was determined at different Bregma levels (0.74, -0.26, -0.46, -2.18) in the midline and at a lateral location caudal to the primary somatosensory cortex.

2.8.2 Behavior analysis

For behavioral studies mice were accustomed to an inverted day-night-cycle (light off at 8:00 am) for one week and then to the experimenter by handling for two weeks. Before the experiments mice were transported to the experimental room and left for 5-10 minutes for habituation. Tests started and ended at least 2 h after light offset and 3 h before light onset, respectively. Tracks representing the position of the mice were created and analyzed with EthoVision (Noldus, Wageningen, The Netherlands) (Freitag et al., 2003). Manual scoring of behavior was performed by a trained experimenter blinded to the genotype of the mice using The Observer software (Noldus).

2.8.2.1 Open field and elevated plus maze

To evaluate activity levels and exploratory and anxiety-like behavior mice were evaluated in the open field and elevated plus maze (Carola et al., 2002). A multiple unit open field (OF) consisting of four activity chambers was used. Each OF chamber measured 50 cm (length) x 50 cm (width) x 50 cm (height), was made from white high density and non-porous plastic and was illuminated with 50 lux. Then a mouse was placed in an acrylic glass cylinder located in one corner of each activity chamber. When the cylinder was lifted, the mice could freely move in the arena for 20 or 30 minutes and the distance moved and behavior in the arena was recorded. In addition to the time spent in the center of the arena, the total distance moved and the average distance from the wall, which were analyzed for 20-30 minutes, specific behavior parameters were analyzed only for the first 5 min of the test: rearing on the wall (vertical exploration by standing on the back paws with one or two forepaws touching the wall) rearing the off wall and self-grooming.

The elevated plus maze consisted of a plus shaped arena with four arms, 30 cm long and 5 cm wide, connected with a center zone of 5 x 5 cm. Two opposing arms were bordered with a 2 mm rim (open arm), while other two had a 15 cm high wall (closed arm). The maze was elevated 75 cm from the floor and illuminated with 10 lux. Mice were placed in the center of the maze facing the open arm and observed for 5 minutes. The following parameters were analyzed: open and closed arm entries (calculated when all the four paws were inside the arm), stretch attend posture (SAP, calculated when the mouse stretched forward and retracted to the original position without forward locomotion), self-grooming, and head dips.

2.8.2.2 Marble burying test

To measure repetitive and anxiety-related behavior the marble burying test was used (DeBoer and Koolhaas, 2003). The test was performed under red light in cage with 42 cm x 42 cm x 12 cm length. A 5 cm layer of bedding covered the floor of the cage, and 20 black marbles (diameter 1.5 cm) were placed on top of the bedding. The mice were placed in the corner of the cage and left for 30 min to explore and move in the new environment and the number of marbles buried was counted.

2.8.2.3 Social interaction

Motivation to investigate a social stimulus was tested by giving the experimental mouse the choice to investigate an unfamiliar sex-matched mouse or a familiar mouse (Freitag et al., 2003). The arena used for the open field test (50 x 50 cm) was divided into two identical compartments by a 40 cm high wall with an opening in the middle allowing the mouse access to both the compartments and illuminated with 5 lux. A cylinder with a metal grid mesh allowing olfactory exploration between mice was located in one corner of each compartment containing either a familiar or an unfamiliar mouse. Familiar mice were recruited from heterozygous siblings living in the same cage as the experimental mice. Unfamiliar mice were heterozygous or L1 wild-type mice from different cages that were not used as subjects in the behavior tests. First the familiar and unfamiliar mice were placed under the cylinders and then the subject mouse was placed in the arena and left free to move between compartments for 20 minutes. The room was illuminated with 5 lux during recording of the behavior and distance moved, time spent in each compartment, and time spent in proximity of the two cylinders were determined.

2.8.2.4 Home cage activity

Mice were housed singly in a type II cage with a size of 22 cm × 16 cm × 14 cm for 3 days and then their activity during a 24 h day-night-cycle was recorded with a motion detector (Mouse-E-Motion; Infa-E-Motion, Hamburg, Germany) that was placed on top of the cage. The activity of the mice was recorded in 4-minute time bins and E-motion software was used to analyze the activity of the mice.

2.9.2.5 Rotarod and pole test

To evaluate motor coordination and motor learning of mice the rotarod and pole test were used. For the rotarod test (Dunham and Miya, 1957; Jones and Roberts, 1968) mice were trained on a rotating rod with 3 cm diameter (Rota-rod for mice, UGO BASILE S.R.L., Germany) for two days with two trials with constant speed (4 rpm) for 2 min and three trials of training with acceleration (4-40 rpm) for 4 min. After every training trial, the training was stopped for an interval of 10 min before continuing with the next training phase. For the next three to four consecutive days mice were subjected to the test: mice were located on the 3 cm diameter rod, with acceleration from 4 to 40 rpm within 300 sec (5 min). The tests were performed with red light and the latency to fall from the rod was recorded.

The pole test evaluates the ability of a mouse to grasp a pole and make a t-turn to climb down to its home cage. Mice were placed with their head oriented upward on top of a vertical pole of 48.5 cm length and 0.3 cm diameter made of rough wood and the time mice needed to climb down the vertical pole was measured.

2.8.2.6 Beam walking

The beam walking test was used to evaluate motor balance and coordination. The apparatus consisted of a wooden beam 90 cm long and 5 cm wide, positioned 50 cm from the ground. The end of the beam contained food to further motivate the mouse to cross the beam towards its home cage. The time taken by the animal to cross the bar was counted (with a maximum time of 2 min), and the foot-base angle and heel-tail angle were measured to evaluate the presence of impairments in the hind pawns. Light: 50 lux.

2.8.2.7 Grip strength test

Two-month-old wild-type or L1/858-863 male mice were hold by the tail and the strength of the forelimbs was measured. The strength was measured with a Grip Strength Meter system (TSE Systems, Germany) while the mice grasped to a grip bar attached to a dynamometer. The maximal force the mice needed to hold on the grip bar until the mice released the grip was noted (Morellini et al.,2006). Mice were tested twice.

2.9 Statistics

All numerical data are presented as group mean values with the standard error of the mean (SEM) or standard deviation (SD); for small sample numbers, individual data are additionally indicated. The normal distribution of the data was determined using the Shapiro–Wilk test or the D’Agostino–Pearson test. For data with a normal distribution, Student’s t-test was used to compare two groups, whereas for comparisons of more than two groups, I performed ANOVA followed by Tukey’s post-hoc test for multiple comparisons. Groups containing small sample numbers or data that were not normally distributed were analyzed using the Mann–Whitney U-test for comparing two groups or the Kruskal–Wallis test by ranks followed by Dunn’s multiple comparison test when there were more than two groups. The statistical tests used for comparisons are indicated in the figure legends. Analyses were performed using GraphPad (version: 8; RRID:SCR_000306) software.

3. RESULTS

3.1 Impaired mitochondrial motility in neurons from L1 mutant mice

Mitochondria play an important role in energy metabolism and neurons have a high energy demand to properly release and recycle synaptic vesicles during neurotransmission, for the transport of molecules over large distances in axons and dendrites and protein synthesis, amino acid or steroid synthesis, which are essential for outgrowth, survival, and migration of these cells. L1/858-863 and L1/687 cerebellar neurons show reduced migration and outgrowth under basal conditions and do not respond to the function-triggering L1 antibody 557, while L1-201 cerebellar neurons do not respond to the function-triggering L1 antibody 557 but show normal migration and outgrowth under basal conditions (Congiu et al., 2022, Loers et al., 2021). To investigate if altered mitochondrial functions underlie those impairments, mitochondrial activity, and mitochondrial transport in the L1 mutant cerebellar neurons were determined. Mitochondria of cultured cerebellar neurons from wild-type and L1 mutant mice were labeled and imaging of the mitochondrial transport using time-lapse video microscopy was performed. To compare mitochondrial trafficking in neurons from wild-type and L1 mutant mice, the motility and the mobility were quantified using the kymograph tool from ImageJ. Motility is described as the velocity of dynamic mitochondria in axons represented by diagonal lines in the kymographs, whereas the term mobility specifies the number of stationary mitochondria in neurons represented by vertical lines in the kymographs. Mitochondrial transport can be anterograde or retrograde. Anterograde transport of mitochondria from the cell body to synaptic terminals is crucial during periods of high energy demand, whereas retrograde transport of mitochondria from synaptic terminals to the cell soma is required to remove defective mitochondria that have an impaired membrane potential (Niescier et al., 2016). Direction of mitochondrial transport is indicated by left or right diagonal lines in the kymographs. Depending on the position of the cell soma in the kymograph, left or right diagonal lines indicate anterograde or retrograde movement of mitochondria over time (Fig. 6C) (Marra et al., 2015).

In L1/858-863 and L1/687 neurons velocity and mobility of mitochondria were normal, but mitochondria from L1/858-863 and L1/687 mutant mice moved more retrogradely than mitochondria of wild-type neurons (Fig. 6A-C).

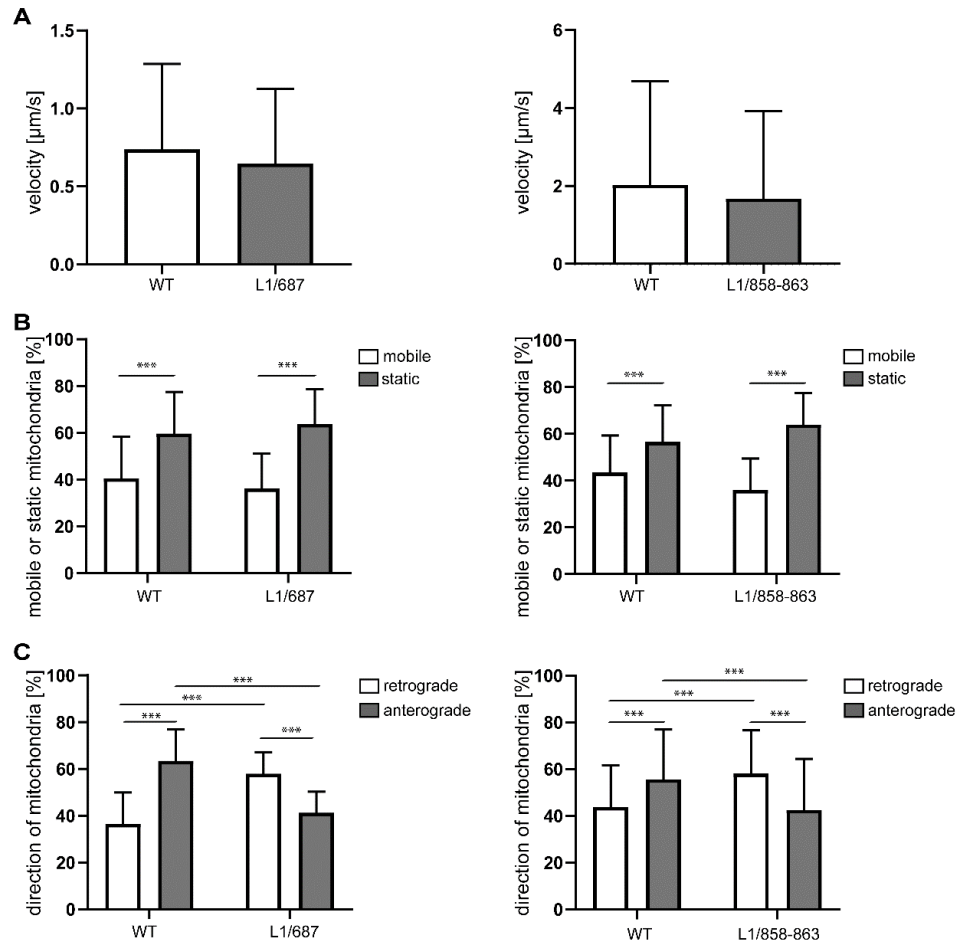


Figure 6. Mitochondria of cerebellar neurons from L1/687 and L1/858-863 mice show normal velocity and mobility but enhanced retrograde transport. Mitochondrial velocity (A), mobility (B) and transport direction (C) were analyzed in cultured cerebellar neurons from 7-day-old male mutants and sex and age matched wild-type littermate mice. Means \pm SD from three independent experiments are shown. *** $p < 0.005$; velocity: Mann–Whitney test; mobility and direction of L1/868-863: Kruskal–Wallis test with Dunn’s multiple comparison test; mobility and direction of L1/687: two-way ANOVA with Tukey’s post-hoc test. (Graphs are taken from Congiu et al., 2022).

Neurons from L1-201 mutant mice showed alterations in mitochondrial functions compared to the neurons from mutant mice lacking L1-70. L1-201 mitochondria also moved more retrogradely than mitochondria of wild-type neurons, but their velocity was enhanced, and their mobility was comparable to that of wild-type neurons (Fig. 7A-C).

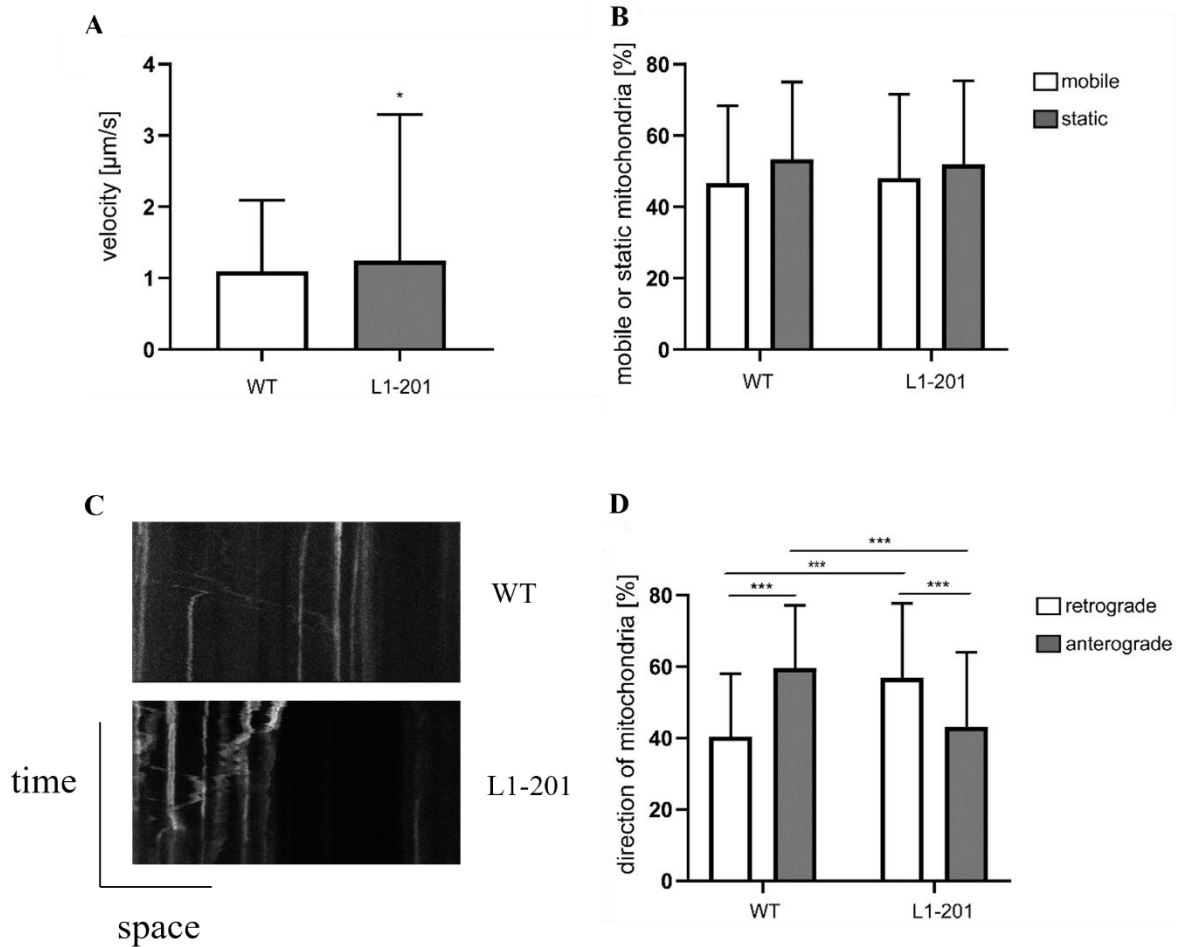


Figure 7. Mitochondria of cerebellar neurons from L1-201 mice show normal mobility and enhanced velocity but move more retrogradely than mitochondria from wild-type neurons. Mitochondrial velocity (A), mobility (B) and transport direction (D) were analyzed in cultured cerebellar neurons from 7-day-old male L1-201 mice and sex and age matched wild-type littermates. Mean values \pm SD are shown. $n = 3$. * $p < 0.05$, *** $p < 0.005$: velocity: Mann-Whitney test; mobility: two-way ANOVA with Tukey's post-hoc test; direction: Kruskal-Wallis test with Dunn's multiple comparison test. Representative images from the kymograph analysis for mitochondrial movement in cerebellar neurons (C) are shown above. (Graphs are taken from Congiu et al., 2022).

Additionally, time lapse video microscopy of labeled mitochondria was performed after treatment of wild-type and L1 mutant neurons with the L1 agonist compound duloxetine. Duloxetine is an FDA approved drug and largely used in the clinical treatment of depression (Knadler et al., 2011, Muscatello et al., 2019). This compound has been shown to trigger some L1-mediated functions, such as neurite outgrowth from spinal motor neurons, dorsal root ganglion neurons, cerebellar

neurons, and cortical neurons as well as proliferation and migration of Schwann cells in vitro, in vitro myelination and regeneration after spinal cord injury in vivo (Kataria et al., 2016).

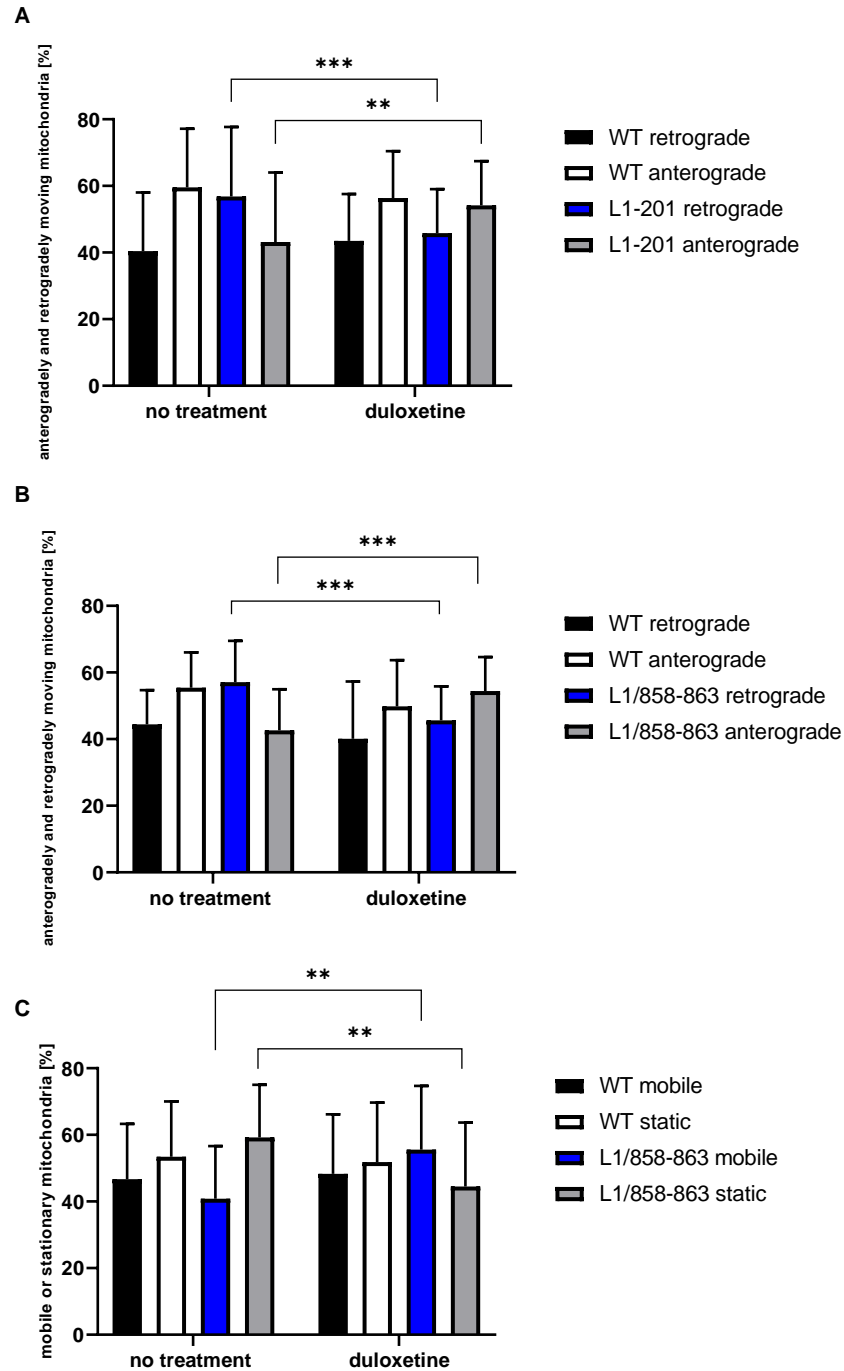


Figure 8. Stimulation with duloxetine increases the percentage of anterogradely moving mitochondria in both L1-201 and L1/858-863 neurons as well as the percentage of mobile

mitochondria in L1/858-863 neurons. Mitochondrial mobility and transport direction were analyzed in cultured cerebellar neurons from 7-day-old male L1-201 (A), L1/858-863 (B, C) mice and wild-type littermates (A-C). Cells were either treated with vehicle solution (no treatment) or the L1 agonist duloxetine before measuring the transport and mobility of mitochondria. Mean values \pm SD are shown. $n = 3$. ** $p < 0.01$, *** $p < 0.005$; three-way ANOVA with Tukey's post-hoc test.

Here, I show that duloxetine increased the percentage of anterogradely moving mitochondria in both wild-type and L1-201 mutant cerebellar neurons, while in cerebellar neurons from L1/858-863 wild-type and mutant mice this compound increased not only the percentage of anterogradely moving mitochondria but also the percentage of mobile mitochondria (Fig. 8A-C).

In conclusion, absence of L1-70 does not seem to be the main cause of the increased retrograde movement of mitochondria since the same impairment is present in both L1-mutant lines. On the other hand, variations of mitochondrial motility are visible only when L1-70 is not expressed, suggesting that this fragment might regulate this specific mitochondrial function.

3.2 The mitochondrial membrane potential is differently impaired in neurons of L1/858-863 and L1-201 mice

To elucidate if an altered energetic or health status is responsible for the enhanced retrograde transport of mitochondria in the L1 mutant mice, the energetic status of mitochondria was evaluated in both L1-70 lacking and L1-201 mice by measuring the polarization of the inner membrane of mitochondria. To measure the membrane potential, the dual-emission potential-sensitive probe JC-1 iodide was used. JC-1 crosses the mitochondrial inner membrane and shows a potential-dependent accumulation: at higher mitochondrial membrane potentials red fluorescent "J-aggregates" are formed in mitochondria, while in cells with a lower mitochondrial membrane potential the dye leaks out of mitochondria and is present as green fluorescent monomer in the cytosol. Neurons of the L1/858-863 mutant mice exhibited a lower mitochondrial membrane potential when compared to their wild-type littermates (Congiu et al., 2022; Fig. 9). Interestingly, the membrane potential of neurons from L1-201 mice is higher compared to that of their wild-

type littermates, showing that mitochondria from this mutant are differently damaged in comparison to mitochondria from L1-70 lacking neurons (Fig. 9).

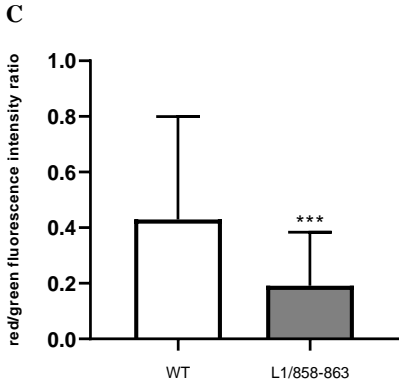
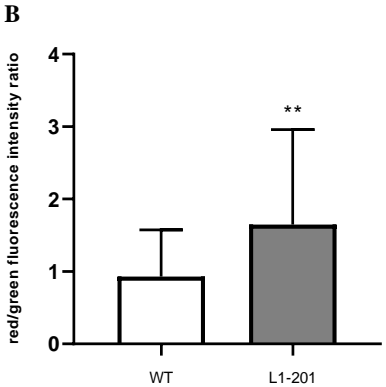
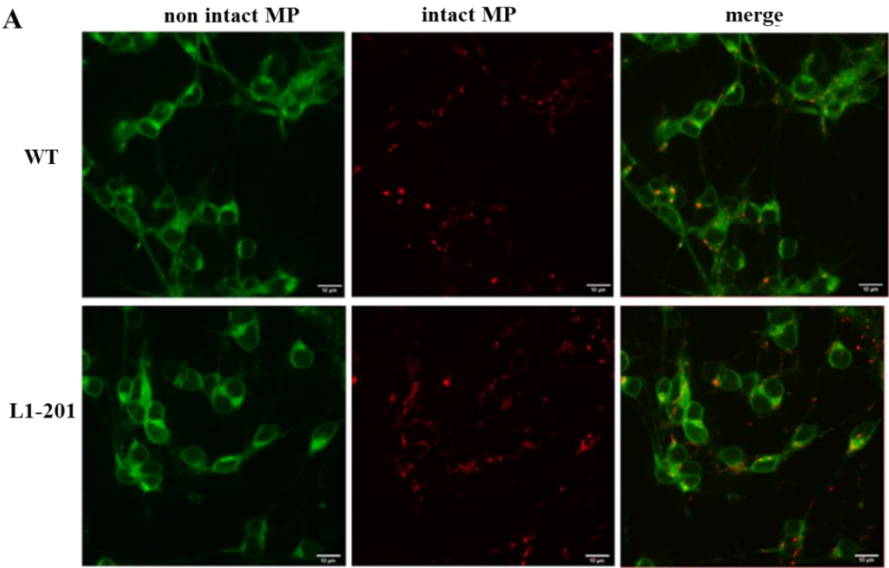


Figure 9. Mitochondria in cerebellar neurons from L1-201 mice show an enhanced membrane potential while in neurons of L1/858-863 mice the mitochondrial membrane potential is reduced. (A)

Representative images of cerebellar neurons from wild-type and L1-201 mice stained with JC-1 show mitochondria with intact membrane potential in red and cells with disrupted membrane potential show green fluorescent staining in the cytosol. Scale bars: 7 μ m. (B, C) The mitochondrial membrane potential was determined in cultured cerebellar neurons from 7-day old male L1-201 (B), L1/858-863 (C) and their respective wild-type (WT) littermate mice (B, C). Means \pm SD are shown. n = 3; ** p < 0.01; *** p < 0.005; L1-201: Student's t-test; L1/858-863: Mann-Whitney test. (Graphs are taken from Congiu et al., 2022).

3.3 Complex 1 activity and ATP production are differently affected in neurons of L1-201 and L1/858-863 mice

Previous studies showed that L1 interacts with glyceraldehyde 3-phosphate dehydrogenase (GAPDH), an important mitochondrial protein (Makhina et al., 2009, Loers et al., 2012), involved in the regulation of mitochondrial oxidative phosphorylation (Ramzan et al., 2013). Furthermore, the L1-70 fragment, which is present in the cytoplasm of wild-type and L1-201 mice (Lutz et al., 2012), is imported into mitochondria in wild-type neurons through the interaction with TOM70 and inside mitochondria this fragment interacts with GAPDH and NDUFV2 (Kraus et al., 2018a). To produce ATP, mitochondria use the oxidative phosphorylation machinery that comprises the electron transport chain containing the enzymes of complex I-V of the inner mitochondrial membrane. To verify that the L1-70 fragment is important for mitochondrial function and to determine whether mutations of L1 can affect mitochondrial metabolism, the activity of complex I, which is the first and largest multisubunit complex of the respiratory chain, and ATP levels in neurons were analyzed.

Complex I activity in brains from L1/858-863 7-day-old mice was reduced, while in young L1-201 mice no impairment was detected (Fig. 11). Interestingly, adult L1/858-863 and L1-201 mice showed a normal complex I activity (Fig. 10), suggesting activation of a possible compensatory mechanism which can explain also why L1 mutant mice survive longer, compared to the L1-deficient mice.

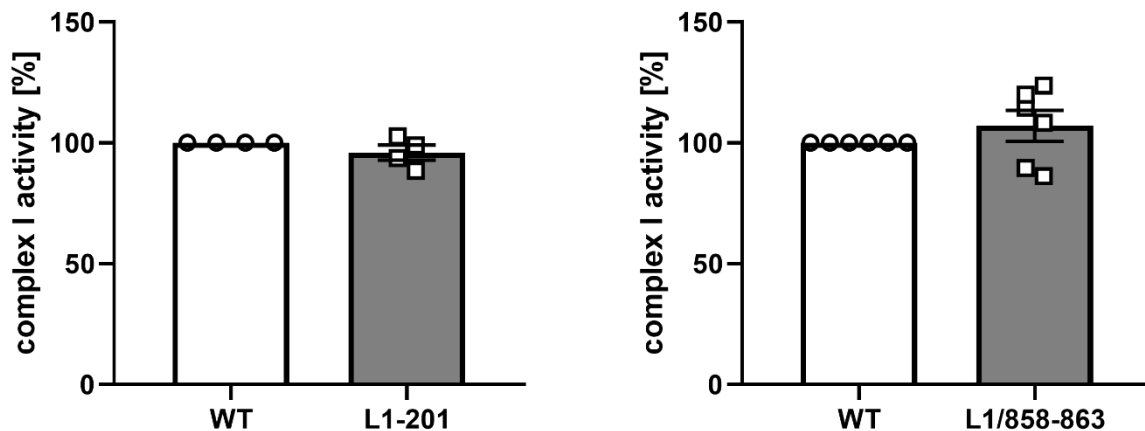


Figure 10. Normal complex I activity in mitochondria from L1-201 and L1/858-863 adult mice. Mitochondrial complex I activity was determined using isolated mitochondria from whole brains of 5-month-old male L1-201 and L1/858-863 (gray bars) and wild-type (WT, white bars) littermate mice. Average values \pm SEM and values from individual mice are shown. $n=4$ (L1-201) and $n=6$ (L1/858-863).

Furthermore, L1/858-863 neurons showed a tendency for lower ATP levels (p -value = 0.06) compared to the wild-type neurons, while neurons from L1-201 mice tended to produce more ATP in comparison to neurons from their wild-type littermates. Since ATP levels in brains of 7-day-old L1/858-863 mice showed a tendency to be reduced, ATP levels were also determined in cultured cerebellar neurons to elucidate if the ATP production in L1-70-lacking neurons is impaired. In addition, cells were treated with antibody 557, tacrine and duloxetine to determine if triggering of L1 changes ATP production in wild-type neurons that generate L1-70 and to discover if L1-70 plays a role in ATP production or consumption (Fig. 12). Since no significant change in the ATP production was observed after the stimulation of wild-type cells and L1/858-863 cells, it can be hypothesized that ATP production in neurons is not influenced by activation of L1 by duloxetine and antibody 557 treatment and the results suggest that L1-70 does not regulate ATP production or consumption of neurons.

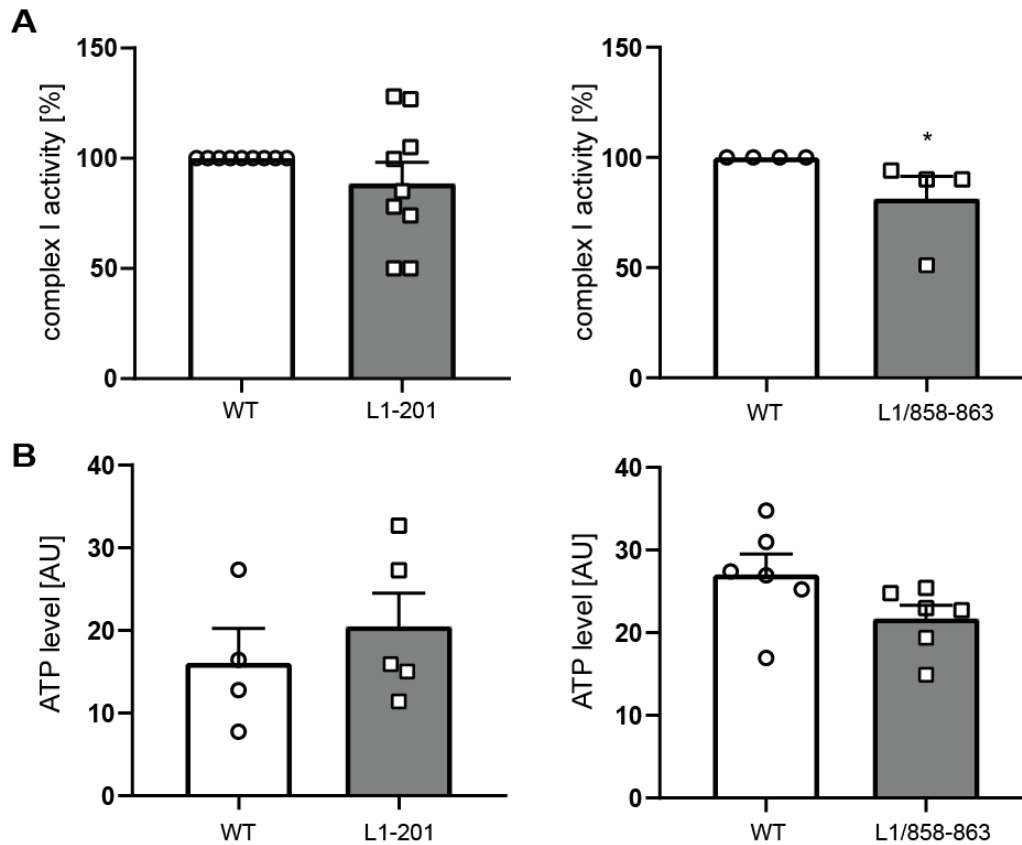


Figure 11. Normal complex I activity and normal ATP levels in mitochondria from L1-201 mice and reduced complex I activity and normal ATP levels in L1/858-863 mice. (A) Mitochondrial complex I activity was determined using isolated mitochondria from whole brains of 7- to 9-day-old male L1-201 and L1/858-863 (gray bars) and wild-type (WT, white bars) littermate mice. Average values \pm SEM and values from individual mice are shown. $n=9$ (L1-201) and $n=4$ (L1/858-863). (B) Mitochondrial ATP levels were determined in cultured cerebellar neurons from 7-day old male L1-201, L1/858-863 (gray bars) and wild-type littermate (WT, white bars) mice. $n=5$ for L1-201 and $n=6$ for L1/858-863. * $p < 0.05$, Mann-Whitney test. (Graphs are taken from Congiu et al., 2022).

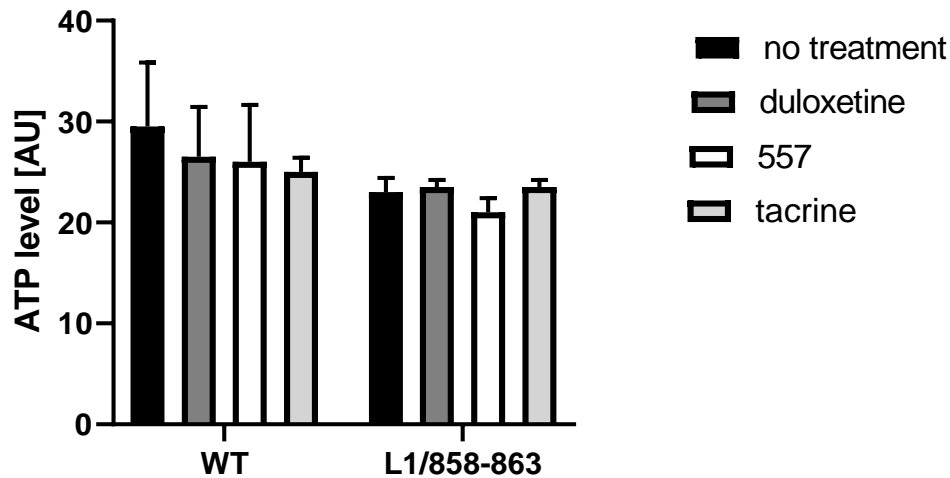


Figure 12. Normal ATP production in cerebellar neurons from L1/858-863 mice after stimulation with L1-agonist compounds duloxetine and tacrine and with 557 antibody. Mitochondrial ATP levels in cerebellar neurons from 7-day old male L1/858-863 and wild-type littermate mice were determined after stimulation with duloxetine, L1 antibody 557 and tacrine. Average values + SD are shown. n= 3 mice per genotype. Three-way ANOVA.

3.4 Cerebellar neurons from L1-201 and L1/858-863 mice show enhanced levels of reactive oxygen species

When their function is impaired, mitochondria contribute to severe pathologies of the nervous system, not only due to metabolic insufficiency but also due to the production of reactive oxygen species (ROS) and activation of caspases, with the highest basal rate of ROS production being in the brainstem and cerebellum. Since L1-deficient mice and L1 mutant mice show impairments in mitochondrial function, they might also exhibit enhanced ROS levels. Therefore, ROS levels in cultured cerebellar neurons were determined. Cerebellar neurons from L1-201 and L1/858-863 mice show higher ROS levels compared to cerebellar neurons from wild-type mice, while levels in neurons from L1-deficient mice only tend to be higher (Fig. 13). To also evaluate whether the treatment with L1-agonist compounds can reduce ROS levels in cerebellar neurons, cells were stimulated with 100 nM duloxetine. Analysis post treatment highlights a restorative effect of duloxetine in decreasing ROS production in both L1-201 and L1/858-863 neurons (Fig. 13).

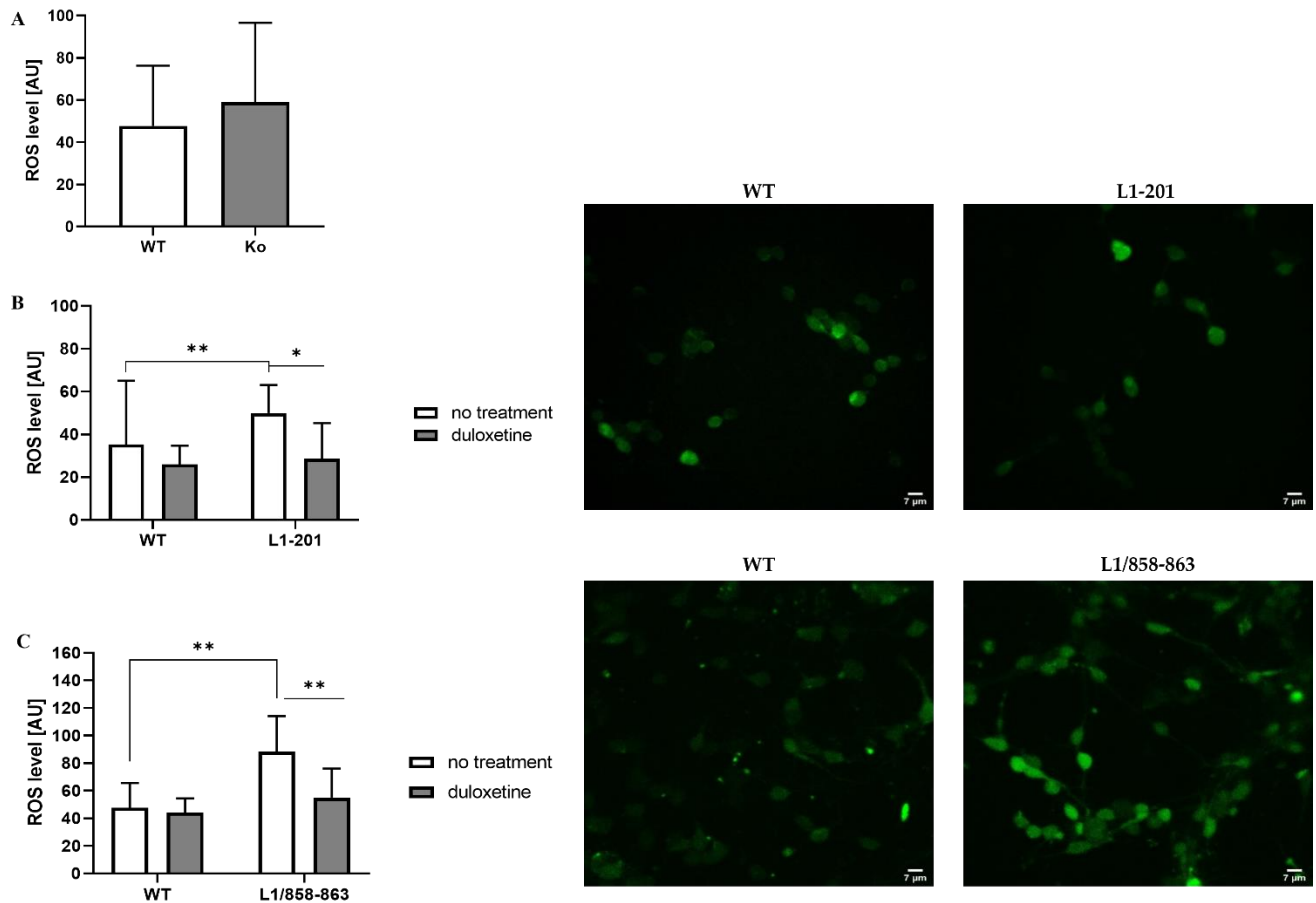


Figure 13. Enhanced ROS levels in neurons from L1-201 and L1/858-863 mice are reduced after stimulation with duloxetine. ROS levels were determined in cultured cerebellar granule cells from 6- to 7-day-old male L1-ko, L1-201 and L1/858-863 mice and their wild-type male littermates. (A, B and C) Representative images from L1-201, L1/858-863 and their respective wild-type littermate cerebellar neurons stained with DCFH-DA are shown. (B and C) Graphs show ROS levels in L1-ko (A), L1-201 (B) and L1/858-863 neurons (C). (B, C) Neurons from L1-201 and L1/858-863 mice were also treated with vehicle (no treatment) or 100 nM duloxetine. Means \pm SD are shown. $n=3$; ** $p < 0.01$, * $p < 0.05$ (Mann-Whitney test and two-way ANOVA).

The ability of duloxetine to restore normal ROS levels is visible when L1-70 is expressed and also when it is not express, suggesting that this compound exerts its effect through mechanisms

that do not only involve L1-70. Further analysis to investigate how duloxetine interacts with mitochondria to ameliorate oxidative stress in cells will be required.

3.5 Oxidative stress is higher in young but not in adult brains of L1-mutant mice

To further investigate whether the oxidative damage affects not only the neurons in the cerebellum but also the whole brain and to determine if oxidative stress augments with age, brains from 10-day-old and 8-month-old wild-type and L1 mutant male mice were collected and the concentration of malondialdehyde (MDA), the major product of polyunsaturated fatty acids peroxidation, was measured.

Interestingly, brains from 10-day-old L1-201 and L1/858-863 mice showed a slight tendency for higher concentrations of MDA compared to the wild-type brains, while levels in brains of adult wild-type and mutant mice were similar (Fig. 14).

Thiobarbituric acid-reactive substances are formed as a byproduct of lipid peroxidation and a marker of oxidative stress and the antioxidant status in the tissue. The slight increase in oxidative stress observed in the whole brain of both L1-201 and L1/858-863 mice at 10-days of age could be a consequence of the mitochondrial damage in neurons but it is probably not linked to L1-70 action since L1-70 lacking and L1-70 expressing cells showed a similar phenotype. However, the same scenario does not occur for animals from both L1-mutant lines in adulthood. Since the brain contains not only neurons but also astrocytes and oligodendrocytes which do not express L1 and which protect neurons from stress *in vivo*, it is conceivable that the overall oxidative stress in brain is lower compared to the stress seen in isolated neurons.

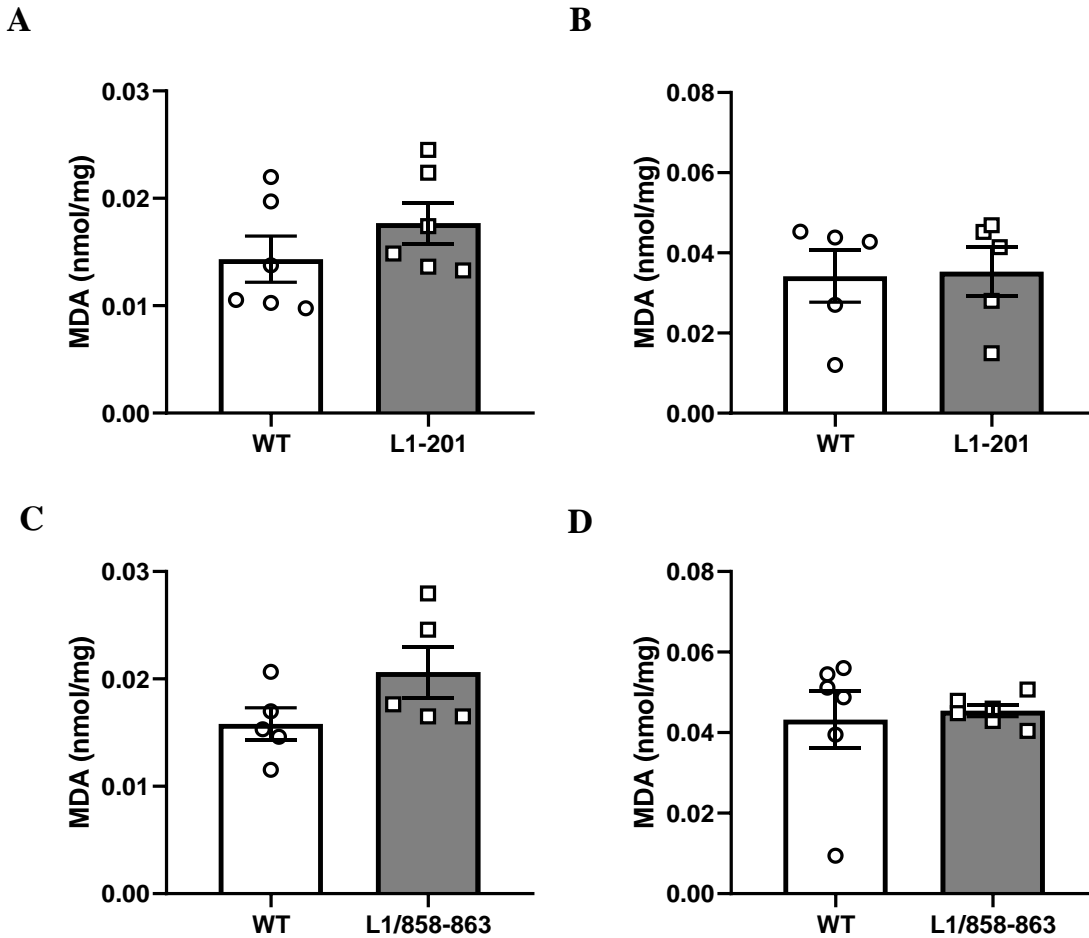


Figure 14. The total MDA concentration is not significantly altered in brains of young and adult L1 mutant mice. Brains of 10-day-old (A, C) and 8-month-old (B, D) L1-201 and L1/858-863 male mice and their wild-type littermates were collected, and the concentration of MDA was measured. Means \pm SEM and single values are shown. $n=5/6$; Mann-Whitney test.

3.6 Phospho-AMPK/AMPK levels are normal in 10-day-old L1-201 mice

Adenosine monophosphate-activated protein kinase (AMPK) has been identified in the past few years to act as a central integrator of mitochondrial homeostasis by controlling various aspects of the mitochondrial life cycle, from biogenesis and dynamics to removal by mitophagy (Herzig et al., 2018). AMPK is activated under conditions in which mitochondrial function and mitochondrial production of ATP are compromised. Since neurons from L1-201 mice show an

impaired mitochondrial activity and a tendency to produce more ATP compared to the wild-type neurons, I further investigated the mechanism that could underly these impairments. For this aim, the ratio between the phosphorylated and non-phosphorylated AMPK was evaluated in cytosolic fractions from brains of 10-day-old mice. Cytosolic proteins from L1-201 and wild-type mice were applied to Western blot analysis using antibodies against the phospho- α AMPK subunit and the α -AMPK subunit. Beta-actin was analyzed to control for loading. Results show no significant difference in phospho-AMPK and total AMPK levels between mutant mice and wild-type mice (Fig. 15).

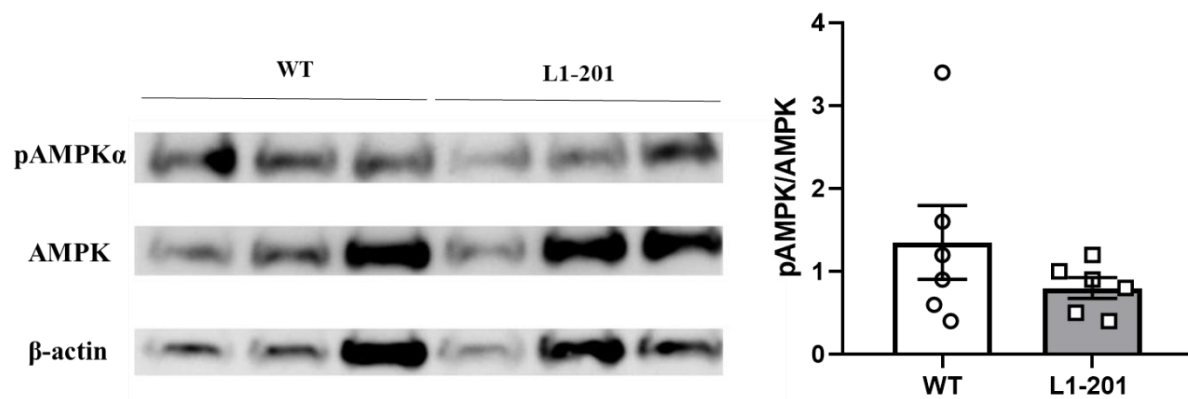


Figure 15. Phospho-AMPK and total AMPK protein levels are normal in L1-201 mouse brains. No difference was observed in the levels of phospho-AMPK between brains of 10-day-old L1-201 mice and their aged-matched wild-type littermates. β -actin was used as loading control. A representative Western blot out of two independent experiments is shown. Means \pm SEM are shown; n=6; Mann-Whitney test.

3.7 Schwann cell process formation is impaired in L1-201 neurons

Not only neurons, but also Schwann cells express L1 (Martini et al., 1994, Haney et al., 1999) and it has been shown that L1 is able to trigger Schwann cell functions, such as proliferation and process formation (Haney et al., 1999). To evaluate whether the L1-201 mutation affects Schwann cell functions, their process formation in wild-type and L1-201 cells was investigated. Process formation was reduced by 20% in L1-201 Schwann cells in comparison to wild-type littermate cells (Fig. 16), showing that L1-201 expressing Schwann cells are impaired in this function. Furthermore, L1 mimetic treatment was performed to evaluate whether there might be a restorative effect on the impaired L1 function. Duloxetine was chosen from the L1 agonists since it showed strongest effects on in vitro myelination by wild-type Schwann cells (Kataria et al., 2016). L1-201-expressing Schwann cells showed enhanced process formation, and process lengths were comparable to the process length of wild-type cells, indicating that the L1 mimetic duloxetine can rescue the defective phenotype (Loers et al., 2021) (Fig. 16).

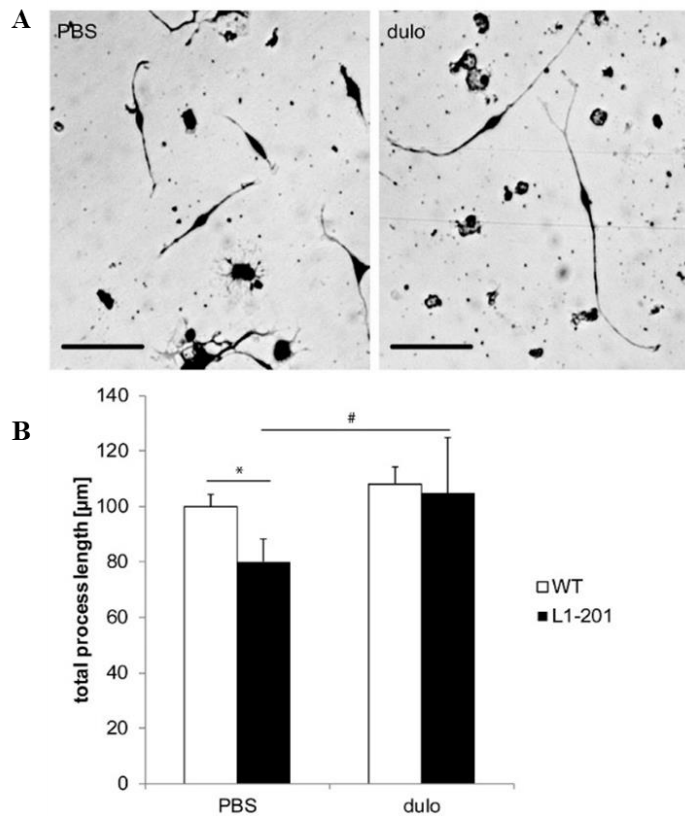


Figure 16. L1-201 Schwann cells show impaired process formation that can be ameliorated with the L1 mimetic duloxetine. A and B, wild-type (WT) and L1-201 Schwann cells were cultured on PLL in the

presence of phosphate-buffered saline, pH 7.4 (PBS) or 100 nM duloxetine (dulo). (A) Representative images of L1-201 Schwann cells maintained on PLL without compound (PBS) and on PLL with duloxetine (dulo). Scale bars: 50 μ m. (B) Graph shows lengths of processes measured from at least 100 cells per treatment and genotype. Mean values + SEM are shown. # $p < 0.001$ compared to values obtained on the PLL substrate; * $p < 0.001$ compared to the respective WT values. The experiment was performed independently three times with two mice per genotype and experiment. (Data and figure were taken from Loers et al., 2021).

Taken together, my results suggest that the L1-70 fragment is involved in the regulation of the mitochondrial membrane potential, complex I activity and ATP production. Mitochondrial activity is differently impaired in L1-201 and L1/858-863 mutant lines. While the increased ROS production in the L1/858-863 neurons might be a consequence of the decreased complex I activity and ATP production, the higher production of ROS in the L1-201 neurons could be due to ATP overproduction or other oxidative mechanisms and do not involve over-phosphorylation of AMPK. Treatment with duloxetine reduces ROS levels in cultured neurons from both lines, suggesting that its therapeutic property does not depend on the presence of L1-70.

Furthermore, mice with D201N mutation show a 20% reduction of process length of Schwann cells and this impairment can be rescued also by stimulation with duloxetine.

3.8 Behavior

3.8.1 Body weight and grip strength

To investigate whether L1-70 absence can induce alterations in body weight or strength of mice, the body weight and grip strength of mice were evaluated. No obvious difference in the appearance of L1/858-863 compared to their wild-type (WT) littermates was observed when mice were examined starting from postnatal day 21 till five month of age (weight average \pm SD: two-month-old mice - WT males 27.17 ± 0.74 g, L1/858-863 males 27.20 ± 2.18 g, WT females 25.83 ± 1.80 g, L1/858-863 females 22.70 ± 1.08 g; five-month-old mice - WT males 31.47 ± 2.62 g, L1/858-863 males 32.18 ± 3.99 g, WT females 23.38 ± 1.43 g, L1/858-863 females 23.47 ± 2.17 g). When evaluating quadriceps muscle function in the beam walking test, L1/858-863 mice needed a similar time to cross the beam and plantar stepping abilities were the same as their wild-type littermates (Fig. 17).

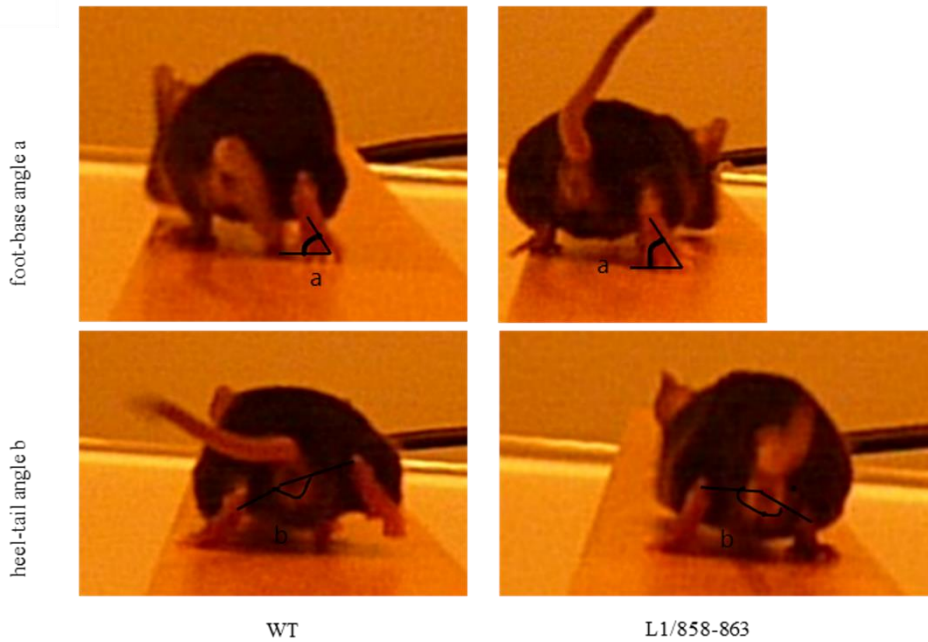
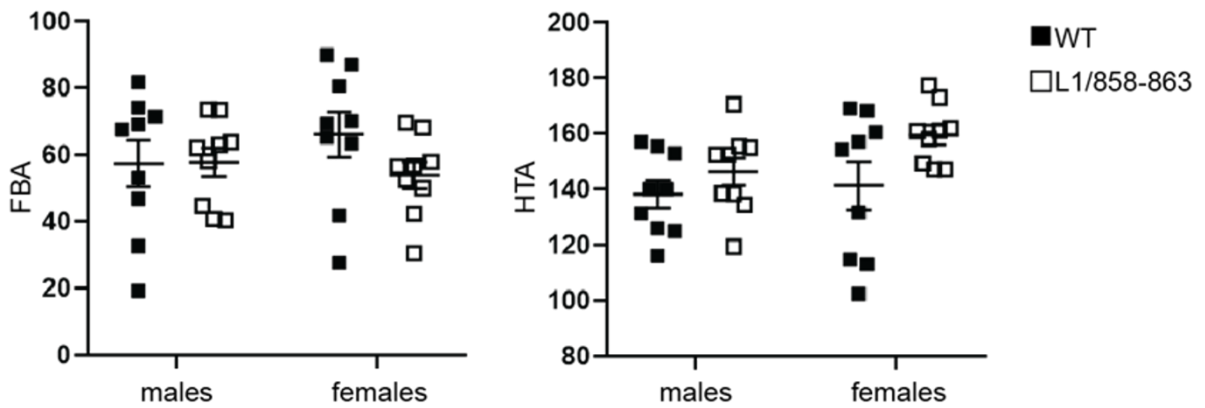
A**B**

Figure 17. Normal quadriceps muscle function in L1/858-863 mice. Male and female L1/858-863 mice and their wild-type littermates were subjected to the beam walking test and foot-base-angle (FBA) and heels-tail-angle (HTA) were measured. (B) Representative images of mice walking on the beam and recorded from behind are shown. (A) Single values and average values with SEM are shown. N = 8-10 mice per group; two-way ANOVA with Tukey's post hoc test.

3.8.2 Open field

The open field test is commonly used to evaluate motor activity and exploratory behavior of mice by observing their distance moved, mean velocity and rearing on the hind limbs. As open spaces like the center of an arena are an anxiogenic stimulus for mice, thigmotaxis (the tendency to stay and move along the wall of the arena) is used to measure anxiety. No differences were detected for mean velocity of L1/858-863 males and females and their corresponding wild-type animals and velocity decreased in males and females of both genotypes with habituation to the new environment (Fig. 18a, b).

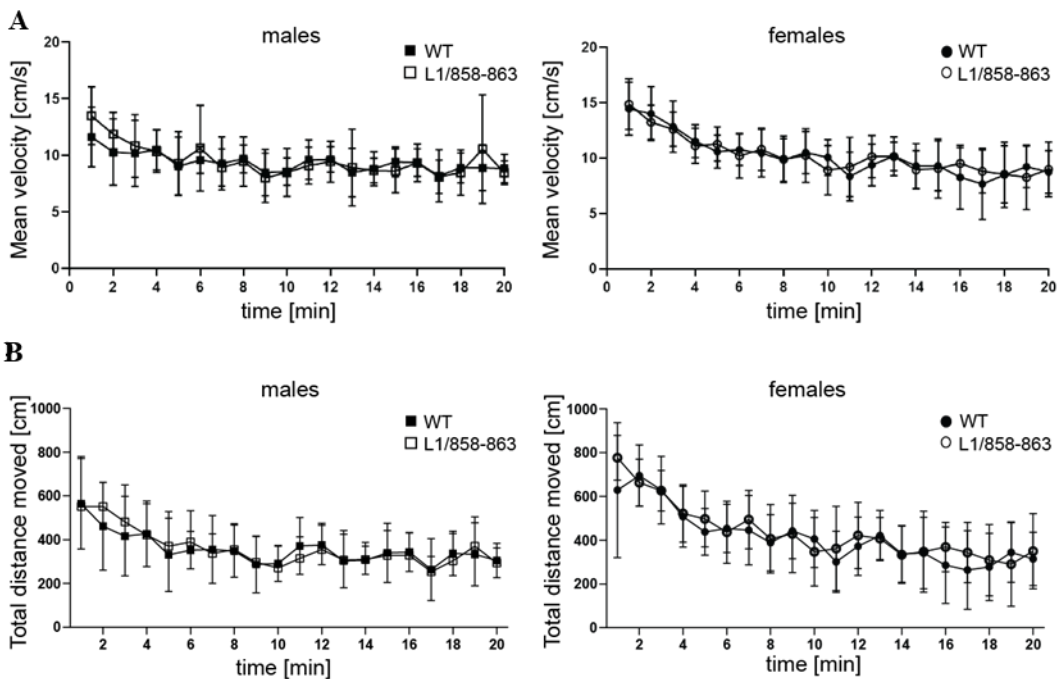


Figure 18. Normal velocity and total distance moved of L1/858-863 mice in the open field. Male and female L1/858-863 mice and their wild-type littermates were subjected to the open field and the velocity (A), and distance moved (B) was determined over 20 minutes. Average values with SD are shown. N = 10 mice per group; two-way ANOVA RM with Tukey's post hoc test.

Time in the center zone in the first minutes of the test was higher for L1/858-863 females but not for L1/858-863 males (Fig. 19A). The frequency to visit the center zone was not changed for L1/858-863 males and females and compared to their wild-type littermates (Fig. 19B). The total distance moved in the center zone was also not changed for L1/858-863 males and females compared to their wild-type littermates (Fig. 19C). In contrast, the distance from the wall was

higher for the L1/858-863 females during the first 10 minutes of the test, while it was not changed for L1/858-863 males (Fig. 19D). No differences between genotypes were found for the other behavioral parameters analyzed (stretch attend posture, self-grooming, and rearing on and off wall; data not shown). Results show reduced anxiety-like behavior of female L1/858-863 mice and normal behavior of male L1/858-863 mice.

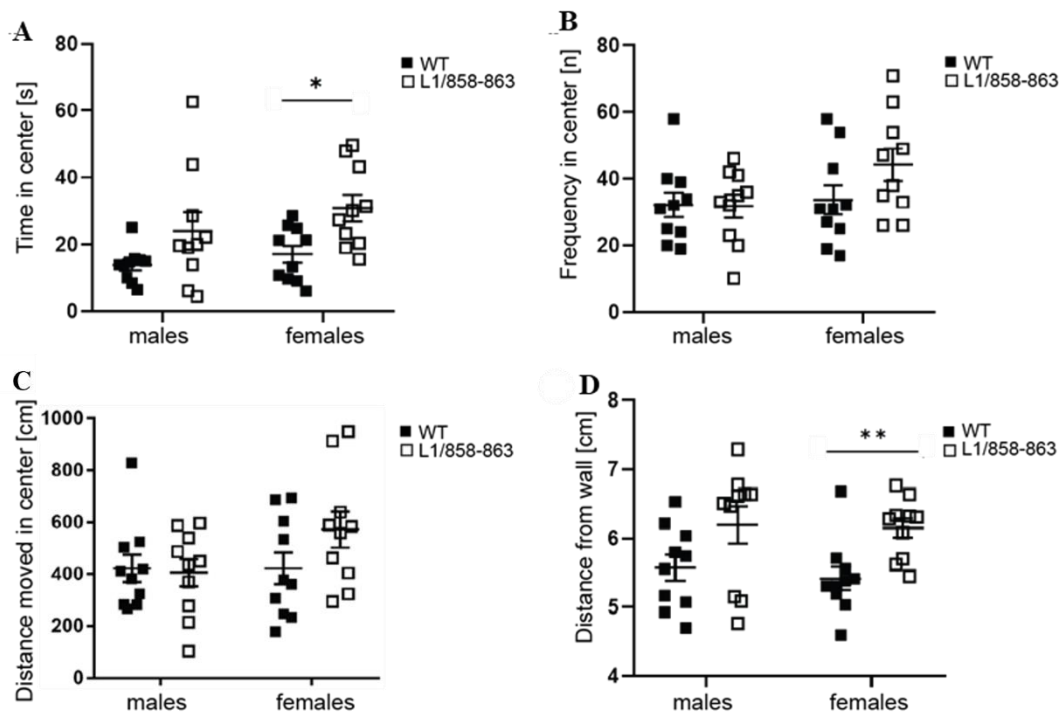


Figure 19. Female, but not male L1/858-863 mice spend an increased time in the center zone and move at a higher distance from the wall in the open field. Male and female L1/858-863 mice and their wild-type littermates were subjected to the open field and the time spend in the center zone during the first 10 min (A), the frequency to enter the center zone during 20 min (B), the distance moved in the center during 20 min (C) and the distance from the wall during 20 min (D) were determined. Single values and average values with SEM are shown. N = 8-10 mice per group; * $p < 0.05$, ** $p < 0.01$, two-way ANOVA (for distance and time in the center) with Tukey's Post Hoc Test and two-way ANOVA (for the frequency in the center).

3.8.3 Elevated plus maze

To further measure anxiety-like behavior the elevated plus maze was used. The test is based on the analysis of natural fear of mice for open and elevated areas, as well as on their natural spontaneous exploratory behavior in novel environments. No difference was detected between the genotypes for all the parameters analyzed: L1/858-863 mice did not show differences in the number of entries or time spent in the open and closed arm compared to their wild-type littermates (Fig. 20A-D). Results support the observation that L1/858-863 mice show normal risk assessment and in contrast to the open field test female L1/858-863 mice did not show alterations in anxiety levels in the elevated plus maze.

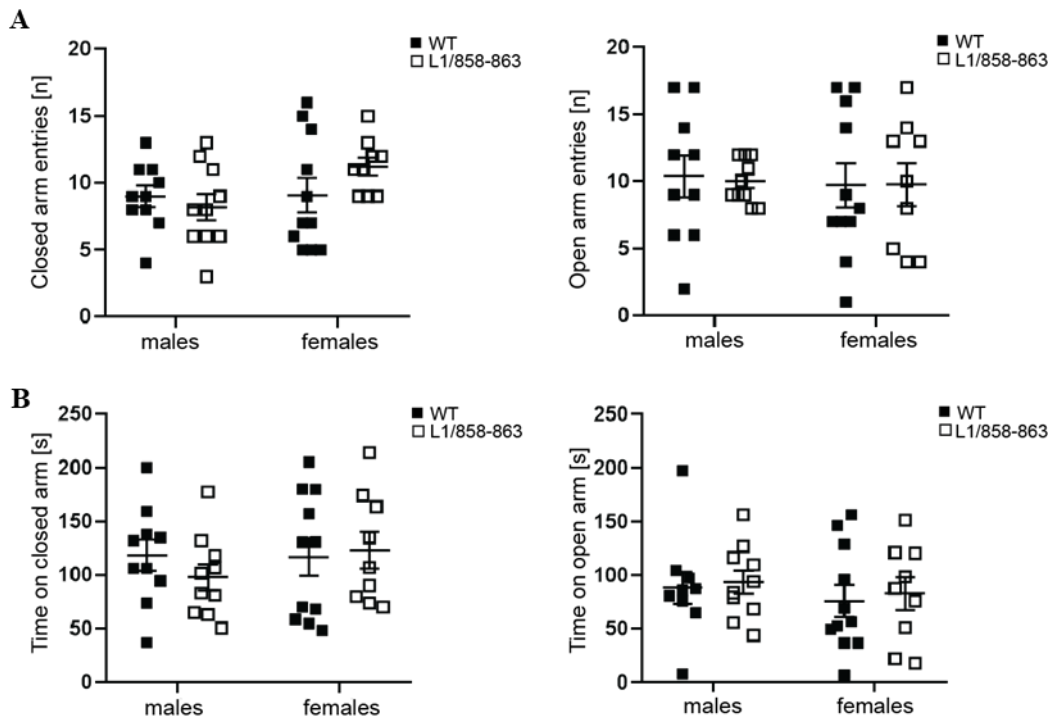


Figure 20. L1/858-863 mice do not show differences in anxiety states in the elevated plus maze. Male and female L1/858-863 mice and their wild-type littermates were subjected to the elevated plus maze and the open and closed arm entries (A) and the time spent in the open and closed arm (B) were determined. Single values and average values with SEM are shown. N = 8-10 mice per group; two-way ANOVA and Tukey's Post Hoc test.

3.8.4 Social interaction

To assess olfaction, memory, and social interest the social interaction test was performed. Mice tend to investigate more intensively unfamiliar mice compared to familiar ones. In this test, social preference is tested by measuring the time mice spend close to familiar versus unfamiliar mice. Male and female L1/858-863 mice and their wild-type littermates stayed at the same distance to the familiar and unfamiliar mouse and only a slightly longer time at the unfamiliar mouse compared to the familiar mouse (Fig. 21a-c). The frequency of visits at the familiar and unfamiliar mouse was similar for L1/858-863 males and their wild-type littermates, while female L1/858-863 mice visited the unfamiliar mouse more often than their wild-type littermates (Fig. 22).

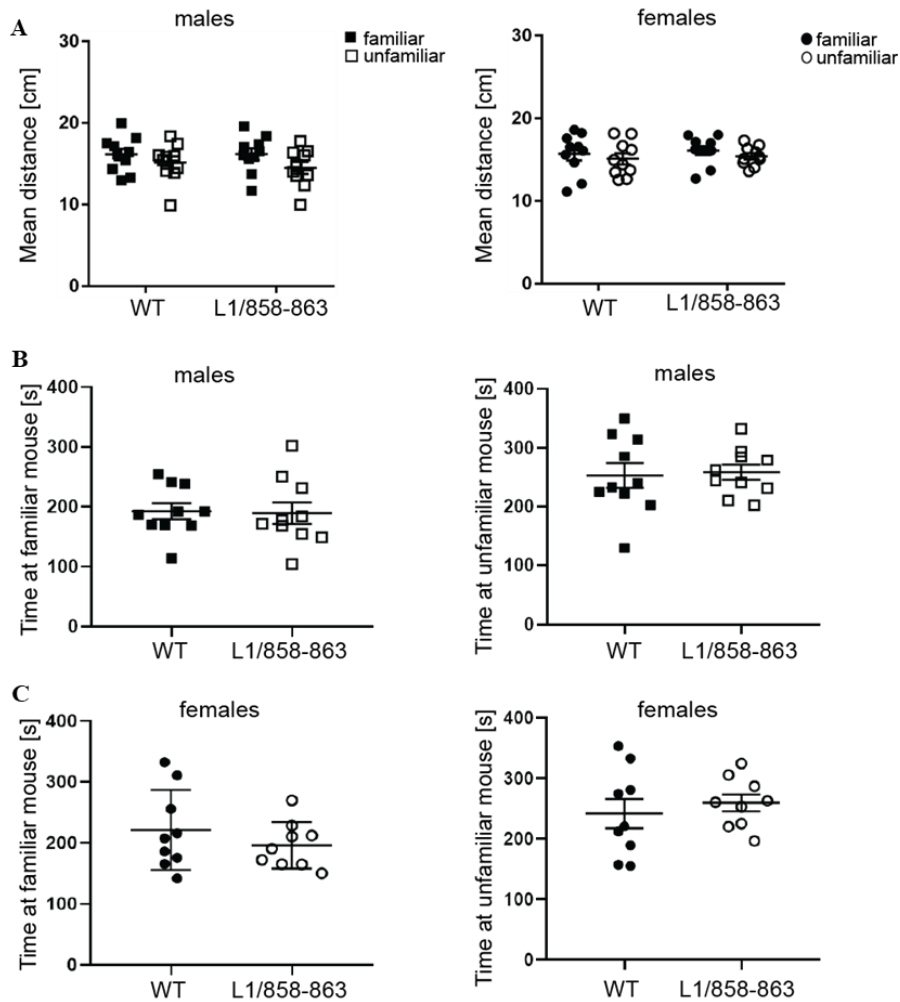


Figure 21. Unaltered social interest of L1/858-863 mice. Male and female L1/858-863 mice and their wild-type littermates were subjected to the social interaction test and distance to the familiar and

unfamiliar mouse (a), and the time spent with the familiar and unfamiliar animal (b, c) were recorded for 10 min. Single values and average values with SEM are shown. N = 8-10 mice per group; two-way ANOVA and Tukey's multiple comparison Post Hoc test.

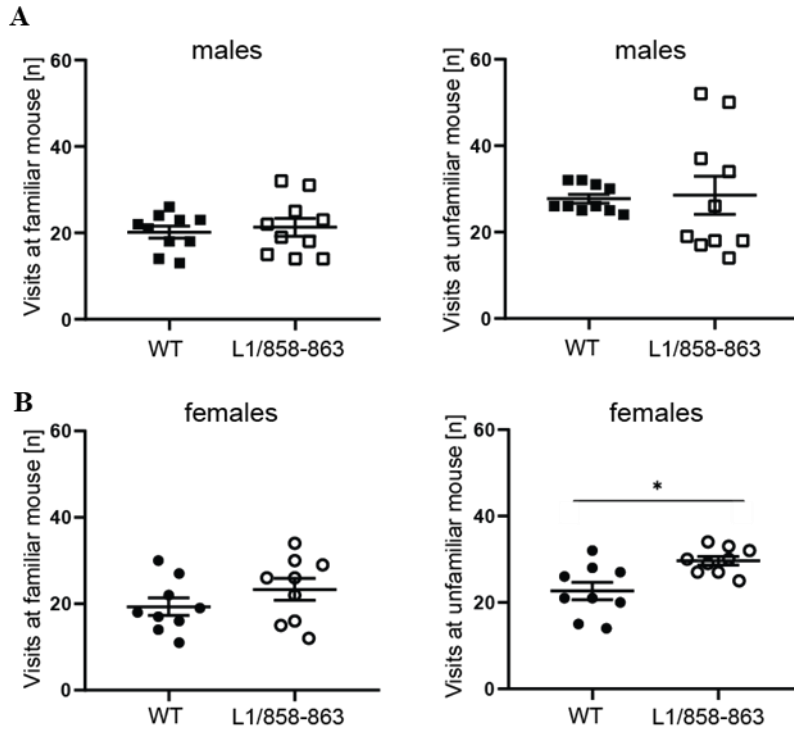


Figure 22. Social interest of L1/858-863 mice. Male and female L1/858-863 mice and their wild-type littermates were subjected to the social interaction test and the frequency of visits of male (a) and female (b) mice at the familiar and unfamiliar mouse was determined after 10 min of the test. Single values and average values with SEM are shown. N = 8-10 mice per group; * $p < 0.05$; two-way ANOVA and Tukey's multiple comparison Post Hoc test.

3.8.5 Circadian activity

The circadian activity of single-housed mice was also measured for 24 h to evaluate their general motor activity. As expected, all mice were more active during the dark phase compared to the light phase (Fig. 23) and male and female transgenic mice did not show differences in activity compared to their wild-type littermates. Results demonstrate that the L1/858-863 mice have a proper circadian rhythm and normal spontaneous behavior in the home cage.

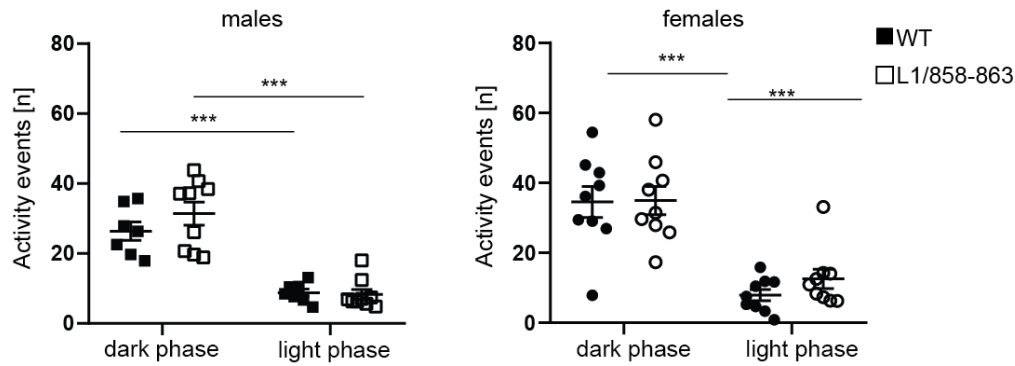


Figure 23. L1/858-863 mice have a normal circadian rhythm and normal spontaneous activity. Activity of male and female L1/858-863 mice and their wild-type littermates was recorded in the home cage for 24 h every 4 min. All mice were more active in the dark phase compared to the light phase and the number of activity events did not differ between genotypes. Single values and average values \pm SEM are shown. N = 8 per genotype; *** p < 0.001; two-way ANOVA and Tukey's multiple comparison Post Hoc test.

3.8.6 Rotarod and pole test

Motor performance of L1/858-863 mice was evaluated to test if they show motor impairments like L1-ko mice and L1-deficient mice transduced to express mutated L1 that could not be cleaved to generate the L1-70 fragment. The L1-deficient mice and mice transduced to express mutated L1 had a lower latency to fall off an accelerating rod compared to wild-type mice and to L1-deficient mice transduced to express wild-type L1 (Kraus et al., 2018a). Here, two-month-old and five-month-old male and five-month-old female L1/858-863 mice were used. On the accelerating Rotarod, transgenic male and female mice showed the same latency to fall from the rotating rod as their wild-type littermates (Fig. 24). Interestingly, especially the two-month-old wild-type males had a higher latency to fall compared to the five-month-old wild-type males, while this effect was not seen for the females. In the pole test no differences between the genotypes were seen and time to climb down and ability to turn 180° was similar in all examined mice (Fig. 25). Results show that L1/858-863 mice do not show impaired motor coordination.

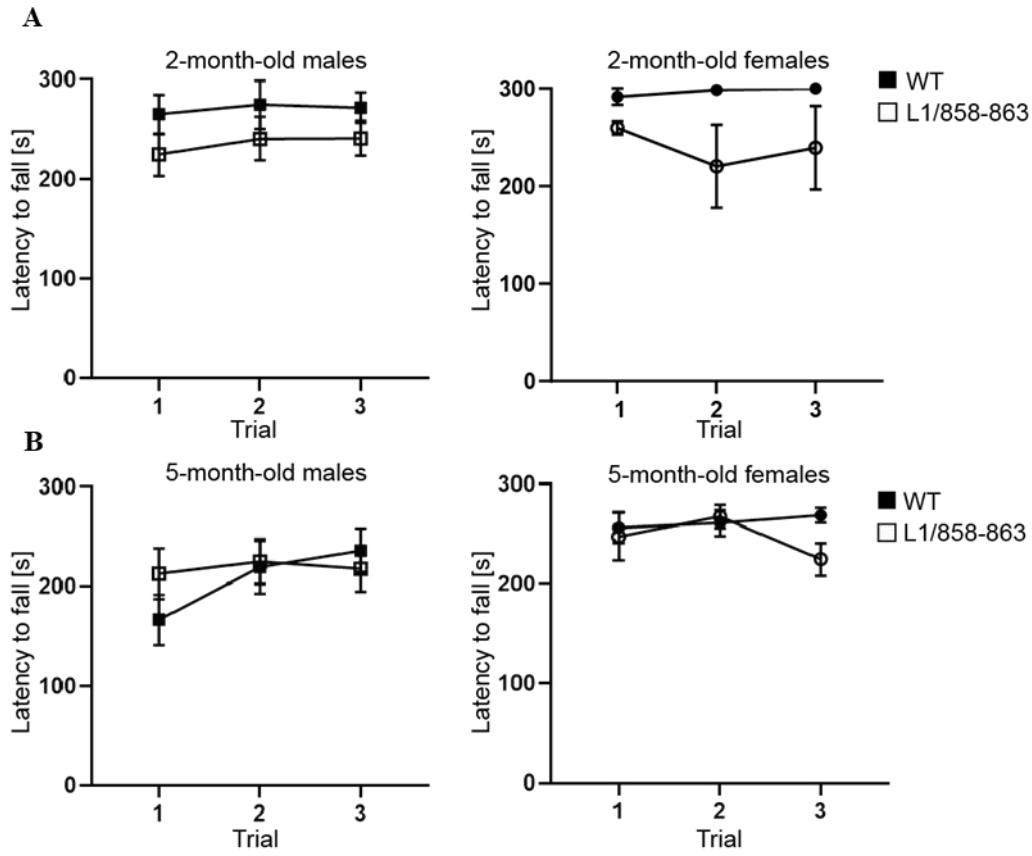


Figure 24. Normal motor performance of L1/858-863 mice in the Rotarod test. Two-month-old male and female L1/858-863 (a) and five-month-old male and female L1/858-863 (b) mice and their wild-type littermates were subjected to the Rotarod test and the latency to fall from the accelerating Rotarod on 3 consecutive trials was determined. Average values \pm SEM are shown; $n = 10$ mice per group; two-way ANOVA RM and Tukey's multiple comparison Post Hoc test.

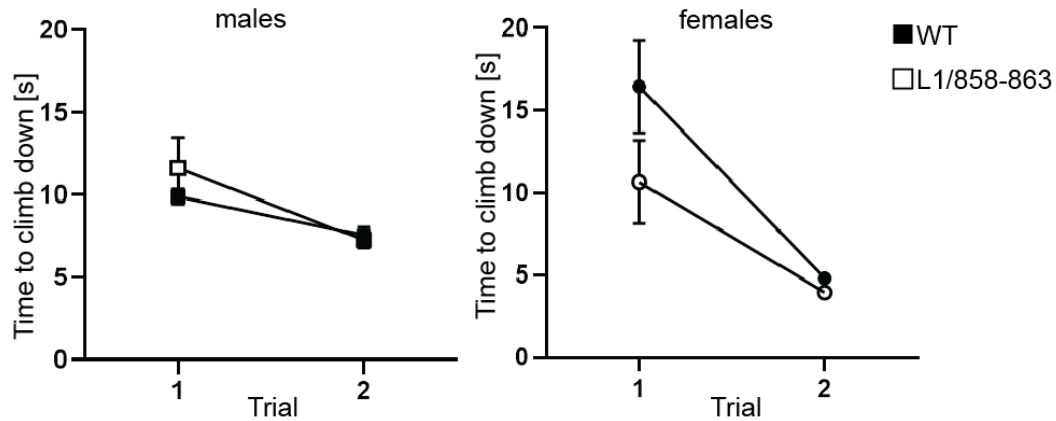


Figure 25. Normal motor performance of L1/858-863 mice in the pole test. Male and female L1/858-863 and their wild-type littermate mice were subjected to the pole test and the time needed to climb down on two consecutive trials was measured. N = 10 mice per group; two-way ANOVA and Tukey’s multiple comparison Post Hoc test.; average values \pm SEM are shown.

3.8.7 Marble burying

Previous studies showed that heterozygous L1-deficient female mice exhibit an increased density of neurons in the neocortex and basal ganglia which could be indicative for an autistic-like phenotype (Schmid et al., 2013). Furthermore, L1 was shown to interact with methyl CpG binding protein 2 (MeCP2) (Loers et al., 2021) and mutations in MeCP2 were shown to cause the Rett syndrome, which is an X-linked autism-spectrum disorder (Good et al., 2021). This suggests that mutations in L1 might also cause autism-spectrum disorder phenotypes. Thus, we performed the marble burying test to detect repetitive, compulsive-like behaviors using L1/858-863 males and females and their corresponding wild-type littermates. This test exploits the species-specific behavior of rodents, i.e., digging or collection, allowing to quantify compulsive manifestations which involve repetitive actions (Dixit et al., 2020). L1/858-863 males buried more marbles as their male wild-type littermates, while female L1/858-863 mice buried the same number of marbles as their female wild-type littermates (Fig. 26). These results show that especially in male individuals the mutation in the dibasic sequence in the 3rd FNIII region of L1 leads to obsessive-like behavior.



Figure 26. Increased marble burying of male L1/858-863 mice. Male and female L1/858-863 mice and their wild-type littermates were subjected to a cage containing 20 black marbles and the number of marbles buried within 30 min was counted. Results show single values and average values \pm SEM; males: $n = 7$; females: $n = 5$; * $p < 0.05$; two-way ANOVA and Tukey's Post Hoc Test.

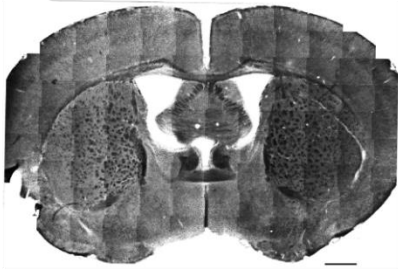
3.9 Morphological analysis

3.9.1 L1/858-863 mice have normal ventricle size and corpus callosum thickness

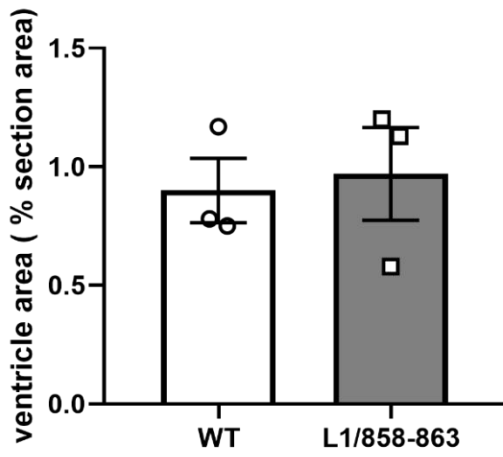
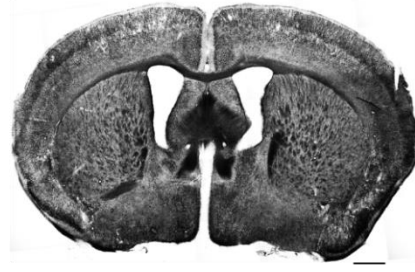
Previous morphological analysis of L1-deficient mice and L1-201 mice revealed several brain abnormalities (Dahme et al., 1997, Cohen et al., 1998, Fransen et al., 1998, Loers et al., 2021), demonstrating that normal L1 processing and functioning is important for normal development of brain structures. To investigate whether L1 mutant mice lacking the L1-70 fragment also present abnormalities of brain structures, histopathological features in L1/858-863 adult male mice were studied by quantification of the brain ventricle size and corpus callosum thickness from coronal brain sections (Fig. 26). The size of the lateral ventricles was normal at different bregma levels. Corpus callosum thickness was measured at the midline and its lateral projection at different bregma levels. The mean thickness at each bregma level was slightly reduced in L1/858-863 male mice compared to male wild-type littermates, but this difference did not reach statistical significance (Fig. 27).

A

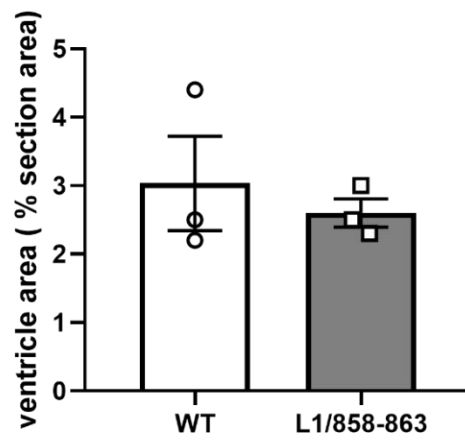
WT



L1/858-863



bregma 0.74



bregma -0.34

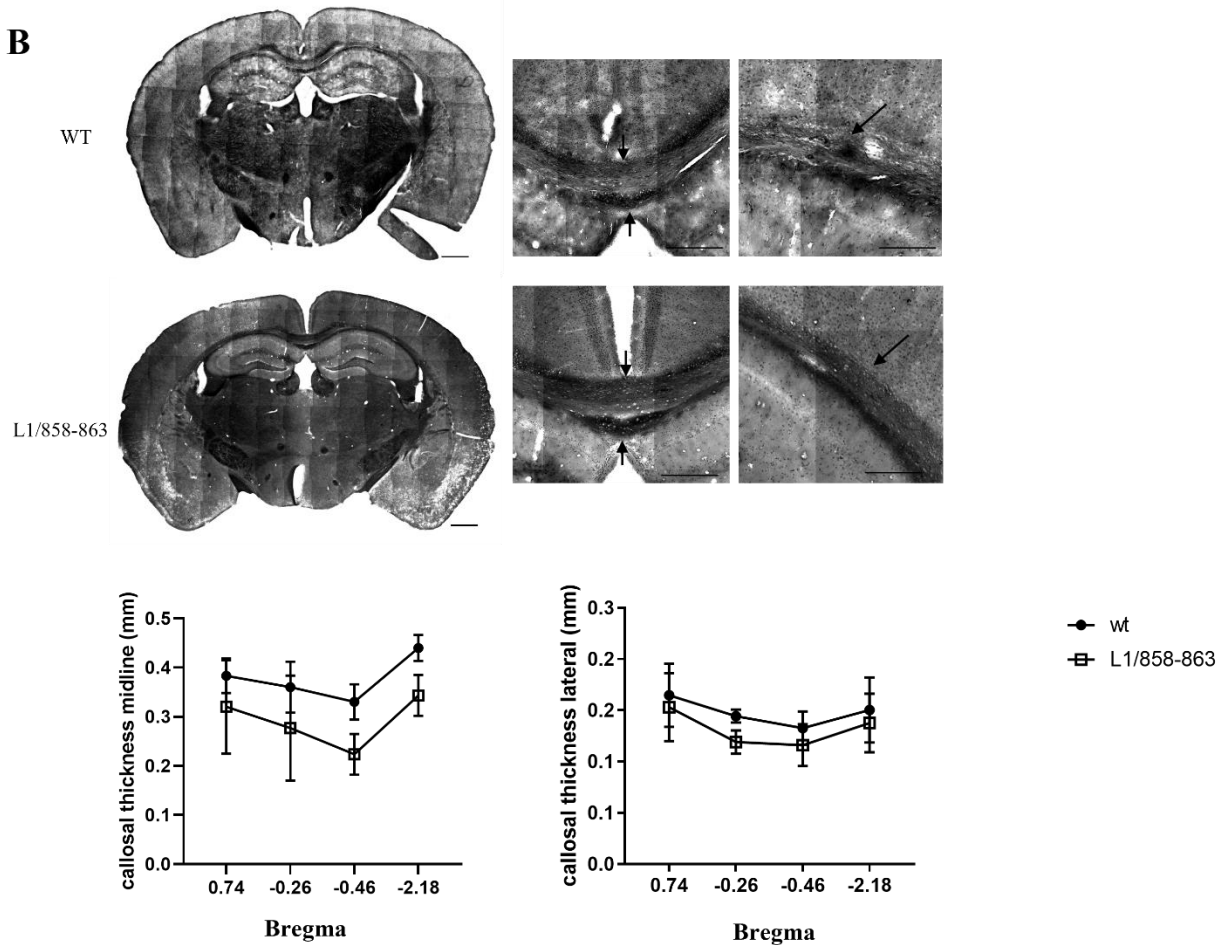


Figure 27. Thickness of the corpus callosum and ventricle size are normal in L1/858-863 mice. Coronal sections from brains of male L1/858-863 mice and their wild-type littermates were stained with Luxol fast blue and Cresyl violet. (A) Representative overview from two different bregmas (-0.34 (A) and -2.18 (B)) and midline and lateral corpus callosum (bregma -2.18, (B)). Scale bars: 250 μ m and 500 μ m. Ventricle size was quantified at bregma 0.74 and -0.34 (A). Arrows point to the corpus callosum. Graphs show callosal thickness from lateral and midline at different bregmas (B). Average values with SEM are shown. N = 3-4 mice per group; two-way ANOVA with Tukey Post Hoc Test for corpus callosum thickness, Mann-Whitney test for ventricle size measurement.

3.9.2 Spine density and spine type determination in L1-201 male mice

Studies of the histopathological features in mice carrying the D201N mutation showed enlarged ventricle size and a marked reduction of corpus callosum thickness (Loers et al., 2021).

Furthermore, behavioral characterization of male L1-201 mice highlights the presence of neurological deficits and increased locomotor activity (Loers et al., 2021). These abnormalities were also detected in L1-deficient mice (Kraus et al., 2018a, Rolf et al., 2020). Therefore, I wanted to go deeper into the study of brain morphology of this L1 mutant line to evaluate if the motor and cognitive impairments result from some changes in the neuronal arborization and dendritic spine density.

For this purpose, coronal section of prefrontal and motor cortex from adult L1-201 and wild-type mice were collected and stained with the Golgi-Cox method for Sholl analysis and evaluation of spine density and discrimination of the single spine type (Fig. 28).

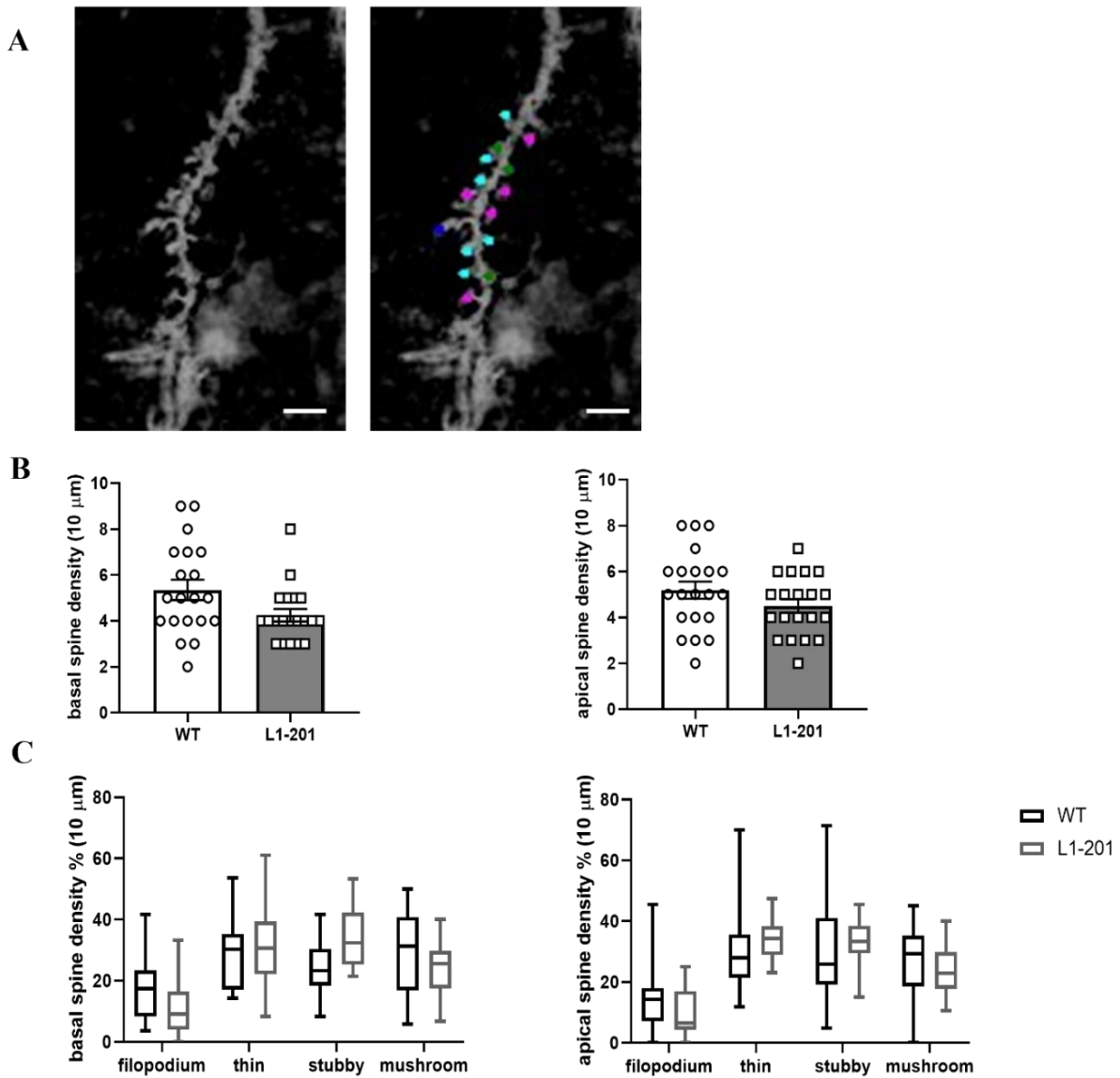


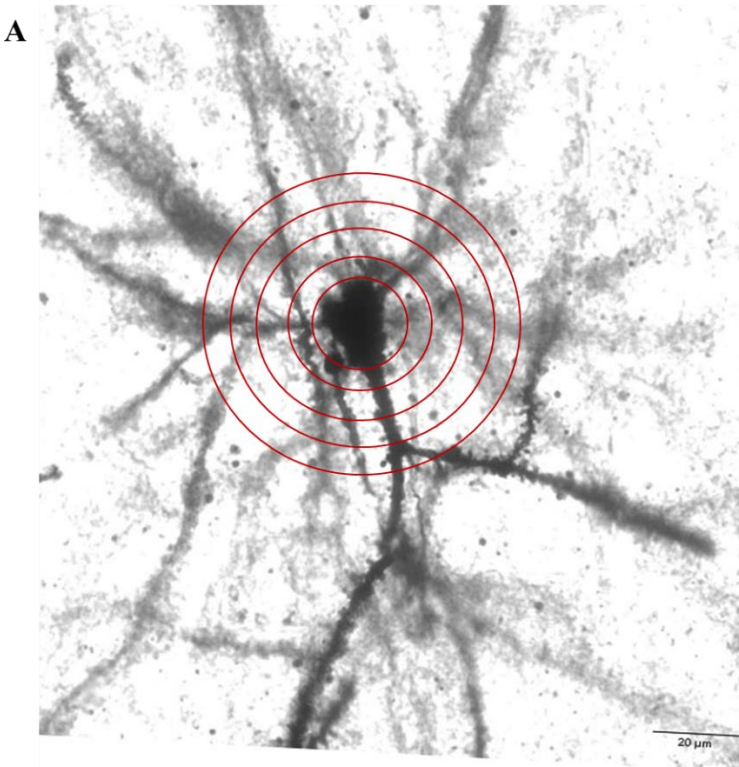
Figure 28. L1-201 mice display no alteration in dendritic spine density and spine type. Golgi-Cox staining of pyramidal neurons from coronal sections of motor and prefrontal cortex of adult L1-201 and wild-type mice was performed. (A) A dendrite and its spines from a L1-201 neuron are shown (scale bars: 10 μm). The different colors in the right image depict the different spine types: filopodium (blue), thin (light blue), stubby (fuchsia), mushroom (green). (B) Graphs show quantification of the spine density per 10 μm dendrite length. (C) Box plots show quantification of single spine types in percentage per 10 μm dendrite length. No difference in the number of spines per 10 μm of dendrite length, as well as no alteration in the number of single spine types were observed (B) Quantification of total number of spines per 10 μm dendrite length. N = 20 dendrites per genotype; n=5 mice per genotype. Mann-Whitney test.

(C) Quantification of spine types (%) per 10 μm dendrite length. N = 20 dendrites per genotype; 5 mice per genotype. Two-way ANOVA.

Density of total spines, as well as the density of the single spine types from L1-201 mice is comparable to the spine density of neurons in the wild-type mice brains, thus the L1-201 mutation does not affect dendritic spine growth and development in the motor cortex.

3.9.3 Normal arborization of dendrites from pyramidal neurons in the prefrontal cortex of L1-201 male mice

Sholl analysis was also performed to evaluate the distribution and ramification of dendrites from pyramidal neurons in the prefrontal cortex. Measurement was done for both apical and basal portions of each neuron per 150 μm dendrite length. Results show no abnormalities in ramification of dendrites in L1-201 neurons compared to the neurons of the control group (Fig. 29).



B

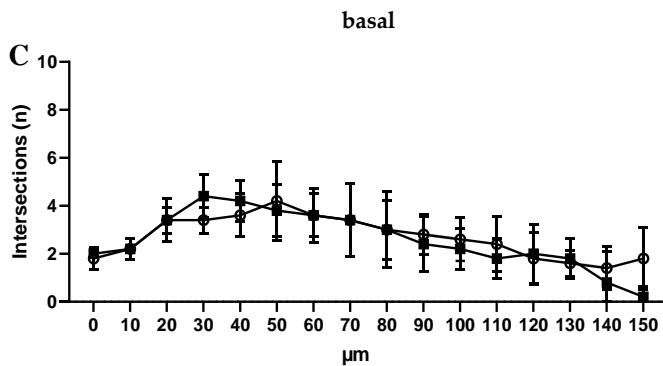
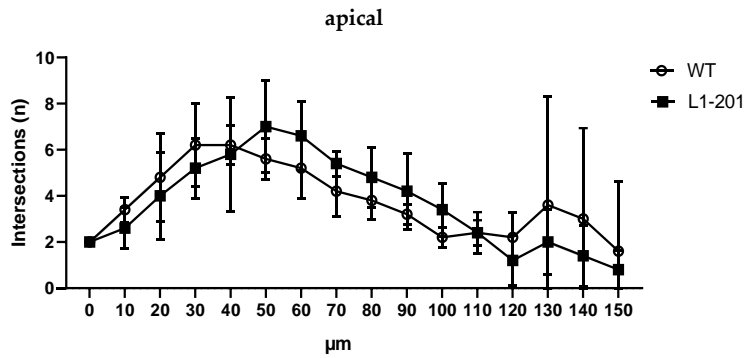


Figure 29. Sholl analysis from pyramidal neurons of the PFC shows no difference in the number of intersections between L1-201 and wild-type mice. (A-C) Golgi-Cox staining of pyramidal neurons from the prefrontal cortex was performed to measure the number of intersections in 150 μm dendrite length in the apical and basal part of the neurons. (A) Representative picture of a pyramidal neuron from a L1-201 mouse with concentric circles used to detect intersections. Scale bar: 20 μm . (B, C) Graphs show number of apical (B) and basal (C) intersections. No difference is present between L1-201 and wild-type neurons. Average values \pm SD, $n=5$ mice per genotype, two-way ANOVA RM.

To conclude, my morphological analysis provides an overview of the dendritic arborization and spine density in both motor and prefrontal cortex from L1-201 and wild-type adult mice. No severe differences were observed for both measured parameters, meaning that mice with L1/D201N mutation that reach adulthood do not develop pathological changes that alter neuronal development and ramification in the PFC.

4. DISCUSSION

My project was focused on the characterization of several functional aspects of different L1 mutant mouse models. The major investigation point was to determine how the L1-70 fragment affects molecular, morphological, and behavioral functions in these different models.

- 1) I first studied the role of L1-70 in mitochondrial dynamics, evaluating how and if absence of this specific fragment is responsible for mitochondrial impairments.
- 2) I also evaluated whether absence of the L1-70 fragment enhances oxidative stress in cells and tissue.
- 3) Brain morphology was analyzed to further investigate the influence of L1-70 during neuronal development.
- 4) Behavioral tests were performed using L1/858-863 mutant mice to characterize the influence of L1-70 on social, cognitive, and motor performance.

Furthermore, the effect of the point mutation D201N, which leads to the L1 syndrome in humans, was studied.

4.1 The L1-70 fragment regulates mitochondrial membrane potential and complex I activity

In previous studies it has been shown that L1-70 is transported from the cytosol to intracellular organelles, such as mitochondria and the nucleus (Kraus et al., 2018a, b). In our laboratory we demonstrated that this 70 kDa fragment, generated by the proteolytic cleavage of L1 by MBP, can interact with NADH dehydrogenase ubiquinone flavoprotein 2 subunit from mitochondrial complex I (Kraus et al., 2018a). L1-deficient mice show a severe impairment of mitochondrial activity characterized by lower membrane potential, lower complex I activity and altered motility (Kraus et al., 2018a). It was hypothesized that lack of L1-70 is responsible for the reduction of complex I activity and mitochondrial membrane potential. The experiments I have performed to confirm this theory show that the mitochondrial membrane potential and complex I activity from L1/858-863 and L1-201 mice are differently impaired depending on the expression of L1-70. Absence of L1-70 leads to a reduced neuronal mitochondrial membrane potential, reduced complex I activity and a strong tendency for lower ATP production, while complex I activity and

ATP levels were normal and the membrane potential was enhanced in neurons of L1-201 mice, demonstrating that L1-70 is indeed a key player in regulating mitochondrial membrane potential and complex I activity (Congiu et al., 2022). Furthermore, stimulation of L1 with L1-agonist compounds duloxetine and tacrine did not alter ATP production in both lines. This is consistent with the fact that there are no significant alterations in the ATP level and so duloxetine and tacrine do not exert any restorative effect.

It is known from previous studies that inhibition of the ETC at the site of complex I induces a depolarization of the mitochondrial membrane potential (Pravdic et al., 2012). Complex I is located in the inner mitochondrial membrane, and it consists of a hydrophobic membrane arm and a hydrophilic peripheral arm that form a L-shaped structure which protrudes into the matrix (Hofhaus et al., 1991, Guénebaut et al., 1997, Friedrich and Bottcher, 2004). The peripheral arm has two independent functions: the electron transfer mediated by the so called N-module (which contains NDUFV2) and the NADH oxidation site that give the electron input, and the electrons transfer mediated by the Q-module, which gives the electron output by transferring electrons to the ubiquinone reduction site (Mathiesen and Hägerhäll, 2002, Sazanov, 2015). A direct interaction between L1-70 and NDUFV2 was previously shown (Kraus et al., 2018a). Therefore, changes of complex I activity could be due to a direct influence of L1-70 on the core subunit of the hydrophilic side of the complex I. The evidence that *in vitro* import of L1-70 into L1-lacking mitochondria enhanced complex I activity (Kraus et al., 2018a) further supports this theory.

Interestingly, while cerebellar neurons from L1-70 lacking mice showed a reduced complex I activity, depolarization of the mitochondrial membrane potential and a trend for lower production of ATP, cerebellar neurons of L1-201 mice show no impairments of complex I activity but a higher mitochondrial membrane potential and a tendency for enhanced ATP production compared to mitochondria from wild-type mice.

Several factors can contribute to hyperpolarization of the mitochondrial membrane. Change of glucose levels (Siewiera et al., 2016) as well as elevated concentrations of intracellular ADP and ATP regulate cytosolic levels of free Ca^{2+} (Szewczyk et al., 1999), which contributes to platelet activation in blood and can alter mitochondrial membrane potential (Varga-Szabo et al., 2009). Furthermore, accelerated substrate oxidation may also result in increased mitochondrial membrane potential and the overproduction of reactive oxygen species (Yamagish et al., 2001).

Higher glucose levels can alter mitochondrial metabolism not only in platelets but also in neurons in a dose dependent manner, leading to a mitochondrial hyperpolarization and higher production of ATP, which is probably due to a change in the quantity or function of complex V (ATP-synthase) (Siewiera et al., 2016).

Mitochondrial dysfunctions are a hallmark of Alzheimer's disease. In fact, a relationship between amyloid precursor protein, amyloid beta and mitochondria is well established (Gabuzda et al., 1994, Devi et al., 2006) as well as a strong correlation between mitochondrial membrane potential, APP mitochondrial localization, and A β secretion (Wilkis et al., 2022). APP and A β localize to mitochondria, where APP blocks mitochondrial translocases and inhibits the import of nuclear DNA-encoded mitochondrial proteins and where A β could be produced by a resident γ -secretase. Next, A β can interact with mitochondrial proteins leading to mitochondrial dysfunctions (Wilkis et al., 2022). A β interacts with a mitochondrial enzyme, A β binding alcohol dehydrogenase, which inhibits NAD⁺ binding (Lustbader et al., 2004). A β also inhibits cytochrome oxidase (COX) activity, reduces ATP production, increases reactive oxygen species levels, and depolarizes the mitochondria. On the other hand, the mitochondrial membrane potential also affects mitochondrial APP targeting. With mitochondrial membrane depolarization more APP localizes to mitochondria and with mitochondrial membrane hyperpolarization less APP localizes to mitochondria (Wilkis et al., 2022). Elevated levels of L1 were detected in the cerebrospinal fluid of patients with AD, vascular dementia and dementia of mixed type (Strekalova et al., 2006). It has been reported that adeno-associated viral mediated overexpression of L1 in neurons and astrocytes results in a reduction of amyloid plaque load, decreases astrogliosis and leads to a better preservation of inhibitory synaptic terminals on pyramidal cell bodies in the hippocampus (Djogo et al., 2013). L1 is able to exert this action due to its ability to directly bind to A β via the FN domains, thus suggesting that stimulation of L1 functions might be beneficial for the clinical treatment of AD (Djogo et al., 2013).

Altogether, we find ourselves faced with two opposite scenarios regarding the functional damage of complex I and the mitochondrial membrane potential. While the absence of L1-70 might explain the functional impairments of mitochondria in L1/858-863 mice, further investigations are required to understand what causes the over-activation of mitochondria in the L1-201 mice.

Interestingly, these two different kind of impairments lead to the same result: enhanced oxidative stress and higher production of reactive oxygen species in cerebellar neurons.

4.2 L1-70 fragment is not responsible for the increased oxidative stress in both L1-201 and L1/858-863 neurons

Previous studies revealed that an impaired membrane potential is linked to an unhealthy status of mitochondria and that complex I is the main source of ROS in mitochondria under a pathological status (Jung et al., 2020). When their function is impaired, mitochondria contribute to severe pathologies of the nervous system, including Alzheimer's disease, Parkinson's disease, motor neuron disease and Huntington's disease (Jung et al., 2020). Under pathological conditions, mitochondria extensively generate ROS or/and are targeted by free radicals, with the highest basal rate of ROS production being in the brainstem and cerebellum (Vinokurov et al., 2021).

As mentioned above, L1/858-863 and L1-201 mice showed mitochondrial dysfunction culminating in a significant increase of ROS production in cerebellar neurons. However, my results highlight that enhanced oxidative stress is probably present only in primary neurons. When I went to investigate whether the oxidative stress affects also the whole brain, I found that 10-day-old brains from both L1/858-863 and L1-201 mutant lines present a higher, although not statistically significant concentration of thiobarbituric acid-reactive species, while no differences were observed in the brains from L1/858-863 and L1-201 adult mice. This result suggests that oxidative stress occurs only in the cerebellum, where the number of glial cells that could degrade the ROS and protect the neurons is very low, and thus different mutations of L1 do not affect ROS production in the whole brain.

It has been reported that in L1 syndrome individuals, the phenotypic expression of the hydrocephalus is very heterogeneous and an intrafamilial heterogeneity in carriers of L1CAM mutations has been observed (Serville et al., 1992). This heterogeneity might also explain why some individuals do not develop severe mitochondrial impairments and have better chances to survive. Furthermore, this heterogeneity is also seen in mice. L1-deficient and L1-201 mice bred and maintained on C57Bl6 background have massively enlarged ventricles and die at a higher rate than L1-deficient mice and L1-201 mice on 129 background.

The rate of ROS production, mitochondrial membrane potential and the activity of the complexes of the ETC are interdependent (Votyakova and Reynolds, 2001). Therefore, dissipation of the mitochondrial membrane potential could increase ROS generation when respiration is inhibited. At the same time, hyperpolarization of mitochondria could also lead to an increase in ROS production. Thus, the production of ROS in the ETC depends on the release of electrons out of the electron transport chain followed by the formation of free radicals. The process of the release of electrons could be induced by the reverse flux of electrons and the activity of complexes I and II as donors of electrons and partial inhibition of the complexes by hyperpolarization of the mitochondrial membrane, ischemic conditions, or chemical compounds (Angelova and Abramov, 2016). Despite the fact that the respiratory chain is a major ROS producer in mitochondria under resting conditions, several matrix proteins and complexes, including enzymes of the tricarboxylic acid cycle (e.g., aconitase, pyruvate dehydrogenase and α -ketoglutarate dehydrogenase), could produce free radicals such as O_2^- (Gibson et al., 2015, Starkov et al., 2004). Some inner mitochondrial membrane proteins (various cytochrome P450 enzymes, glycerol-3-phosphate dehydrogenase) can regulate ROS production depending on the mitochondrial membrane potential. Furthermore, outer membrane enzymes and proteins, such as enzyme monoamine oxidase and cytochrome b5 reductase, use monoamines to produce aldehydes, hydrogen peroxide and other ROS (Angelova and Abramov, 2016).

Redox balance in the mitochondrial matrix is maintained by an effective antioxidant system comprising manganese superoxide dismutase (MnSOD) in the mitochondrial matrix, copper- and zinc-containing superoxide dismutase (Cu,Zn-SOD) in the intermembrane space, and catalase and glutathione peroxidase (GPx). The SODs convert superoxide radicals into hydrogen peroxide and molecular oxygen (O_2), while the catalase and peroxidases convert hydrogen peroxide into water and in the case of catalase to oxygen and water (Weydert et al., 2010). SODs and catalase do not need co-factors to function, while GPx not only requires several co-factors and proteins but also has five isoenzymes. In the glutathione system, glutathione reductase and glucose-6-phosphate dehydrogenase do not act on ROS directly, but they enable the GPx to function. The permeable H_2O_2 participates in signaling cascades and it is removed by the enzymes catalase, glutathione peroxidase and peroxiredoxin 3 (Forman et al., 2010, Mukherjee et al., 1982).

I speculate that one of the reasons why I observed an increase in oxidative stress in neurons from L1-201 mice could be found in a possible malfunction of the above-described antioxidant system.

In addition, stimulation with duloxetine was able to reduce ROS production in neurons from both mutant lines. Since its effect was similar when L1-70 was expressed or not, it is likely that this compound does not require the production of L1-70 in the cells to mediate a protective effect. Duloxetine can exert its neuroprotective activity through the modulation of the transient receptor potential Mu and the transient receptor potential vanilloid 1 which regulate the entry of Ca^{2+} and they are also activated by ROS (Demirdas et al., 2016). Furthermore, duloxetine can also modulate the phosphatidylinositol 3-kinase/protein kinase B/NF-E2-related factor-2/heme oxygenase 1 pathway, which leads to an increased production of brain-derived neurotrophic factor (Engel et al., 2018). In addition, L1 signaling is triggered by treatment of cultured neurons with duloxetine and the expression of full-length L1 and L1-70 were enhanced in neurons after duloxetine application (Kataria et al., 2016). Thus, duloxetine could also exert its neuroprotective action by enhancing L1 expression and by triggering of L1 signaling which is also known to activate phosphatidylinositol 3-kinase (Loers et al., 2005).

Lastly, mitochondrial homeostasis and metabolism are monitored by AMPK, which controls various aspects of the mitochondrial life cycle, from biogenesis and dynamics to removal by mitophagy. Under low energy conditions, AMPK phosphorylates specific enzymes to increase ATP generation and decrease ATP consumption, ensuring optimal mitochondrial function (Herzig and Shaw, 2018). Almost every mitochondrial insult or defect activates AMPK, including respiratory chain complex inhibitors such as the diabetes drug metformin, the Parkinson disease-causing herbicide rotenone, proton ionophores, ATP synthase inhibitors and mitochondrial DNA depletion or mutation (Herzig and Shaw, 2018). Given the importance of AMPK in controlling mitochondrial homeostasis, I evaluated if changes of the ratio between AMPK and its phosphorylated form could be one of the causes of mitochondrial dysfunctions in L1-201 mice. My results revealed that there was no significant difference in the pAMPK/AMPK ratio, suggesting that other metabolic pathways are responsible for mitochondrial function impairments in this L1-mutant line. It remains to be evaluated whether the absence of the L1-70 fragment can alter AMPK activity.

4.3 L1-70 fragment absence reduces mitochondrial motility but is not responsible for the increased retrograde transport of mitochondria

Regions with high energetic requirements, such as growth cones and presynaptic terminals, contain a higher number of mitochondria compared to other cellular compartments. Mitochondria move bidirectionally: anterogradely, from the cell soma to distal axons and synaptic terminals, and retrogradely, from the distal axons back to the soma, where they are degraded (Kim et al., 2007). When they reach the synaptic terminals, mitochondria remain stationary to support synaptic transmission by supplying ATP and buffering Ca^{2+} . Throughout their movements in the axon, mitochondria can quickly switch between anterograde and retrograde movement, and their net direction in cultured neurons results primarily from the modulation of the fraction of time spent moving anterogradely (Morris and Hollenbeck, 1993). Cerebellar neurons from the three L1 mutants tested in my study exhibited more retrogradely moving mitochondria, suggesting that these mitochondria were less healthy. Since lack of L1-70 and the D201N mutation lead to a similar phenotype, the enhanced retrograde transport is not caused by the lack of L1-70 in the neurons. In contrast, the percentage of static mitochondria is significantly higher in L1/858-863 and L1/687 neurons compared to the wild-type neurons while neurons from L1-201 mice do not show any alteration regarding the mobility of mitochondria. It is thus likely that the L1-70 fragment is indeed a regulator of mitochondrial motility, since its absence leads to an enhancement of static mitochondria not only in the L1/858-863 and L1/687 mice (Congiu et al., 2022), but also in L1-deficient mice (Kraus et al., 2018a).

The variability between mitochondrial speeds in the three mutant lines does not allow a final conclusion. In general, I hypothesize that L1-70 is not the only element that regulates the speed of mitochondria, taking into account that in its absence mitochondrial velocity is only slightly reduced compared to that of wild-type mitochondria, while mitochondria from L1-201 neurons are faster compared to those of their wild-type littermates. Interestingly, in contrast to mitochondria of L1-70 lacking neurons from L1/858-863 and L1/687 mice, mitochondria of L1-deficient mice show a reduction in velocity (Kraus et al., 2018a), which suggests that other fragments of L1 or full-length L1 influence mitochondrial velocity. Furthermore, it has been shown that a decreased activity of complex I results in a decreased percentage of moving mitochondria and reduced mitochondrial velocity (Koopman et al., 2007). Here, although complex I activity is reduced, L1-70 lacking neurons do not show alterations in the percentage of

moving mitochondria and only a trend towards reduced velocity. In L1-201 neurons activity of complex I is not significantly altered, and this is consistent with the fact that also motility of L1-201 mitochondria is normal. However, further investigations are required to explain why L1-201 mitochondria have an enhanced velocity.

Duloxetine showed therapeutic properties in enhancing neuronal migration and survival, as well as neurite outgrowth of L1-201 cerebellar neurons, and process formation of L1-201 Schwann cells in culture (Loers et al., 2021). Here, I demonstrated that this compound also ameliorates mitochondrial motility impairments in both L1-201 and L1/858-863 neurons. In L1-201 and L1/858-863 neurons, stimulation with duloxetine enhances the percentage of anterograde moving mitochondria. Furthermore, in L1/858-863 neurons duloxetine is also able to restore a normal balance between the percentage of mobile and static mitochondria. However, further experiments are required to understand through which mechanism this compound exerts its therapeutic action on mitochondria.

4.4 Morphological and histological features of L1-201 mutant mice

Behavioral and histological characterization of male L1-201 mice showed neurological deficits, increased locomotor activity, reduction of corpus callosum thickness, and enlarged ventricles (Loers et al., 2021). Therefore, L1-201 mice display the major pathological features of L1 syndrome, similar to L1-deficient mice (Cohen et al., 1998, Dahme et al., 1997).

A well-known correlation between L1 and Schwann cell function has been established (Haney et al., 1999). In the peripheral nervous system, L1 is indeed expressed in axons and Schwann cells during embryonic and early postnatal development and remains expressed by non-myelinating Schwann cells in the adult (Faissner et al., 1984, Nieke and Schachner, 1985, Martini and Schachner, 1986, and 1988). Here, results highlight a significant reduction of process formation in Schwann cells from L1-201 mice, showing that the D201N mutation affects this specific function in L1-201 expressing Schwann cells. Normal process formation can be restored by stimulation of Schwann cells with the L1-stimulating antibody 557 and the L1 agonist duloxetine, thus demonstrating the high therapeutic potential of duloxetine in rescuing the defective phenotype caused by mutations in L1.

In addition, morphological analysis of the PFC and motor cortex showed no alterations in the dendritic arborization and in the total spine density and single type spine density of pyramidal neurons. This means that mice carrying the D201N mutation do not develop morphological damages of the pyramidal neurons in the PFC and motor cortex, which are persistent till adulthood.

Interestingly, an intrafamilial heterogeneity regarding the different size and lack of hydrocephalus has been observed in boys carrying the D202 mutation (Christaller et al., 2017, Shaw et al., 2015, Sztriha et al., 2002). However, stenosis of the aqueduct of Sylvius, which has been considered as the major cause of congenital hydrocephalus, was not found in L1-deficient mice despite ventricle dilatation (Fransen et al., 1998). Differences in ventricle size in L1-deficient mice might be related to a variability of the genetic background. These different phenotypes can be caused by defective axonal projections through the corpus callosum, which leads to neuronal cell death, reduction of the gray matter and enlarged ventricle size (Loers et al., 2021).

It is also important to consider the fact that the survival rate of L1-syndrome individuals is extremely low, depending on the severity of the signs and symptoms. Severely affected individuals may survive only a short time after birth, while those with mild features live into adulthood. We can thus assume that L1-201 mice that reach adulthood might present mild features that increase their chances of survival. It would be interesting to evaluate dendritic arborization and spine density in young mutant mice, to investigate the presence of age-related impairments or compensatory effects.

4.5 Morphological characterization of adult L1/858-863 mice

Several studies showed changes of corpus callosum thickness and ventricle size in L1-deficient and L1-201 mice (Dahme et al., 1997, Cohen et al., 1998, Fransen et al., 1998, Loers et al., 2021). L1-ko mice exhibit enlarged ventricles and reduced corpus callosum thickness, while L1-201 brains have a markedly enlarged third ventricle and not significantly increased lateral ventricles (Loers et al., 2021). In addition, the mean thickness of the corpus callosum is reduced in male L1-201 mice compared to male wild-type littermates. The neurological and cognitive

symptoms of the L1-syndrome are probably caused by alterations in these morphological features, highlighting the importance of L1 for a normal brain development. Analysis of ventricle size and corpus callosum thickness of L1/858-863 mice showed no severe changes of morphology of these two structures at different bregmas, suggesting that L1-70 is not important for maintenance of ventricle size and development of the corpus callosum.

4.6 Behavioral characterization of adult L1/858-863 mice

In previous studies from our group, it has been shown that stimulation of L1 signaling leads to the generation of a 70-kDa L1 fragment by the serine protease myelin basic protein, which cleaves L1 at Arg687 (Lutz et al., 2012, Lutz et al., 2014a). This fragment is then imported into the cell nucleus and involved in regulating L1-dependent functions (Lutz et al., 2014a). The murine L1 contains an LXXLL motif (L1136LILL) in the transmembrane domain and an FXXLF motif (F1046HILF) in the fifth fibronectin type III repeat. It has been found that both motifs are present on the L1-70 fragment (Kraus et al., 2018b) and that they mediate and affect the interaction of co-activators and co-repressors with nuclear receptors (Smirnov, 2022, Gronemeyer et al., 2004, Bain et al., 2007). Our group demonstrated that the nuclear receptors ER α and ER β , PPAR γ , and RXR β interact with L1-70, and provided evidence that the lack of interaction of nuclear L1 with nuclear receptors is associated with malformation of synaptic contacts in the cerebellum and with dysfunctions in motor coordination and learning (Kraus et al., 2018b).

ER α and ER β are nuclear receptors belonging to the Class I, which includes the steroid receptor family, such as receptors for progesterone, estrogen, androgen, glucocorticoid, and mineralocorticoid. They mediate many of the effects of estradiol, which is an important regulator of the functions and plasticity of the adult central nervous system, and they affect important developmental processes such as proliferation, migration, synapse formation, and apoptosis (Hedges et al., 2012). Estradiol is synthesized in several brain areas, where it plays a key role in the regulation of memory, cognition, behavior, mood, and synaptic plasticity (Gillies et al., 2010, Azcoitia et al., 2011). In the cerebellum, estradiol directs cerebellar development, and affects cerebellar glutamatergic neurotransmission, and locomotor abilities, as well as other cerebellar functions (Hedges et al., 2012). In addition, estradiol plays a beneficial role in aging by

improving balance, coordination, and mobility of post-menopausal women. It also exerts a neuroprotective action in neurological disorders, such as Alzheimer's disease, Friedreich's ataxia, and premenstrual dysphoric disorder (Hedges et al., 2012).

Peroxisome proliferator-activated receptors (PPARs) and receptors for thyroid hormone, vitamin D, and retinoic X acid (RXRs) are nuclear receptors belonging to the Class II of the thyroid/retinoid family. PPARs act as heterodimers with RXRs and play an important role in the regulation of lipid metabolism and PPARs and RXRs are both expressed in cerebellar granule cells (Kainu et al., 1994, Moreno et al., 2004). Retinoic acid is essential for central nervous system development and the lack of retinoic acid or defective retinoic acid signaling via RXRs is involved in neurodegeneration and it is linked to Alzheimer's disease (Corcoran et al., 2004). Malfunctions of PPARs and RXRs are also associated with neurological and psychiatric disorders, such as attention deficit hyperactivity disorder, bipolar disorders, and autism spectrum disorders (Schuchardt et al., 2010).

Based on the evidence that deficiency of L1 or ablation of the LXXLL and FXXLF motifs present in the L1-70 fragment induce impairments of motor performance and learning (Kraus et al., 2018b), I hypothesize that mutation in the dibasic sequence of L1 exchanging wild-type RKHSKR for mutant SKHSSS in the 3rd FNIII region would also affect behavior of mice. Moreover, since the interaction of L1-70 with ERs and PPARs/RXRs might modulate estradiol action and affect neurological functions, and since estradiol is regulating cognitive and behavioral performances, cognitive and social skills were tested in adult L1/858-863 mice from both genders.

4.6.1 L1/858-863 female mice show alterations in their anxiety state

Female L1/858-863 mice spent more time in the center of the open field and stayed at a larger distance from the wall, which could hint at a reduced anxiety of L1/858-863 females. Male L1/858-863 mice did not differ from their wild-type littermates in the open field test and velocity and distanced moved in the open field was similar in L1/858-863 males and females compared to the wild-type mice of the same sex. Furthermore, open and closed arm entries and risk assessment in the elevated plus maze were similar in L1/858-863 males and females compared to

their wild-type littermates. Taken together, my data highlight that locomotion of mutant male and female mice is normal and show that L1/858-863 females exhibit reduced anxiety behavior, while L1/858-863 males show unaltered anxiety.

Although differences in behavior of male and female mice are known and always need to be taken into account, in this case the difference regarding the anxiogenic status of transgenic females might not be related to lack of L1-70. Different phases of the estrus cycle or hormone level fluctuations might explain why mutant females were less anxious compared to the wild-type females, but whether absence of the L1-70 fragment underlies this difference is not clear.

4.6.2 L1/858-863 male mice show altered activity in the marble burying test

In humans and mice, mutations in the X chromosome-linked gene L1 cause severe neurological defects in males. Nevertheless, L1 heterozygous female mice with one functional copy of the L1 gene show complex morphological features that are different from L1-deficient males and wild-type littermate mice (Schmid et al., 2013). It has been found that L1 heterozygous mice express an autism-like phenotype, comprised of reduced social behaviors and excessive self-grooming. L1 heterozygous mice also exhibited an increase in sensitivity to light, assessed by a reluctance to enter the lighted areas of novel environments. However, levels of anxiety, stress, motor abilities, and spatial learning in L1 heterozygous mice were similar to those of wild-type mice (Sauce et al., 2015). In addition, a correlation between L1 and autistic-spectrum disorders might be possible due to the interaction of L1 with MeCP2, whose mutation can lead to an autistic phenotype (Good et al., 2021, Kleene et al., 2023, Loers et al., 2021).

My results from the marble burying test show no differences in behavior of the transgenic female mice, while L1/858-863 males buried more marbles compared to their wild-type littermates. Although this test has been used so far to evaluate obsessive-like behaviors and stress-related manifestations, this connection has been recently questioned (Brouwer et al., 2019, Dixit et al., 2020). Therefore, my results could also be interpreted in terms of hyperactivity of L1/858-863 males. Since locomotion of L1/858-863 males in the open field and elevated plus maze was normal, it is likely that the mutant males show an obsessive-like behavior rather than hyperactivity. This increased activity in the marble burying test observed in mutant males might

be explained by the role of L1-70 in modulating neurological functions through its interaction with PPARs and RXRs. We can hypothesize that absence of L1-70 can affect the normal function of these two nuclear receptors, thus leading to neurological defects. However, further investigations are required to test this theory since female mice lacking L1-70 did not show alterations.

4.6.3 Normal social interest of L1/858-863 mice

Social performance of L1/858-863 mice from both genders was evaluated to determine if olfaction, memory, and social interest were affected by the absence of L1-70.

Normally, mice have a preference for a new stimulus (objects, places, unfamiliar mice). In the social interaction test, I observed a normal social performance from mice of both sexes, measured as time spent with the familiar and the unfamiliar mouse and number of visits to the familiar and unfamiliar mouse cage. The only difference was detected for L1/858-863 females, which prefer to visit the unfamiliar mouse more often compared to their wild-type littermates. All taken, absence of L1-70 fragment does not alter the social-related skills of these mice.

4.6.4 Lack of L1-70 fragment does not influence motor performance and general motor coordination

L1/858-863 and wild-type male and females mice at two different ages (5-month-old and 2-month-old) were tested to analyze their motor abilities and learning skills. First, evaluation by the grip strength test and the beam-walking test highlights that for both genders and genotypes muscles strength and balance are normal. Next, motor coordination was evaluated by the rotarod and the pole test.

Results from the rotarod test show no severe impairments of motor skills in male and female transgenic mice of different age. Even though, two-month-old male and female L1/858-863 mice have a slightly non-significant lower latency to fall compared to their wild-type littermates.

Pole test results show no difference between genotypes and genders at both ages considered.

Finally, circadian rhythm and general activity were assessed, and results show normal activity of these mice. Since all tests with exception of the marble burying test did not show signs of hyperactivity in transgenic mice it is conceivable that transgenic males show compulsive-like behavior.

As mentioned above, motor and balance impairments occur in L1-deficient mice and L1-deficient mice transduced with AAV1 coding for mutated L1 which cannot be cleaved by MBP (Kraus et al., 2018b). Ablation of L1 and mutations of the intracellular part of L1 lead to impaired balance and motor performance (Fransen et al., 1998, Nakamura et al., 2010). Furthermore, L1-deficient mice have a lower latency in falling off the accelerating rotarod than wild-type mice, and their performance does not improve over the consecutive trials. L1-deficient mice transduced with AAV1 coding for mutated L1 did not increase their performance level as compared to the level of L1-ko mice. In the pole test, L1-deficient mice needed more time to climb down from the top of a vertical beam than wild-type mice and repeatedly fell off the top of the pole. L1-deficient mice transduced with AAV1 coding for mutated L1 performed as bad as the L1-deficient mice, but unlike them, they did not show any learning skills during the consecutive trials (Kraus et al., 2018b).

In conclusion, it is possible that L1-70 is not the only element involved in the regulation of motor activity. Indeed, decreased performances on the rotarod and in the pole test are visible when L1 is not expressed, while the D201N mutation leads to increased locomotor activity. I hypothesize that mutation of the dibasic sequence in the 3rd FNIII region leads to a less severe phenotype due to the activation of compensative mechanisms.

Finally, my results from the morphology evaluation are extremely helpful to also explain why motor and cognitive performances, that are strongly compromised in L1-deficient and L1-201 mice (Kraus et al., 2018a, Loers et al., 2021), are normal in adult L1/858-863 mice.

5. SUMMARY

Adhesion molecules regulate cell adhesion, proliferation, migration, survival, neuritogenesis, synapse formation and synaptic plasticity during nervous system development and in the adult. Among such molecules, the neural cell adhesion molecule L1 contributes to these functions. Proteolytic cleavage of L1 by different proteases is essential for these functions. A proteolytic fragment of 70 kDa comprising part of the extracellular domain and the transmembrane and intracellular domains was shown to interact with mitochondrial proteins and is suggested to be involved in mitochondrial functions. Furthermore, a mutation of aspartic acid at position 201 in the extracellular part of murine L1, has been shown to be responsible for an L1-syndrome phenotype in mice. In my study, I report that L1-201 mice show higher mitochondrial membrane potential, normal complex I activity and ATP levels, as well as enhanced retrograde mitochondrial transport and higher levels of reactive oxygen species. In contrast, mitochondria from L1-70 deficient mice exhibit a lower mitochondrial membrane potential, lower ATP levels, enhanced retrograde transport and reduced complex I activity as well as enhanced production of reactive oxygen species, compared to mitochondria from their wild-type littermates. In addition, stimulation with the L1-agonist compound duloxetine rescued the defective phenotype of mitochondria in both L1-201 and L1/858-863 cerebellar neurons by enhancing anterograde transport and the percentage of mobile mitochondria, and by decreasing the ROS production. Analysis of the oxidative stress status of the brain in L1-201 and L1/858-863 young and adult mice showed no enhanced lipid peroxidation and the ratio between phospho-AMPK and total AMPK in the L1-201 brains is normal.

Morphological and histological characterization of L1-201 mice show that L1-201 Schwann cells exhibit an impairment in process formation that can be ameliorated with the L1 mimetic duloxetine. Golgi staining of coronal sections of the prefrontal cortex and motor cortex from adult L1-201 mice reveal normal arborization of pyramidal neurons and normal density of dendritic spines as well as normal density of the single spines type.

I also measured ventricle size and corpus callosum thickness of adult L1/858-863 mice to further investigate the presence of L1-syndrome features in this L1 mutant line. Results show no changes of the morphology of these brain structures.

Finally, behavioral assessment shows an enhanced obsessive-like behavior in adult male L1/858-863 mice and reduced anxiety in L1/858-863 females while social and motor performances as well as circadian activity were normal in transgenic male and female mice.

Altogether, the present study reveals the importance of the L1-70 fragment for mitochondrial homeostasis. However, absence of L1-70 does not affect the development of brain structures or motor performances in adult male and female mice. Mutation of the dibasic sequence in the 3rd FNIII region could induce an obsessive-like behavior in males, suggesting a possible correlation between L1-70 and autism-spectrum disorders. Importantly, my data suggest that different mutations of L1 may lead to enhanced oxidative stress of neurons and cell death, thus increasing the risk to develop neurodegenerative pathologies.

6. ZUSAMMENFASSUNG

Adhäsionsmoleküle regulieren Zelladhäsion, Proliferation, Migration, Zellüberleben, Neuritogenese, Synapsenbildung und synaptische Plastizität während der Entwicklung des Nervensystems und im Erwachsenenalter. Von den Zelladhäsionsmolekülen trägt das neurale Zelladhäsionsmolekül L1 maßgeblich zu diesen Funktionen bei. Die proteolytische Spaltung von L1 durch verschiedene Proteasen ist für diese Funktionen essentiell. Es wurde gezeigt, dass ein proteolytisches L1-Fragment von 70 kDa, das einen Teil der extrazellulären Domäne und der transmembranen und intrazellulären Domänen umfasst, mit mitochondrialen Proteinen interagiert und vermutlich an mitochondrialen Funktionen beteiligt ist. Darüber hinaus wurde gezeigt, dass die Mutation von Asparaginsäure an Position 201 im extrazellulären Teil von murinem L1 zu einem L1-Syndrom Phänotyp bei Mäusen führt. In meiner Studie konnte ich zeigen, dass Neurone von L1-201 Mäusen ein höheres mitochondriales Membranpotential, normale mitochondriale Komplex I-Aktivität und einen unveränderten ATP-Spiegel sowie einen erhöhten retrograden mitochondrialen Transport und erhöhte Mengen an reaktiver Sauerstoffspezies aufweisen. Im Gegensatz dazu wiesen Mitochondrien in Neuronen von L1-70-defizienten Mäusen im Vergleich zu Mitochondrien von ihren Wildtyp-Wurfgeschwistern ein niedrigeres Membranpotential, niedrigere ATP-Spiegel, einen erhöhten retrograden Transport und eine reduzierte Komplex I-Aktivität sowie eine erhöhte Produktion von reaktiven Sauerstoffspezies auf. Darüber hinaus führt die Stimulation der L1-201- und der L1/858-863-Neuronen mit dem L1-Agonisten Duloxetine zu einer Verbesserung des Phänotyps der Mitochondrien. Durch die Behandlung werden sowohl der anterograde Transport der Mitochondrien reduziert als auch der Prozentsatz mobiler Mitochondrien erhöht und Verringerung der Produktion von ROS. Die Analyse des oxidativen Stresses im Gehirn bei jungen und erwachsenen L1-201- und L1/858-863-Mäusen zeigt keine erhöhte Lipidperoxidation, und das Verhältnis zwischen phosphoryliertem AMPK- und totalem AMPK-Gehalt in den L1-201-Gehirnen ist normal.

Die morphologische und histologische Charakterisierung von L1-201-Mäusen zeigt eine Beeinträchtigung bei der Fortsatzbildung durch der Schwann'sche Zellen, die mit dem L1-Mimetikum Duloxetine aufgehoben werden konnte. Die Golgi-Färbung der Koronalschnitte des PFC und des motorischen Kortexes von erwachsenen L1-201-Mäusen zeigt eine normale

Verzweigung von Fortsätzen der Pyramidalneuronen und eine normale Dichte von dendritischen Dornen sowie eine normale Dichte des Typs der einzelnen Dornen.

Ich habe außerdem die Größe der Ventrikel und des Corpus callosum bei erwachsenen L1/858-863-Mäusen bestimmt, um das Vorhandensein von L1-Syndrom Merkmalen in dieser L1-Mutantenlinie weiter zu untersuchen. Die Ergebnisse zeigen keine Veränderungen der Morphologie dieser Gehirnstrukturen.

Die Untersuchung des Verhaltens der L1/858-863 Mäuse zeigte ein verstärktes obsessives Verhalten der erwachsenen männlichen Tieren, während angstbezogenes Verhalten, soziale und motorische Leistungen bei männlichen Mäusen unverändert war. Weibliche L1/858-863 Mäuse zeigten reduziertes Angstverhalten und normale soziale und motorische Leistungen. In männlichen und weiblichen L1/858-863 Tieren ist die zirkadiane Rhythmik unverändert.

Insgesamt zeigt die vorliegende Studie die Bedeutung des L1-70-Fragments für die mitochondriale Homöostase. Das Fehlen von L1-70 beeinflusst jedoch nicht die Entwicklung von Gehirnstrukturen oder neurologische und motorische Leistungen bei erwachsenen Mäusen. Die Mutation der dibasischen Sequenz in der 3. FNIII-Region ruft ein obsessives Verhalten bei männlichen Mäusen hervor, was auf eine mögliche Korrelation zwischen dem L1-70 Fragment und Autismus-Spektrum-Störungen hindeutet. Wichtig ist, dass meine Daten darauf hindeuten, dass verschiedene Mutationen von L1 zu oxidativem Stress und Zelltod führen können, wodurch das Risiko erhöht wird, neurodegenerative Pathologien zu entwickeln.

6. ABBREVIATIONS

A, Ala alanine

AAV1 adeno-associated virus 1

ABAD A β binding alcohol dehydrogenase

AD Alzheimer's disease

ADP adenosine diphosphate

AMPK adenosine monophosphate-activated protein kinase

AR androgen receptor

Arg, R arginine

ATP adenosine triphosphate

A β amyloid beta

APP amyloid precursor protein

BCA bicinchoninic acid

BHT butylhydroxytoluol

BSA bovine serum albumine

CAM cell adhesion molecule

CAMKK Ca²⁺/calmodulin-dependent kinase kinase

CHL1 close homolog of L1

CoQ coenzyme Q

COX cytochrome oxidase

CREB cAMP-response element binding protein

CTCF corrected total cell fluorescence

Cu,ZnSOD copper- and zinc-containing superoxide dismutase

DCFH-DA 2',7'-dichlorofluorescein diacetate

DMEM Dulbecco's modified Eagle medium

DMSO dimethyl sulfoxide

DNA deoxyribonucleic acid

Drp1 dynamin-related protein 1

DTT dithiothreitol

EDTA ethylenediaminetetraacetic acid

EGTA ethylene glycol-bis(β -aminoethyl ether)-N,N,N',N'-tetraacetic acid

EPM elevated plus maze

ERM ezrin-radixin-moesin

ER α/β estrogen receptor α/β

ETC electrons transport chain

F, Phe phenylalanine

FADH₂ flavin adenine dinucleotide

FBA foot-based angle

FMN flavin mononucleotide

FNIII fibronectin type 3 domain

G-6-PD glucose-6-phosphate dehydrogenase

GAPDH glyceraldehyde 3-phosphate dehydrogenase

GPX glutathione peroxidase

GR glutathione reductase

GTPase guanosine triphosphatase

His histidine

H⁺ proton

HBSS Hank's balanced salt solution

HEPES 4-(2-hydroxyethyl)-1-piperazineethanesulfonic acid

HRP horse radish peroxidase

HTA heels-tail angle

I, Ile isoleucine

Ig immunoglobulin

IMM inner mitochondrial membrane

JC-1 iodide 1,1',3,3'-tetraethyl-5,5',6,6'-tetrachloroimidacarbocyanine iodide

kDa kilo dalton

L, Leu leucine

L1-/y L1-deficient mice

L1+/y L1 wild-type mice

LBD ligand-binding domain

LKB1 liver kinase B1

MBP myelin basic protein

MDA malondialdehyde

MeCP2 methyl CpG binding protein 2

MFF mitochondrial fission factor

MIA mitochondrial intermembrane space assembly

MIB mitochondrial isolation buffer

Miro mitochondrial rho guanosine triphosphatase

MnSOD manganese superoxide dismutase

MO armadillo repeat scaffolding-like protein

MP membrane potential

mRNA messenger ribonucleic acid

Na₂EDTA disodium ethylenediaminetetraacetate dihydrate

NAD⁺ oxidized nicotinamide adenine dinucleotide

NADH nicotinamide adenine dinucleotide

NDUFV2 NADH:ubiquinone oxidoreductase core subunit V2

NMDA N-methyl-D-aspartate receptors

NP-1 neuropilin-1

NP-40 nonyl phenoxy polyethoxy ethanol

OF open field

OMM outer mitochondrial membrane

OXPHOS oxidative phosphorylation

PA phosphatidic acid

PAM presequence translocase-associated motor

PBS phosphate buffered saline

PBS-T phosphate buffered saline-Tween-20

PFA paraformaldehyde

PFC prefrontal cortex

PGC-1 α peroxisome proliferator-activated receptor gamma coactivator 1 alpha

Pi phosphate

PLL poly-L-lysine

PMF proton motive force

PPAR γ peroxisome proliferator activated receptor γ

rho ras homolog family member

RIPA radioimmunoprecipitation assay

ROS reactive oxygen species

RXR β retinoid X receptor β

SAM sorting and assembly machinery

SD standard deviation

SDS sodium dodecyl sulfate

SEM standard error of the mean

Sema3A semaphorin 3A

REST RE-1-silencing transcription factor

SOD superoxide dismutases

TBA 2-thiobarbituric acid

TBARS 2- thiobarbituric acid reactive substances

TBS Tris-buffered saline

TBS-T Tris-buffered saline-Tween-20

TCA tricarboxylic acid cycle

TIM translocase of inner mitochondrial membrane

TM transmembrane

TOM translocase of outer mitochondrial membrane

WB Western blot

Wt wild-type

X any amino acid

Y, Tyr tyrosine

7. REFERENCES

- Appel F, Holm J, Conscience JF, Schachner M. (1993) Several extracellular domains of the neural cell adhesion molecule L1 are involved in neurite outgrowth and cell body adhesion. *J Neurosci* 13(11):4764-75.
- Azcoitia I, Yague JG, Garcia-Segura LM. (2011) Estradiol synthesis within the human brain. *Neurosci* 191:139–47.
- Ball SG, Desai D, Zhang Q, Thase ME, Perahia DG. (2013) Efficacy and safety of duloxetine 60 mg once daily in major depressive disorder: a review with expert commentary. *Drugs Context* 2013:212245.
- Basel-Vanagaite L, Straussberg R, Friez MJ, Inbar D, Korenreich L, Shohat M, Schwartz CE. (2006) Expanding the phenotypic spectrum of L1CAM-associated disease. *Clin Genet* 69(5):14-419.
- Cadenas E, Davies KJ. (2000) Mitochondrial free radical generation, oxidative stress, and aging. *Free Radic Biol Med* 29: 222-30.
- Carola V, D'Olimpio F, Brunamonti E, Mangia F, Renzi P. (2002) Evaluation of the elevated plus-maze and open-field tests for the assessment of anxiety-related behaviour in inbred mice. *Behav Brain Res* 134(1–2):49-57.
- Chacinska A, Koehler CM, Milenkovic D, Lithgow T, Pfanner N. (2009) Importing Mitochondrial Proteins: Machineries and Mechanisms. *Cell* 138(4):628-44.
- Christaller WA, Vos Y, Gebre-Medhin S, Hofstra RM, Schäfer MKE. (2017) L1 syndrome diagnosis complemented with functional analysis of L1CAM variants located to the two N-terminal Ig-like domains. *Clin Genet*. 91:115-20.
- Cohen NR, Taylor JS, Scott LB, Guillery RW, Soriano P, FurleyAJ. (1998) Errors in corticospinal axon guidance in mice lacking the neural cell adhesion molecule L1. *Curr Biol* 8:26–33.

Colombo F, Meldolesi J. (2015) L1-CAM and N-CAM: From Adhesion Proteins to Pharmacological Targets. *Trends in Pharmacol Sci* 36(11):769-81.

Congiu L, Granato V, Loers G, Kleene R, Schachner M. (2022) Mitochondrial and Neuronal Dysfunctions in L1 Mutant Mice. *Int J Mol Sci* 23(8):4337.

Corcoran JP, So PL, Maden M. (2004) Disruption of the retinoid signalling pathway causes a deposition of amyloid beta in the adult rat brain. *Eur J Neurosci* 20(4):896–02.

Dahme M, Bartsch U, Martini R, Anliker B, Schachner M, Mantei N. (1997) Disruption of the mouse L1 gene leads to malformations of the nervous system. *Nat Genet* 17:346–49.

Demirdaş A, Nazıroğlu M, Övey, İS. (2017) Duloxetine Reduces Oxidative Stress, Apoptosis, and Ca²⁺ Entry Through Modulation of TRPM2 and TRPV1 Channels in the Hippocampus and Dorsal Root Ganglion of Rats. *Mol Neurobiol* 54: 4683–95.

Devi L, Prabhu BM, Galati DF, Avadhani NG, Anandatheerthavarada HK. (2006) Accumulation of amyloid precursor protein in the mitochondrial import channels of human Alzheimer's disease brain is associated with mitochondrial dysfunction. *J Neurosci* 26: 9057–68.

Djogo N, Jakovcevski I, Müller C, Lee HJ, Xu JC, Jakovcevski M, Kügler S, Loers G, Schachner M. (2013) Adhesion molecule L1 binds to amyloid beta and reduces Alzheimer's disease pathology in mice. *Neurobiol Dis* 56:104-15.

Echtay KS, Murphy MP, Smith RA, Talbot DA, Brand MD. (2002) Superoxide activates mitochondrial uncoupling protein 2 from the matrix side. Studies using targeted antioxidants. *J Biol Chem* 277:47129–35.

Eichner LJ, Giguère V. (2011) Estrogen related receptors (ERRs): a new dawn in transcriptional control of mitochondrial gene networks. *Mitochondrion* 11:544–52.

Emerling B, Weinberg F, Snyder C, Burgess Z, Mutlu G, Viollet B, Budinger G, Chandel N. (2009) Hypoxic activation of AMPK is dependent on mitochondrial ROS but independent of an increase in AMP/ATP ratio. *Free Radic Biol Med* 46:1386–91.

Engel DF, de Oliveira J, Lieberknecht V, Rodrigues ALS, de Bem AF, Gabilan NH. (2018) Duloxetine Protects Human Neuroblastoma Cells from Oxidative Stress-Induced Cell Death Through Akt/Nrf-2/HO-1 Pathway. *Neurochem Res* 43:387–96.

Fischer G, Kunemund V, Schachner M. (1986) Neurite outgrowth patterns in cerebellar microexplant cultures are affected by antibodies to the cell surface glycoprotein L1. *J Neurosci* 6(2):605-12.

Forman HJ, Maiorino M, Ursini F. (2010) Signaling functions of reactive oxygen species. *Biochem* 49: 835–42.

Fransen E, D'Hooge R, Van Camp G, Verhoye M, Sijbers J, Reyniers E, Soriano P, Kamiguchi H, Willemsen R, Koekkoek SK, De Zeeuw CI, De Deyn PP, Van der Linden A, Lemmon V, Kooy RF, Willems PJ. (1998) L1 knockout mice show dilated ventricles, vermis hypoplasia and impaired exploration patterns. *Hum Mol Genet* 7(6):999–1009.

Friedman JR, Nunnari J. (2014) Mitochondrial form and function. *Nature* 505(7483):335-43.

Gabuzda D, Busciglio J, Chen LB, Matsudaira P, Yankner BA. (1994) Inhibition of energy metabolism alters the processing of amyloid precursor protein and induces a potentially amyloidogenic derivative. *J Biol Chem* 269: 13623–28.

Gandhi S, Abramov AY. (2012) Mechanism of oxidative stress in neurodegeneration. *Oxid Med Cell Longev* 2012: 428010.

Gavert N, Conacci-Sorrell M, Gast D, Schneider A, Altevogt P, Brabletz T, Ben-Ze'ev A. (2005) L1, a novel target of b-catenin signaling, transforms cells and is expressed at the invasive front of colon cancers. *J Cell Biol* 168: 633–42.

Geismann C, Arit A, Bauer J, Pfeiffer M, Schirmer U, Altevogt P, Muerkoster SS, Schäfer H. (2011) Binding of the transcription factor Slug to the L1CAM promoter is essential for transforming TGF- β -induced L1CAM expression in human pancreatic ductal adenocarcinoma cells. *Int J Oncol* 38: 257–66.

Gibson GE, Blass JP, Beal MF, Bunik V. (2005) The alpha-ketoglutarate-dehydrogenase complex: a mediator between mitochondria and oxidative stress in neurodegeneration. *Mol Neurobiol* 31: 43–63.

Gillies GE, McArthur S. (2010) Estrogen actions in the brain and the basis for differential action in men and women: a case for sexspecific medicines. *Pharmacol Rev* 62(2):155–98.

Gowans GJ, Hawley SA, Ross FA, Hardie DG. (2013) AMP is a true physiological regulator of AMPactivated protein kinase by both allosteric activation and enhancing net phosphorylation. *Cell Metab* 18:556–66.

Gusarova GA, Trejo HE, Dada LA, Briva A, Welch LC, Hamanaka RB, Mutlu GM, Chandel NS, Prakriya M, Sznajder JI. (2011) Hypoxia leads to Na,K-ATPase downregulation via Ca(2+) releaseactivated Ca(2+) channels and AMPK activation. *Mol Cell Biol*. 31:3546–56.

Halliwell B. (2006) Oxidative stress and neurodegeneration: where are we now? *Neurochem* 97(6):1634–58.

Haney CA, Sahenk Z, Li C, Lemmon VP, Roder J, Trapp BD. (1999) Heterophilic binding of L1 on unmyelinated sensory axons mediates Schwann cell adhesion and is required for axonal survival. *J Cell Biol* 146:1173-84.

Hedges VL, Ebner TJ, Meisel RL, Mermelstein PG. (2012) The cerebellum as a target for estrogen action. *Front Neuroendocrinol* 33(4):403–11.

Herron LR, Hill M, Davey F, Gunn-Moore FJ. (2009) The intracellular interactions of the L1 family of cell adhesion molecules. *Biochem J* 419(3):519-31.

Hortsch M, Nagaraj K, Mualla R. (2014) The L1 family of cell adhesion molecules: a sickening number of mutations and protein functions. *Adv Neurobiol* 8:195-229.

Hortsch M. (1996) The L1 Family of Neural Review Cell Adhesion Molecules: Old Proteins Performing New Tricks. *Neuron* 17(4):587-93.

Iverson TM. (2013) Catalytic mechanisms of complex II enzymes: A structural perspective. *Biochim Biophys Acta* 1827: 648-57.

Jonckheere AI, Smeitink JA, Rodenburg RJ. (2012) Mitochondrial ATP synthase: Architecture, function and pathology. *J Inher Metab Dis* 35: 211-25.

Jung H, Kim SY, Canbakis Cecen FS, Cho Y, Kwon SK. (2020) Dysfunction of mitochondrial Ca(2+) regulatory machineries in brain aging and neurodegenerative diseases. *Front Cell Dev Biol* 8: 599-92.

Kabekkodu SPa, Chakrabarty S, Shukla V, Varghese VK, Singh KK, Thangaraj K, Satyamoorthy K. (2015) Mitochondrial Biology: From Molecules to Disease Symposium. *Mitochondrion* 24:93-8.

Kaepernick L, Legius E, Higgins J, Kapur S. (1994) Clinical aspects of the MASA syndrome in a large family, including expressing females, *Clin Genet* 45: 181–85.

Kainu T, Wikström AC, Gustafsson JÅ, Peltö-Huikko M. (1994) Localization of the peroxisome proliferator-activated receptor in the brain. *Neurorep* 5(18):2481–85.

Kalus I, Schnegelsberg B, Seidah NG, Kleene R, Schachner M. (2003) The proprotein convertase PC5A and a metalloprotease are involved in the proteolytic processing of the neural adhesion molecule L1. *J Biol Chem* 278(12):10381-8.

Kamiguchi H, Lemmon V. (1998) A neuronal form of the cell adhesion molecule L1 contains a tyrosine-based signal required for sorting to the axonal growth cone. *J Neurosci* 18(17):3749-56.

Kenwrick S, Watkins A, De Angelis E. (2000) Neural cell recognition molecule L1: relating biological complexity to human disease mutations. *Hum Mol Genet* 9(6):879-86.

Kim, I, Rodriguez-Enriquez, S, Lemasters, JJ. (2007) Selective degradation of mitochondria by mitophagy. *Arch Biochem Biophys* 462: 245–53.

Kleene R, Lutz D, Loers G, Bork U, Borgmeyer U, Hermans-Borgmeyer I, Schachner M. (2021) Revisiting the proteolytic processing of cell adhesion molecule L1. *J Neurochem* 157:1102–17.

Kovac S, Angelova PR, Holmstrom KM, Zhang Y, Dinkova-Kostova AT, Abramov AY. (2015) Nrf2 regulates ROS production by mitochondria and NADPH oxidase *Biochim Biophys Acta* 1850: 794–801.

Kowitz A, Kadmon G, Eckert M, Schirmacher V, Schachner M, Altevogt P. (1992) Expression and function of the neural cell adhesion molecule L1 in mouse leukocytes. *Eur J Immunol* 22(5):1199-05.

Kraus F, Ryan MT. (2017) The constriction and scission machineries involved in mitochondrial fission. *J Cell Sci* 130:2953–60.

Kraus K, Kleene R, Braren I, Loers G, Lutz D, Schachner M. (2018a) A fragment of adhesion molecule L1 is imported into mitochondria and regulates mitochondrial metabolism and trafficking. *J Cell Sci* 131: 210500.

Kraus K, Kleene R, Henis M, Braren I, Kataria H, Sharaf A, Loers G, Schachner M, Lutz D. (2018b) A Fragment of Adhesion Molecule L1 Binds to Nuclear Receptors to Regulate Synaptic Plasticity and Motor Coordination. *Mol Neurobiol* 55(9):7164-78.

Kujat R, Miragall F, Krause D, Dermietzel R, Wrobel KH. (1995) Immunolocalization of the neural cell adhesion molecule L1 in non-proliferating epithelial cells of the male urogenital tract. *Histochem Cell Biol* 103(4):311-21.

Lev N, Ickowicz D, Melamed E, Offen D. (2008) Oxidative insults induce DJ-1 upregulation and redistribution: implications for neuroprotection. *NeuroToxicology* 29 (3): 397–405.

Li J, Yang L, Pu C, Tang Y, Yun H, Han P. (2013) The role of duloxetine in stress urinary incontinence: a systematic review and meta-analysis. *Int Urol Nephrol* 45(3):679–86.

Lill R. (2009) Function and biogenesis of iron–sulphur proteins. *Nature* 460:831–38.

Lindner J, Rathjen FG, Schachner M. (1983) L1 mono- and polyclonal antibodies modify cell migration in early postnatal mouse cerebellum. *Nature* 305:427-30.

Loers G, Chen S, Grumet M, Schachner M. (2005) Signal transduction pathways implicated in neural recognition molecule L1 triggered neuroprotection and neuritogenesis. *J Neurochem* 92(6):1463-76.

Loers G, Appel D, Lutz D, Congiu L, Kleene R, Hermans-Borgmeyer I, Schäfer MKE, Schachner M. (2021) Amelioration of the abnormal phenotype of a new L1 syndrome mouse mutation with L1 mimetics. *FASEB J* 35(2): 21329.

Lustbader JW, Cirilli M, Lin C, Xu HW, Takuma K, Wang N, Caspersen C, Chen X, Pollak S, Chaney M, Trinchese F, Liu S, Gunn-Moore F, Lue LF, Walker DG, Kuppasamy P, Zewier ZL, Arancio O, Stern D, Yan SS, Wu H. (2004) ABAD directly links Abeta to mitochondrial toxicity in Alzheimer's disease. *Science* 304: 448–52.

Lüthl A, Laurent JP, Figueroa A, Müller D, Schachner M. (1994) Hippocampal long-term potentiation and neural cell adhesion molecules L1 and NCAM. *Nature* 372(6508):777-9.

Lutz D, Wolters-Eisfeld G, Joshi G, Djogo N, Jakovcevski I, Schachner M, Kleene R. (2012) Generation and nuclear translocation of sumoylated transmembrane fragment of cell adhesion molecule L1. *J Biol Chem* 287(21):17161-75.

Lutz D, Loers G, Kleene R, Oezen I, Kataria H, Katagihallimath N, Braren I, Harauz G, Schachner M. (2014a) Myelin basic protein cleaves cell adhesion molecule L1 and promotes neuriteogenesis and cell survival. *J Biol Chem* 289(19):13503-18.

Lutz D, Wolters-Eisfeld G, Schachner M, Kleene R. (2014b) Cathepsin E generates a sumoylated intracellular fragment of the cell adhesion molecule L1 to promote neuronal and Schwann cell migration as well as myelination. *J Neurochem* 128(5):713-24.

Maness PF, Schachner M. (2007) Neural recognition molecules of the immunoglobulin superfamily: signaling transducers of axon guidance and neuronal migration. *Nat Neurosci* 10(1):19-26.

Martini R, Schachner M. (1986) Immunoelectron microscopic localization of neural cell adhesion molecules (L1, N-CAM, and MAG) and their shared carbohydrate epitope and myelin basic protein in developing sciatic nerve. *J Cell Biol* 103(6):2439-48.

Mechtersheimer S, Gutwein P, Agmon-Levin N, Stoeck A, Oleszewski M, Riedle S, Postina R, Fahrenholz F, Fogel M, Lemmon V, Altevogt P. (2001) Ectodomain shedding of L1 adhesion molecule promotes cell migration by autocrine binding to integrins. *J Cell Biol* 155(4):661-73.

Michelson P, Hartwig C, Schachner M, Gal A, Veske A, Finckh U. (2002) Missense mutations in the extracellular domain of the human neural cell adhesion molecule L1 reduce neurite outgrowth of murine cerebellar neurons. *Hum Mut* 20:481-82.

Mikulak J, Negrini S, Klaj A, D'Alessandro R, Mavilio D, Meldolesi J. (2012) Dual REST-dependence of L1CAM: from gene expression to alternative splicing governed by Nova2 in neural cells. *J Neurochem* 120: 699-709.

Moos M, Tacke R, Scherer H, Teplow D, Früh K, Schachner M. (1988) Neural adhesion molecule L1 as a member of the immunoglobulin superfamily with binding domains similar to fibronectin. *Nature* 334(6184):701-3.

Moreno S, Farioli-Vecchioli S, Cerù MP. (2004) Immunolocalization of peroxisome proliferator-activated receptors and retinoid X receptors in the adult rat CNS. *Neurosci* 123(1):131–45.

Morris, R.L.; Hollenbeck, P.J. (1993) The regulation of bidirectional mitochondrial transport is coordinated with axonal outgrowth. *J Cell Sci* 104(3): 917–27.

Mukherjee SP and Mukherjee C. (1982) Similar activities of nerve growth factor and its homologue proinsulin in intracellular hydrogen peroxide production and metabolism in adipocytes. Transmembrane signalling relative to insulin-mimicking cellular effects. *Biochem Pharmacol* 31: 3163–72.

Mungai PT, Waypa GB, Jairaman A, Prakriya M, Dokic D, Ball MK, Schumacker PT. (2011) Hypoxia triggers AMPK activation through reactive oxygen species-mediated activation of calcium release activated calcium channels. *Mol Cell Biol* 31:3531–45.

Nakamura Y, Lee S, Haddox CL, Weaver EJ, Lemmon VP. (2010) Role of the cytoplasmic domain of the L1 cell adhesion molecule in brain development. *J Comp Neurol* 518(7):1113–32.

Nayeem N, Silletti S, Yang X, Lemmon VP, Reisfeld RA, Stallcup WB, Montgomery AM. (1999) A potential role for the plasmin(ogen) system in the posttranslational cleavage of the neural cell adhesion molecule L1. *J Cell Sci* 112 (24):4739-49.

Orrenius S, Gogvadze V, Zhivotovsky B. (2007) Mitochondrial oxidative stress: Implications for cell death. *Annu Rev Pharmacol Toxicol* 47: 143-83.

Otera H, Wang C, Cleland MM, Setoguchi K, Yokota S, Youle RJ, Mihara K. (2010) Mff is an essential factor for mitochondrial recruitment of Drp1 during mitochondrial fission in mammalian cells. *J Cell Biol* 191:1141–58.

Ott M, Amunts A, Brown A. (2016) Organization and Regulation of Mitochondrial Protein Synthesis. *Annu Rev Biochem* 85:77–101.

Pfeiffer M., Schrimmer U., Geismann C., Schäfer H., Sebena S. and Altevogt P. (2010) L1CAM expression in endometrial carcinomas is regulated by usage of two different promoter regions. *BMC Mol Biol* 11: 64.

Pickles S, Vigié P, Youle RJ. (2018) Mitophagy and Quality Control Mechanisms in Mitochondrial Maintenance. *Curr Biol* 28:170–85.

Pravdic D, Hirata N, Barber L, Sedlic F, Bosnjak ZJ, Bienengraeber M. (2012) Complex I and ATP synthase mediate membrane depolarization and matrix acidification by isoflurane in mitochondria. *Eur J Pharmacol* 690(1-3):149-57.

Probstmeier R, Martini R, Tacke R, Schachner M. (1990) Expression of the adhesion molecules L1, N-CAM and J1/ tenascin during development of the murine small intestine. *Differentiation* 44:42-55.

Raveh S, Gavert N, Ben-Ze'ev A. (2009) L1 cell adhesion molecule (L1CAM) in invasive tumors. *Cancer Lett* 282(2):137-45.

Rich PR, Maréchal A. (2010) The mitochondrial respiratory chain. *Essays Biochem* 47:1-23.

Ross FA, MacKintosh C, Hardie DG. (2016) AMP-activated protein kinase: a cellular energy sensor that comes in 12 flavours. *FEBS J* 283:2987–01.

Sadoul K, Sadoul R, Faissner A, Schachner M. (1988) Biochemical characterization of different molecular forms of the neural cell adhesion molecule L1. *J Neurochem* 50(2):510-21.

Sanes JR, Yamagata M. (1999) Formation of lamina-specific synaptic connections. *Curr Opin Neurobiol* 9(1):79-87.

Schapira A.H. (2008) Mitochondria in the aetiology and pathogenesis of Parkinson's disease, *Lancet Neurol* 7(1): 97–109.

Schmid JS, Bernreuther C, Nikonenko AG, Ling Z, Mies G, Hossmann KA, Jakovcevski I, Schachner M. (2013) Heterozygosity for the mutated X-chromosome-linked L1 cell adhesion molecule gene leads to increased numbers of neurons and enhanced metabolism in the forebrain of female carrier mice, *Brain Struct Funct* 218: 1375–90.

Schon EA, Przedborski S. (2011) Mitochondria: the next (neurode)generation. *Neuron* 70:1033–53.

Schuchardt JP, Huss M, Stauss-Grabo M, Hahn A. (2010) Significance of long-chain polyunsaturated fatty acids (PUFAs) for the development and behaviour of children. *Eur J Pediatr* 169(2):149–64.

Seilheimer B, Persohn E, Schachner M. (1989) Neural cell adhesion molecule expression is regulated by Schwann cell-neuron interactions in culture. *J Cell Biol* 108(5):1909-15.

Serville F, Lyonnet S, Pelet A, Reynaud M, Louail C, Munnich A, Le Merrer M. (1992) X-linked hydrocephalus: clinical heterogeneity at a single gene locus. *Eur J Pediatr* 151:515-18.

Shaw M, Yap TY, Henden L, Bahlo M, Gardner A, Kalscheuer VM, Haan E, Christie L, Hackett A, Gecz J. (2015) Identical by descent L1CAM mutation in two apparently unrelated families with intellectual disability without L1 syndrome. *Eur J Med Genet* 58:364-68.

Shpilka T, Haynes CM. (2018) The mitochondrial UPR: mechanisms, physiological functions and implications in ageing. *Nat Rev Mol Cell Biol* 19:109–20.

Silletti S, Mei F, Sheppard D, Montgomery AM. (2000) Plasmin-sensitive dibasic sequences in the third fibronectin-like domain of L1-cell adhesion molecule (CAM) facilitate homomultimerization and concomitant integrin recruitment. *J Cell Biol* 149(7):1485-02.

Starkov AA, Fiskum G, Chinopoulos C, Lorenzo BJ, Browne SE, Patel MS, Beal MF. (2004) Mitochondrial alpha-ketoglutarate dehydrogenase complex generates reactive oxygen species. *J Neurosci* 24: 7779–88.

- Suter M, Riek U, Tuerk R, Schlattner U, Wallimann T, Neumann D. (2006) Dissecting the role of 5'-AMP for allosteric stimulation, activation, and deactivation of AMP-activated protein kinase. *J Biol Chem* 281:32207–16.
- Szewczyk A., Pikula S. (1998) Adenosine 5'-triphosphate: an intracellular metabolic messenger, *Biochim Biophys Acta* 20 (1365): 333–53.
- Sztriha L, Frossard P, Hofstra RM, Verlind E, Nork M. (2000) Novel missense mutation in the L1 gene in a child with corpus callosum agenesis, retardation, adducted thumbs, spastic paraparesis, and hydrocephalus. *J Child Neurol* 15:239-43.
- Sztriha L, Vos YJ, Verlind E, Johansen J, Berg B. (2002) X-linked hydrocephalus: a novel missense mutation in the L1CAM gene. *Pediatr Neurol* 27:293-96.
- Taanman JW. (1999) The mitochondrial genome: structure, transcription, translation and replication. *Biochim Biophys Acta* 1410(2):103-23.
- Tait SWG, Green DR. (2010) Mitochondria and cell death: outer membrane permeabilization and beyond. *Nat Rev Mol Cell Biol* 11:621–32.
- Tilokani L, Nagashima S, Paupe V, Prudent J. (2018) Mitochondrial dynamics: overview of molecular mechanisms. *Essays in Biochem* 62:341–60.
- Togashi H, Sakisaka T, Takai Y. (2009) Cell adhesion molecules in the central nervous system. *Cell Adh Migr* 3(1):29-35.
- Turens JF. (2003) Mitochondrial formation of reactive oxygen species. *J Physiol* 552: 335-44.
- Van der Blik AM, Sedensky MM, Morgan PG. (2017) Cell Biology of the Mitochondrion. *Genetics* 207:843–71.
- Varga-Szabo D, Braun A, Nieswandt B. (2009) Calcium signaling in platelets, *J Thromb Haemost* 7:1057–66.
- Vinogradov AD, Grivennikova VG. (2016) Oxidation of NADH and ROS production by respiratory complex I. *Biochim Biophys Acta* 1857: 863–71.

Vinokurov AY, Stelmashuk OA, Ukolova PA, Zherebtsov EA, Abramov AY. (2021) Brain region specificity in reactive oxygen species production and maintenance of redox balance. *Free Radic Biol Med* 174:195–01.

Votyakova TV, Reynolds IJ. (2001) DeltaPsi(m)-Dependent and -independent production of reactive-oxygen species by rat brain mitochondria. *J Neurochem* 79: 266–77.

Wang Y, Loers G, Pan HC, Gouveia R, Zhao WJ, Shen YQ, Kleene R, Costa J, Schachner M. (2012) Antibody Fragments Directed against Different Portions of the Human Neural Cell Adhesion Molecule L1 Act as Inhibitors or Activators of L1 Function. *PLoS One* 7(12):52404.

Washbourne P, Dityatev A, Scheiffele P, Biederer T, Weiner JA, Christopherson KS, El-Husseini A. (2004) Cell adhesion molecules in synapse formation. *J Neurosci* 24(42):9244-9.

Wei CH, Ryu SE. (2012) Homophilic interaction of the L1 family of cell adhesion molecules. *Exp Mol Med* 44(7):413-23.

Westermann B. (2010) Mitochondrial fusion and fission in cell life and death. *Nat Rev Mol Cell Biol* 11:872–84.

Wu Z, Puigserver P, Andersson U, Zhang C, Adelmant G, Mootha V, Troy A, Cinti S, Lowell B, Scarpulla RC, Spiegelman BM. (1999) Mechanisms controlling mitochondrial biogenesis and respiration through the thermogenic coactivator PGC-1. *Cell* 98:115–24.

Xiao B. (2007) Structural basis for AMP binding to mammalian AMP-activated protein kinase. *Nature* 449:496–500.

Yamagata M, Sanes JR, Weiner JA. (2003) Synaptic adhesion molecules. *Curr Opin Cell Biol* 15(5):621-32

Yamagishi SI, Edelstein D, Du XL, Brownlee M. (2001) Hyperglycemia potentiates collagen-induced platelet activation through mitochondrial superoxide overproduction. *Diabetes* 50:1491–94.

8. ACKNOWLEDGEMENTS

This study has been performed at the Senior Group for Biosynthesis of Neuronal Structures of the Centre for Molecular Neurobiology Hamburg (ZMNH).

First of all, I would like to thank Prof. Dr. Dr. h.c. Melitta Schachner for giving me the opportunity to undertake this PhD which has enriched me both from a professional and human point of view. I am grateful to her for trusting me during these 3 years and for always supporting my research project.

I sincerely thank my supervisors Dr. Ralf Kleene and Dr. Gabriele Loers for their support and help over the years and for all the helpful suggestions during the writing of my thesis. In particular, I would like to thank Gaby for her patience and for being an essential point of reference during my PhD, discussing the results with me and supporting me with her help in any problem I faced during the everyday work and moral support during difficult moments.

I sincerely thank my colleagues Laura, Luciana, Maria and Viviana. Your support and your friendship have been essential during these years. In particular, I thank Viviana for her immense patience and for her support and help during the experiments we did together. I am also thankful to Ute Bork for her technical assistance, her support and commitment in the lab.

I also thank Prof. Matthias Kneussel and all the researchers and technicians of his laboratory for allowing me to use their instruments to perform my experiments, for the technical help I always received and in particular for always making me feel part of their research group. Many thanks to the PhD students of the Kneussel group for being not only wonderful colleagues, but also friends without whom this journey would not have been the same.

I thank my friends from Hamburg for becoming my second family and always supporting and encouraging me in good and bad times. I also thank my lifelong friends, who despite the distance have always encouraged me and given me strength trying to make me feel less homesick.

Last but not least, I thank my family for always being there and for giving me the strength to finish this journey.

9. CURRICULUM VITAE

Name: Ludovica Congiu

Birthdate: 22.05.1992

Place of birth: Cagliari (Italy)

Education and experience:

2011: Classic high school G.M. Dettori (Cagliari)

2011-2015: Bachelor's Degree in Biology

University of Cagliari, Faculty of Biology and Pharmacy, Department of Life and Environmental Science

Internship in the laboratory of Confocal microscopy.

Experimental Thesis: " The role of Purkinje cells in development of dyskinesias after chronic administration of L-DOPA "

2015-2017: Master's Degree in Neuropsychobiology

University of Cagliari, Faculty of Biology and Pharmacy, Department of Life and Environmental Science, Sez.Neuroscience, University of Monserrato, Cagliari (Italy)

Internship in the laboratory of Neuroendocrinology.

Experimental thesis: "Neonatal exposure to estradiol and adrenal-pituitary- hypothalamus axis function"

2017-2019: Predoctoral fellow

University of Cagliari, Department of Life and Environmental Science, Sez. Neuroscience, University of Monserrato, Cagliari (Italy)

Project: "Effect of maternal immune activation on the degeneration induced by Alpha-synuclein in an animal model of Parkinson's disease".

2019-2023: PhD student

Senior Group 'Biosynthesis of Neural Structures' Center for Molecular Neurobiology Hamburg
(ZMNH)

10. Eidesstattliche Versicherung

Ich versichere ausdrücklich, dass ich die Arbeit selbständig und ohne fremde Hilfe verfasst, andere als die von mir angegebenen Quellen und Hilfsmittel nicht benutzt und die aus den benutzten Werken wörtlich oder inhaltlich entnommenen Stellen einzeln nach Ausgabe (Auflage und Jahr des Erscheinens), Band und Seite des benutzten Werkes kenntlich gemacht habe.

Ferner versichere ich, dass ich die Dissertation bisher nicht einem Fachvertreter an einer anderen Hochschule zur Überprüfung vorgelegt oder mich anderweitig um Zulassung zur Promotion beworben habe.

Ich erkläre mich einverstanden, dass meine Dissertation vom Dekanat der Medizinischen Fakultät mit einer gängigen Software zur Erkennung von Plagiaten überprüft werden kann.

Unterschrift: